Geodynamics Lecture #3

Max Rudolph
Department of Earth and Planetary Sciences
University of California, Davis

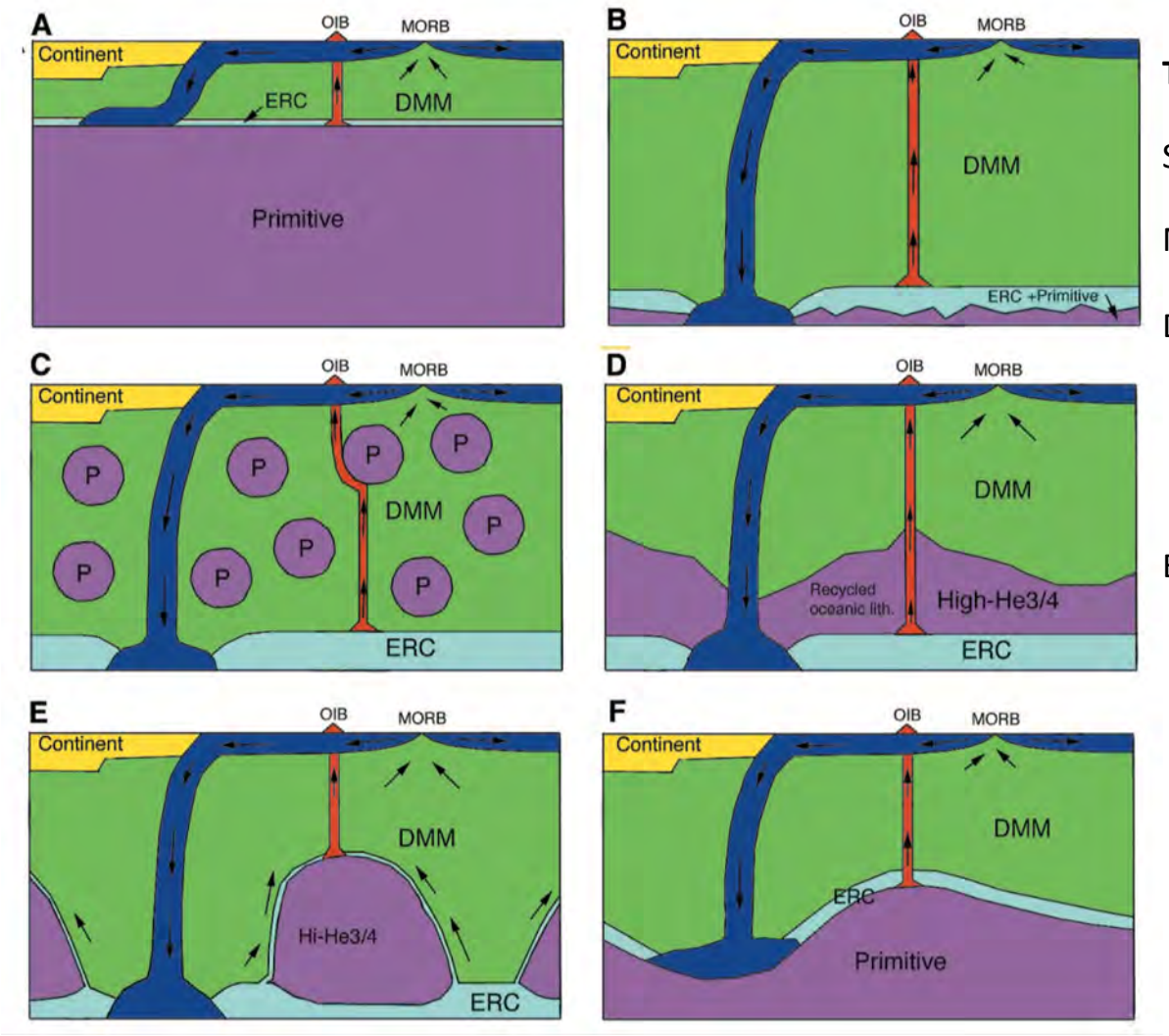

To understand plausibility of models, we need

Seismic images (not the focus of this lecture!)

Material properties and behavior

Deformation of the surface

ERC = Enriched Recycled Crust

Tackley 2000 *Science*

Thermochemical convection in a lava lamp

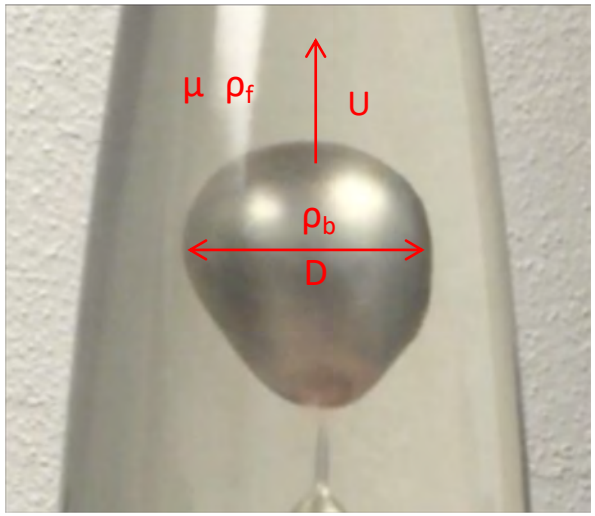

Ascent Timescale:

$$\tau_{\text{ascent}} = \frac{D}{U} = \frac{\frac{a}{2}}{\frac{a^2 g(\rho_f - \rho_b)}{3\mu_f}}$$

Cooling Timescale:

$$\tau_{\text{cooling}} = \frac{a^2}{\kappa}$$

Rayleigh number is related to ratio of time scales

$$Ra = \frac{\tau_{\text{cooling}}}{\tau_{\text{ascent}}} \sim \frac{(\rho_f - \rho_b) g a^3}{\mu_f \kappa}$$

Faster ascent -> Higher Ra -> More vigorous convection
Faster cooling -> Low Ra -> No (or less vigorous) convection

Steady to unsteady transition near Ra 10^5

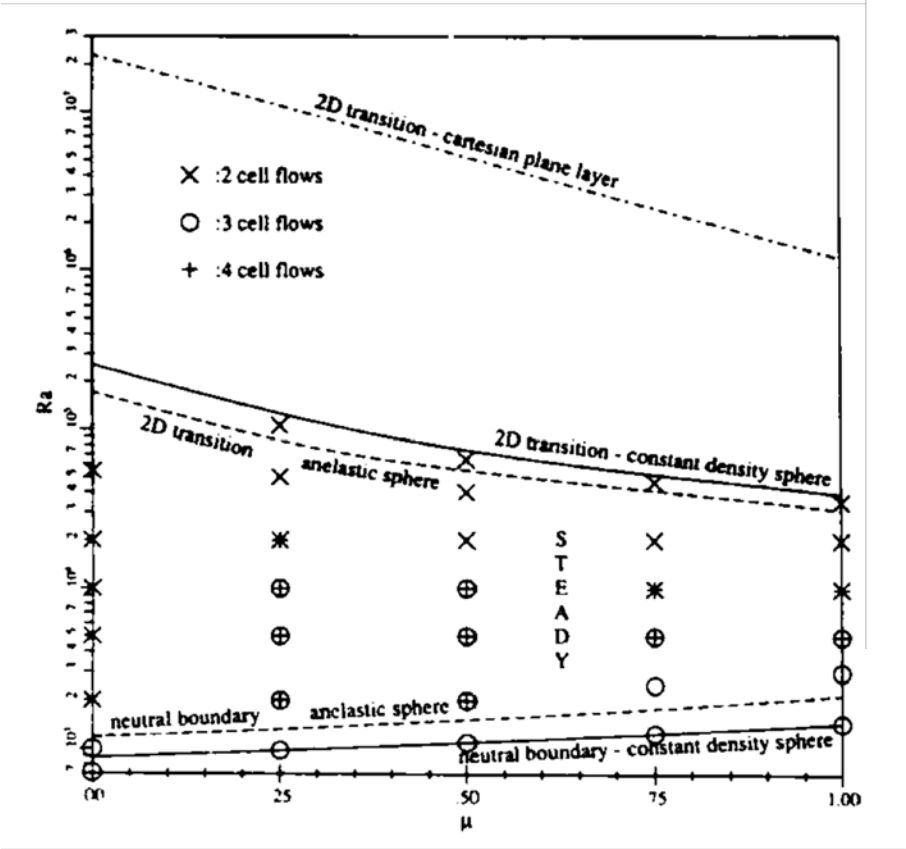

Solheim and Peltier 1990

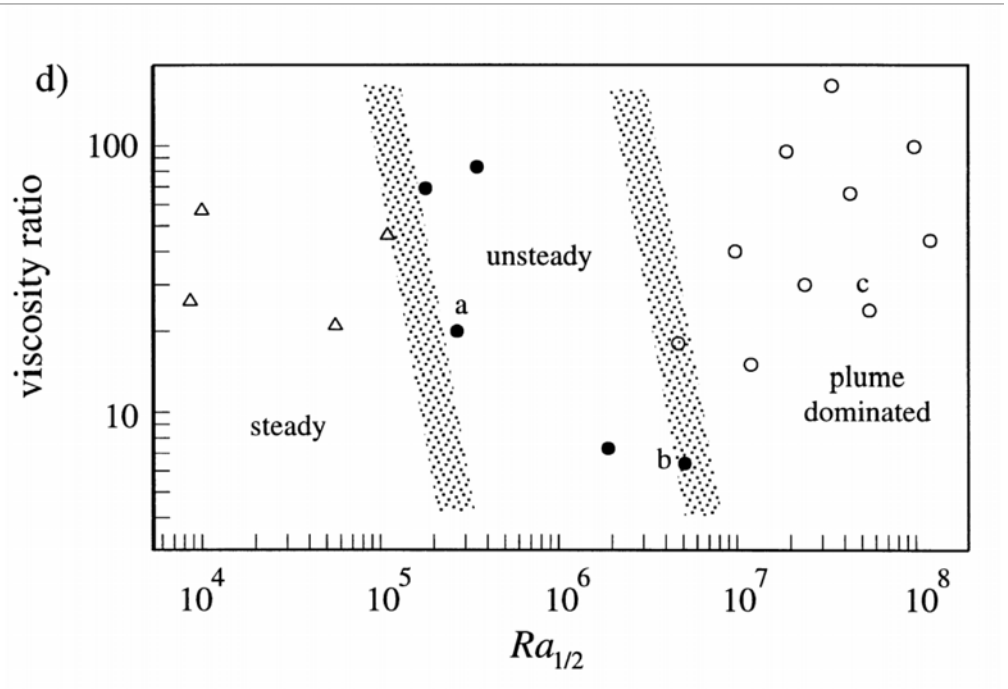

Weeraratne and Manga 1998

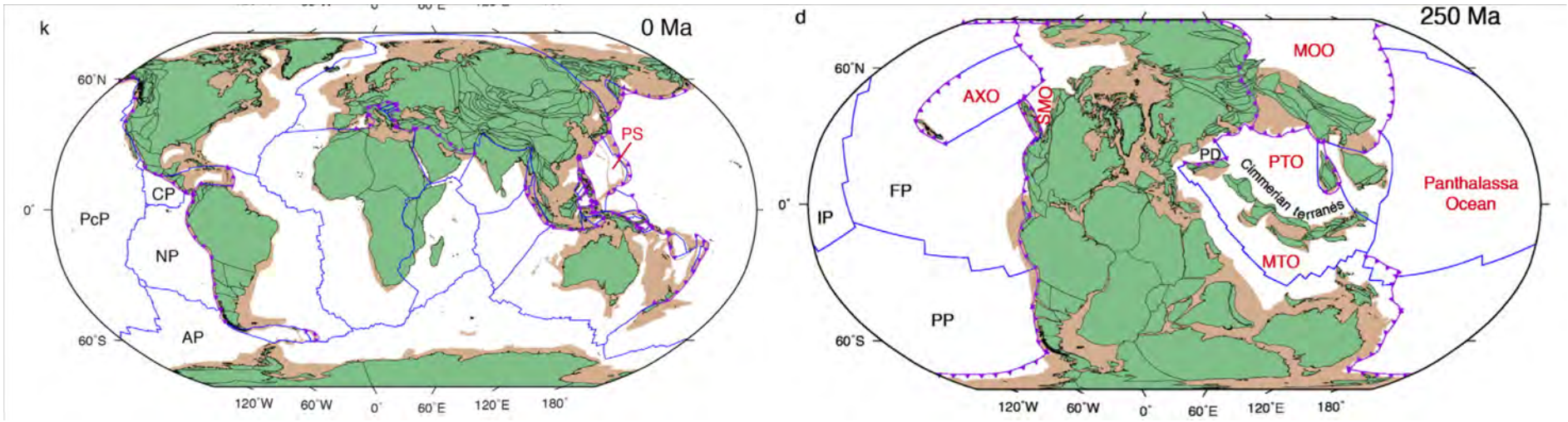

Changing configuration of plate boundaries

Surface motions are clearly unsteady, so flow in mantle must be as well.

Matthews et al. 2016

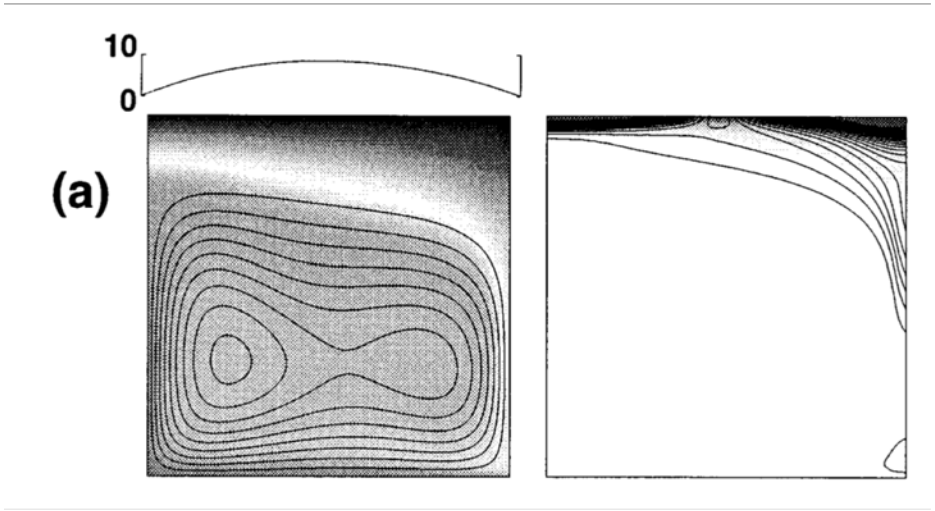

Stagnant lid regime
Ra=10^7
$\Delta\eta=3\times10^4$
$\tau_0=10^6$ (c_0=120 MPa)
$\tau_1=10^7$ (μ=0.013)

$$\tau'_{\text{yield}} = \tau_0 + \tau_1 z',$$

$$\tau_0 = \frac{d^2}{\kappa\eta_0} c_0,$$

$$\tau_1 = \frac{\mu\rho g R a_0}{\alpha\Delta T}$$

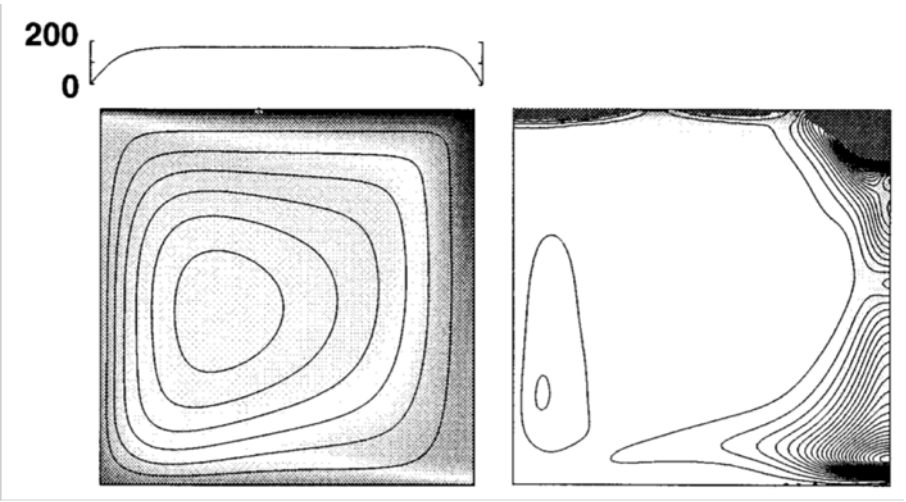

Mobile lid regime
$\tau_0=10^5$ (c_0=12 MPa)

(Moresi and Solomatov 1998)

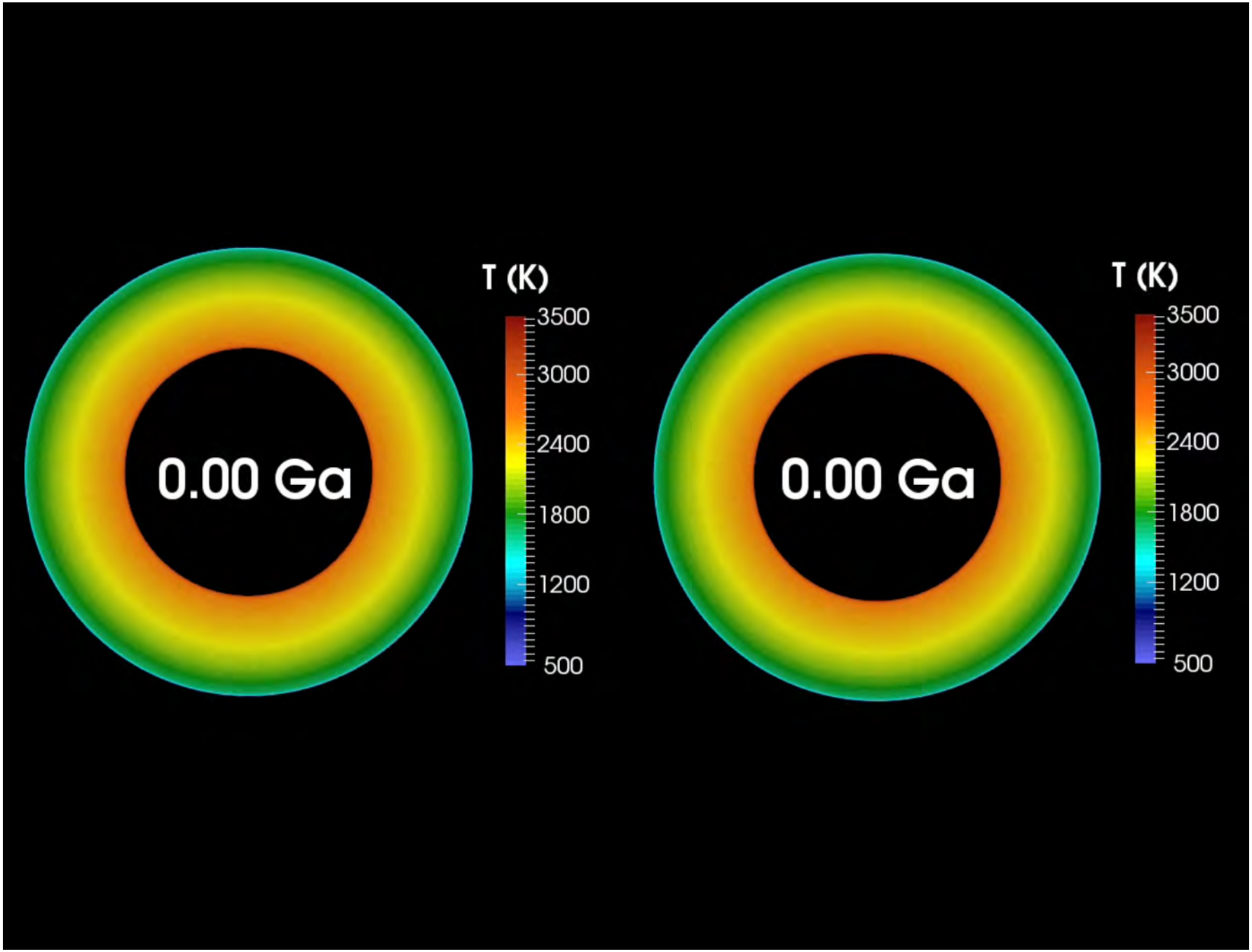

From Diogo Lourenço

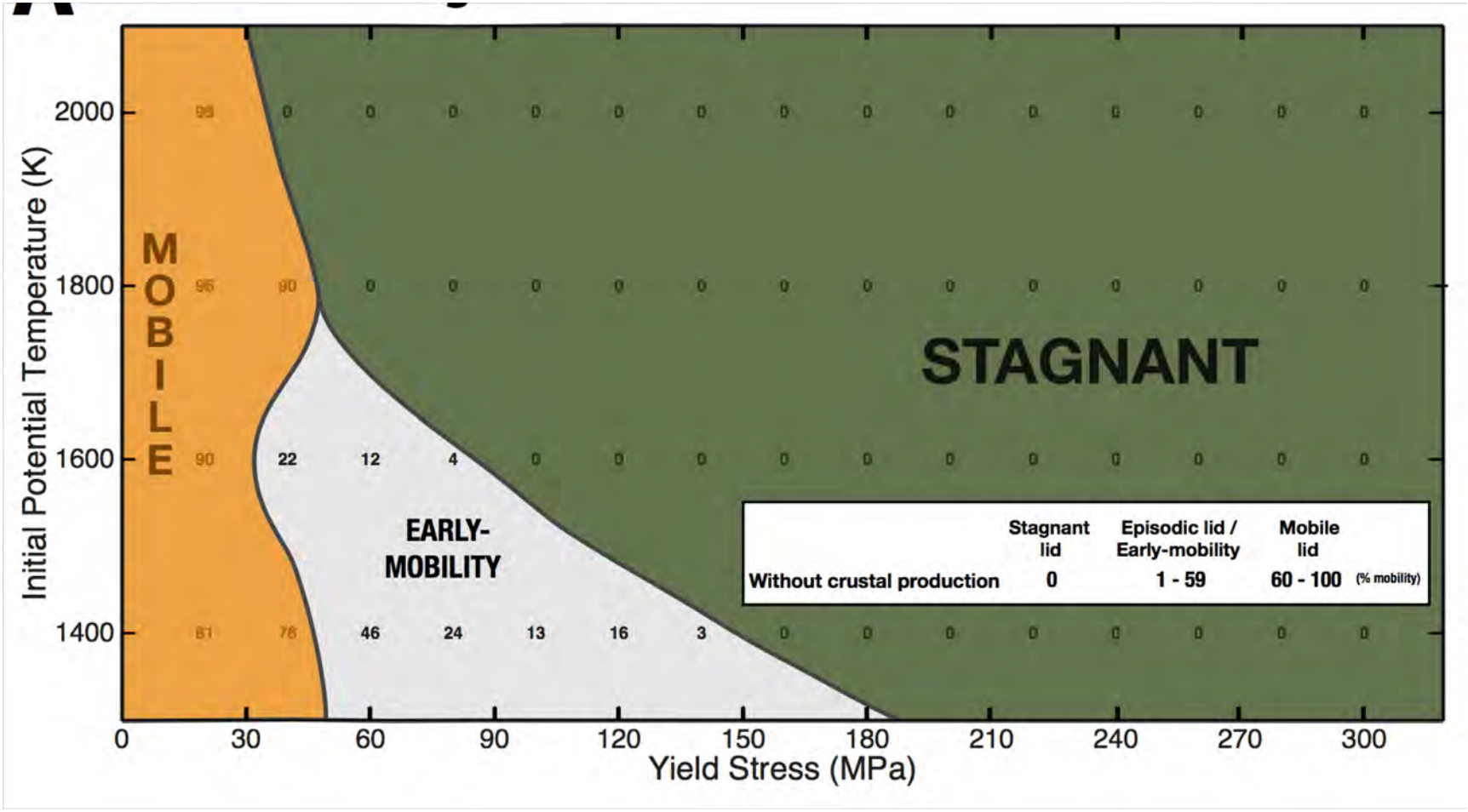

Lourenço et al. 2016 *EPSL*

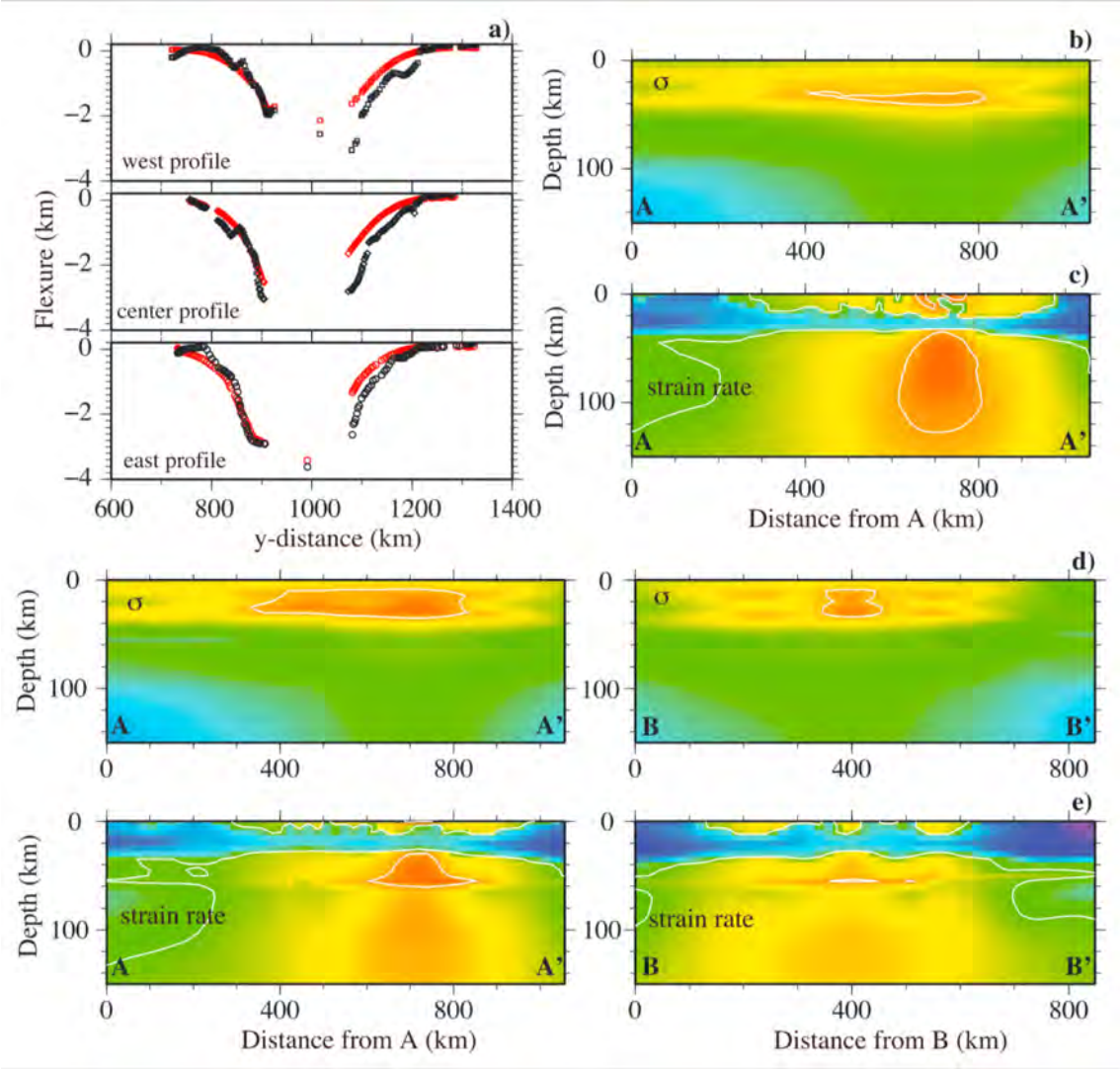

Seamont loading

Load ~ 1/3 A*h/A ~ 150 MPa

Fit:
Flexural topography
Depth distribution of seismicity
Include elasticity, plastic deformation

Result:
Lithospheric stresses are 100-200 MPa

Zhong and Watts 2012 *JGR*

Plate-like flow and mixing

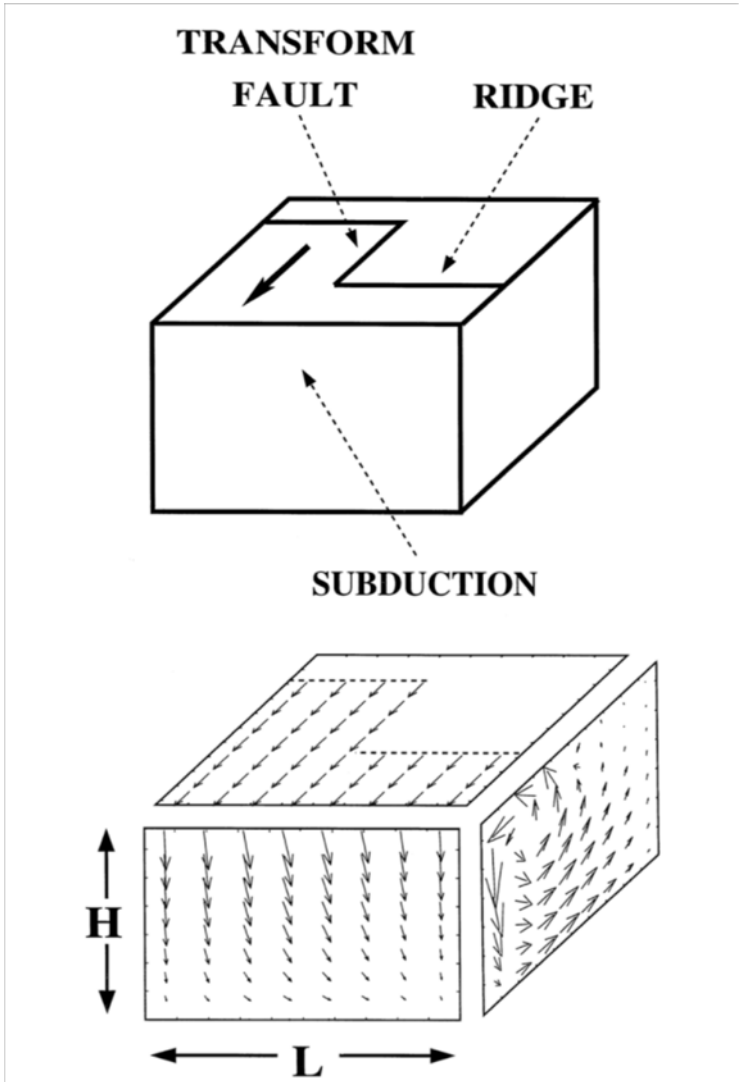

Fig. 1. Box of aspect ratio 2/3 in which the computation is performed. The flow is only driven by a surface motion mimicking a real plate with a segmented ridge, a transform fault and a subduction zone (*top*). The resulting flows at the surface, the front and the right-hand faces are depicted at the bottom.

Ferrachat and Ricard 1998

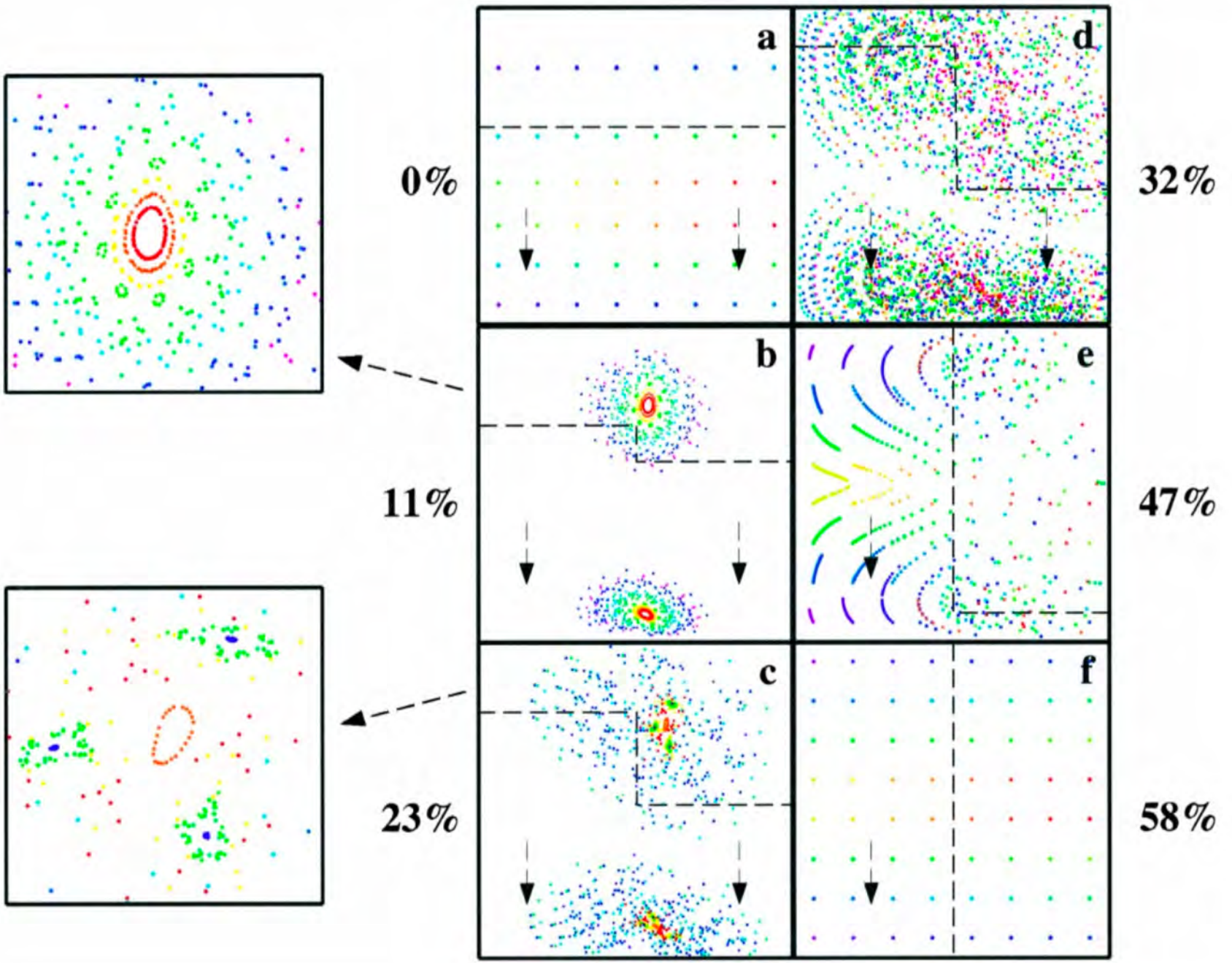

Ferrachat and Ricard 1998

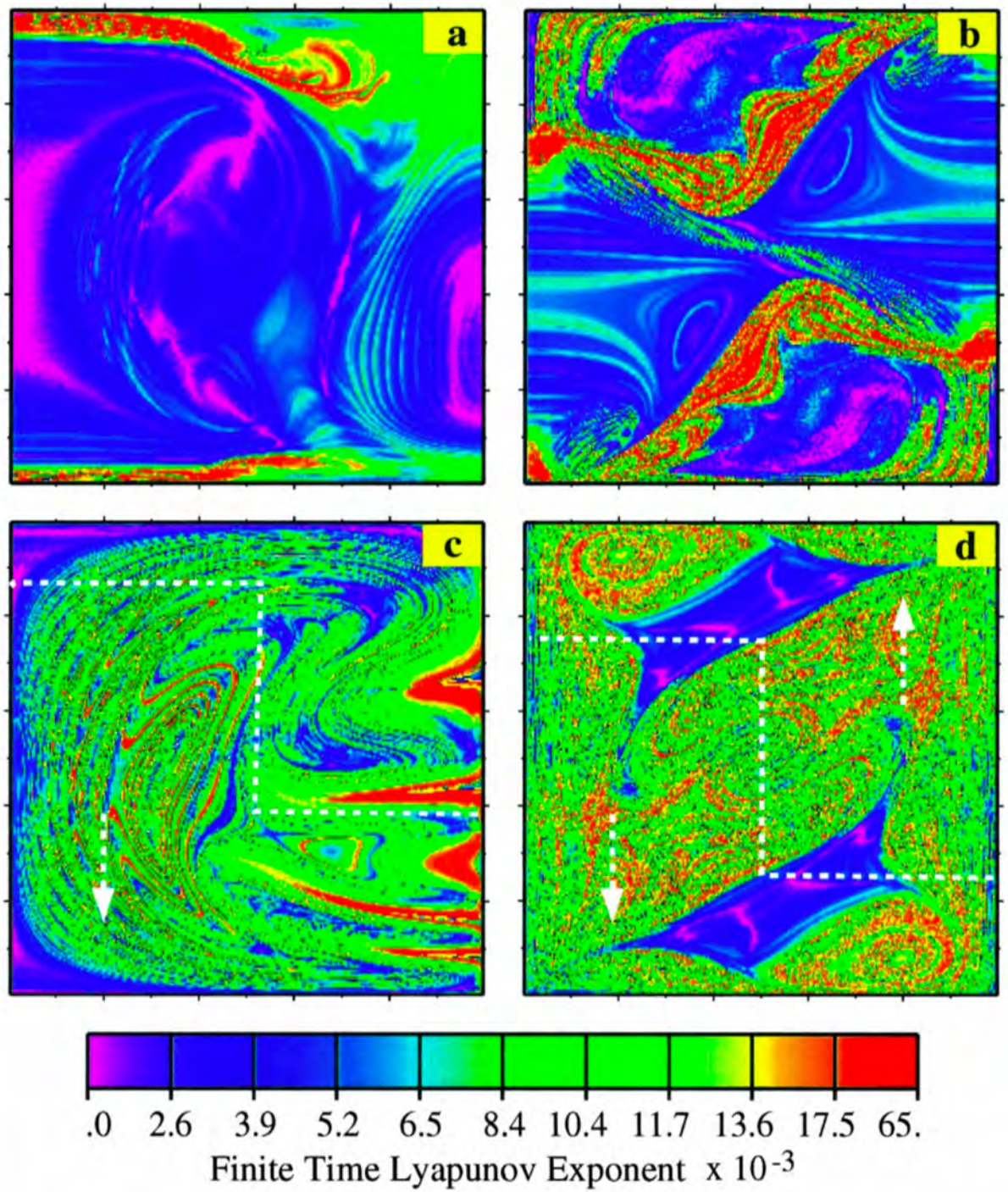

Poloidal only

Plate-driven flow

Mixing in present-day flowfield

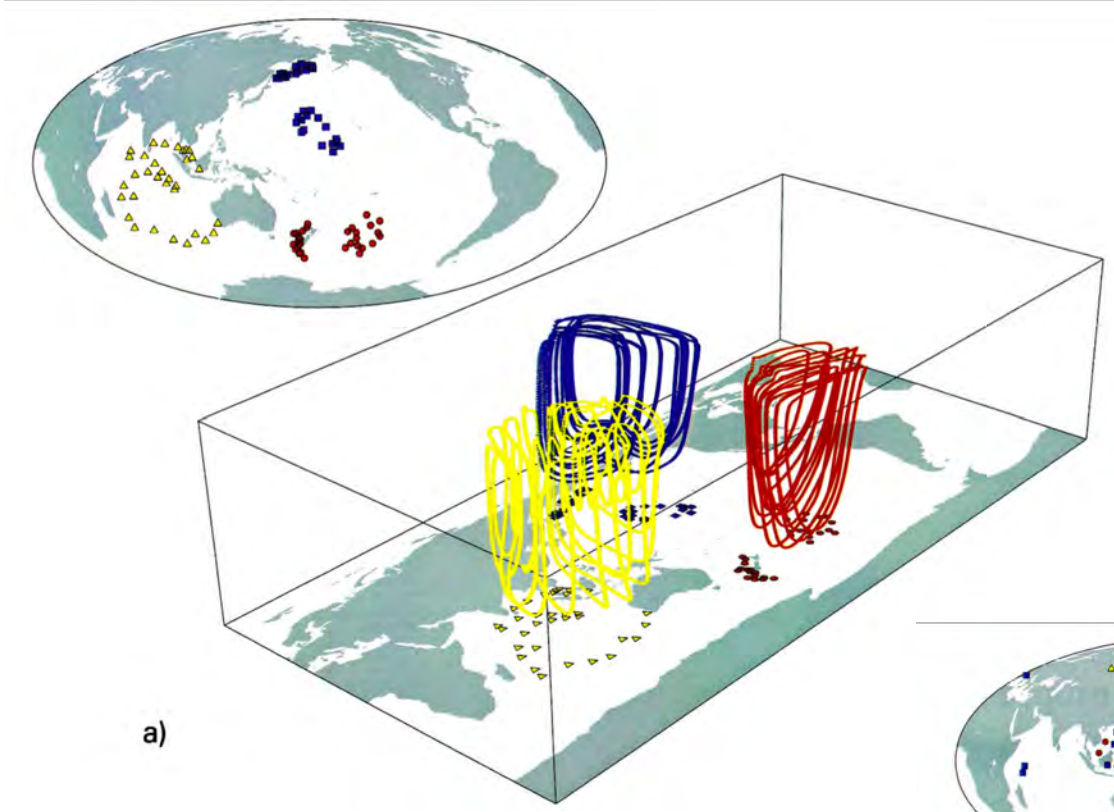

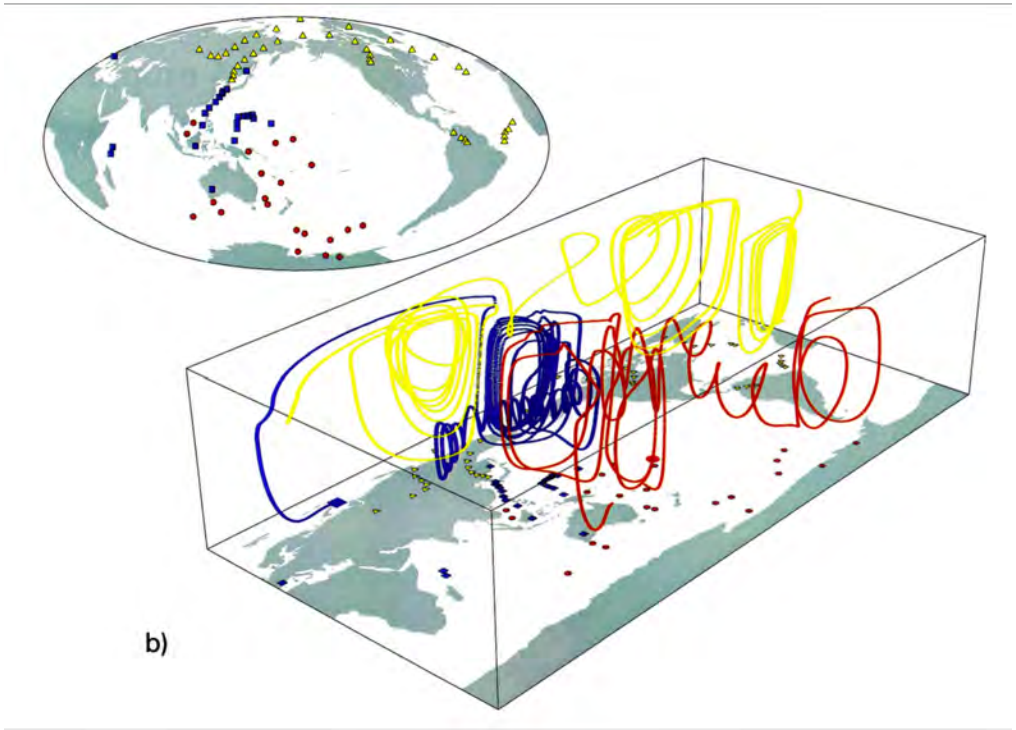

van Keken and Zhong 1999

Wave cut terraces in Nunavut record post-glacial rebound

The Motion of a Viscous Fluid Under a Surface Load

N. A. HASKELL, *Massachusetts Institute of Technology*

(Received April 25, 1935)

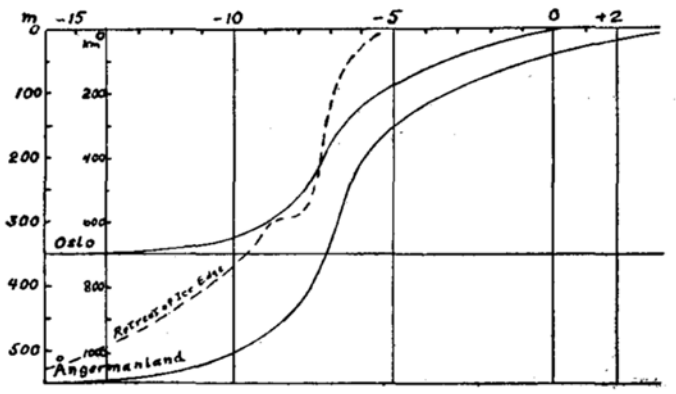

TABLE III. *Values taken for the coefficient of viscosity of various substances.*

MATERIAL	TEMPERATURE	η (g. cm^{-1} sec.$^{-1}$)
Shoemakers wax	15°C	2×10^{8}
Asphalt	15	3×10^{10}
Ice	0	5×10^{12}
Glass	575	1×10^{13}
Lead	20	1×10^{16}
Calcite	18	1.5×10^{16}
Rocksalt	18	2×10^{18}

TABLE I. *Values of the quantities entering in Eq. (5.42) for various times taken as the initial instant.*

$t=0$	a	$b \times 10^{3}$	$\zeta(0, 0)$	$\nu \times 10^{-21}$
5,000 B.C.	3.9	$1.27 \pm .07$	147	2.6 ± 0.2
4,000 "	2.7	$1.19 \pm .09$	118	3.2 ± 0.3
3,000 "	2.2	$1.24 \pm .11$	94	3.0 ± 0.4
2,000 "	1.8	$1.25 \pm .15$	74	2.9 ± 0.5

Mean value: $\nu = 2.9 \times 10^{21}$ cm^2 sec.$^{-1}$

Very close to 10^{21} Pa-s

GOCE geoid

GOCE measurements from ESA

https://dlmultimedia.esa.int/download/public/videos/2016/01/027/1601_027_AR_EN.mp4

Spherical harmonics

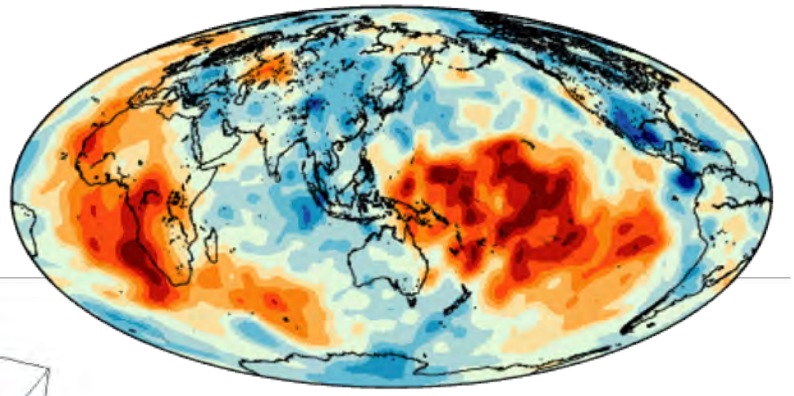

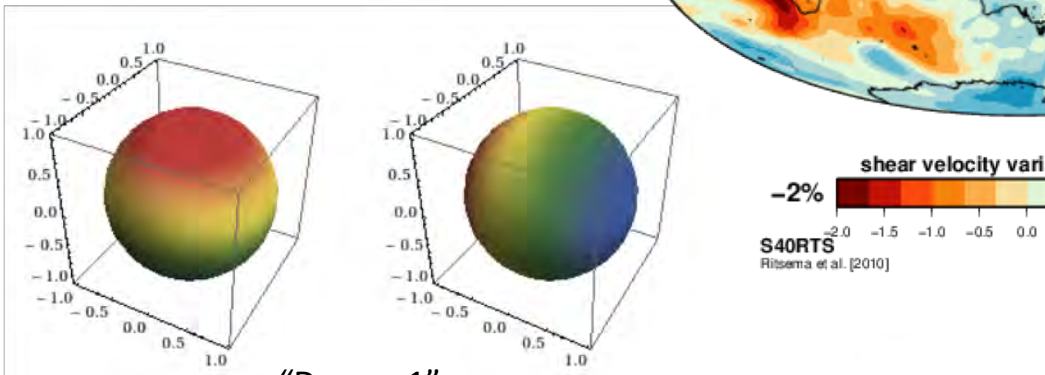

"Degree 1"

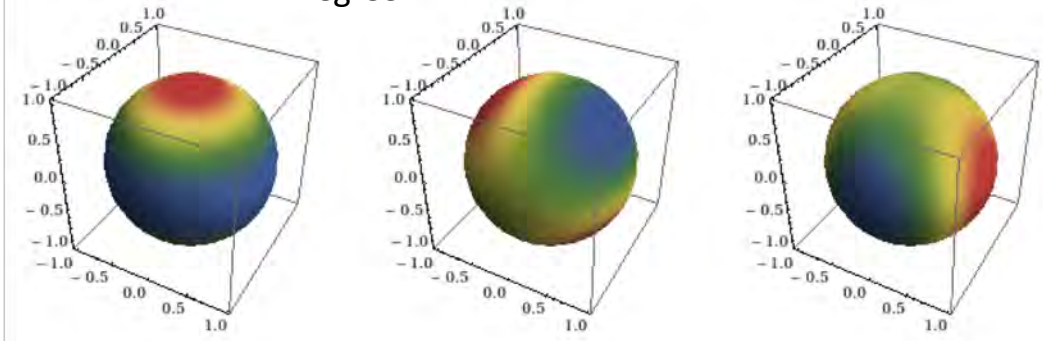

"Degree 2"

Long wavelength geoid: key constraint on mantle viscosity

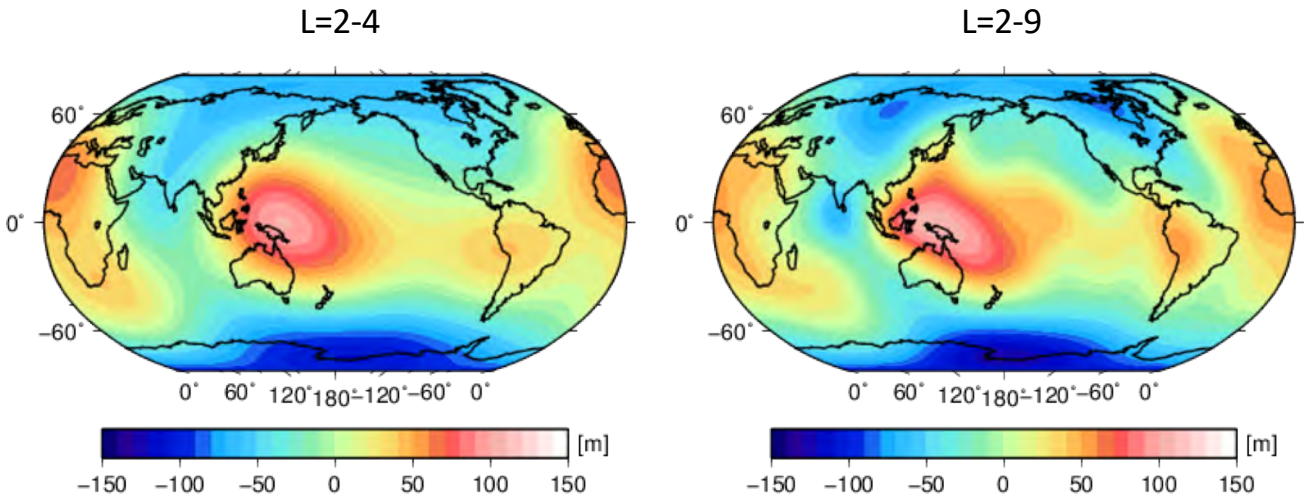

Observed long-wavelength non-hydrostatic geoid

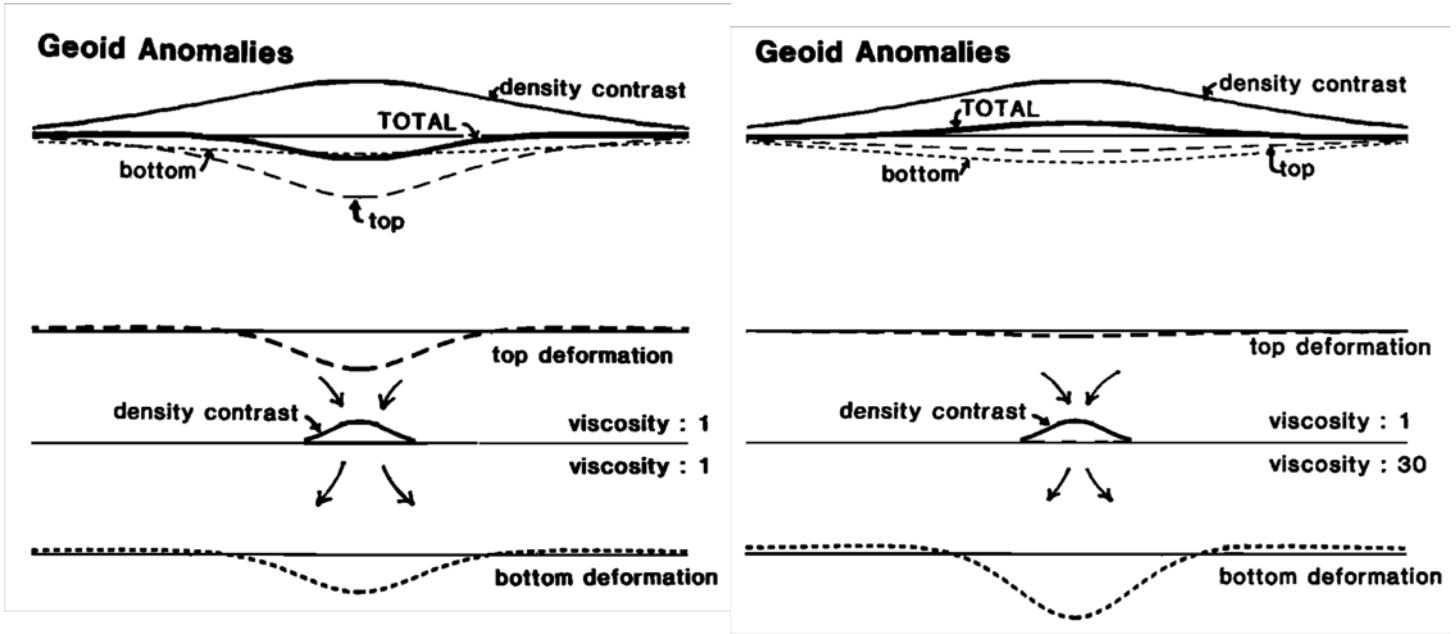

Geoid is sensitive to relative, not absolute, viscosities

From Hager 1984

Predicting geophysical observables using simulations of mantle flow

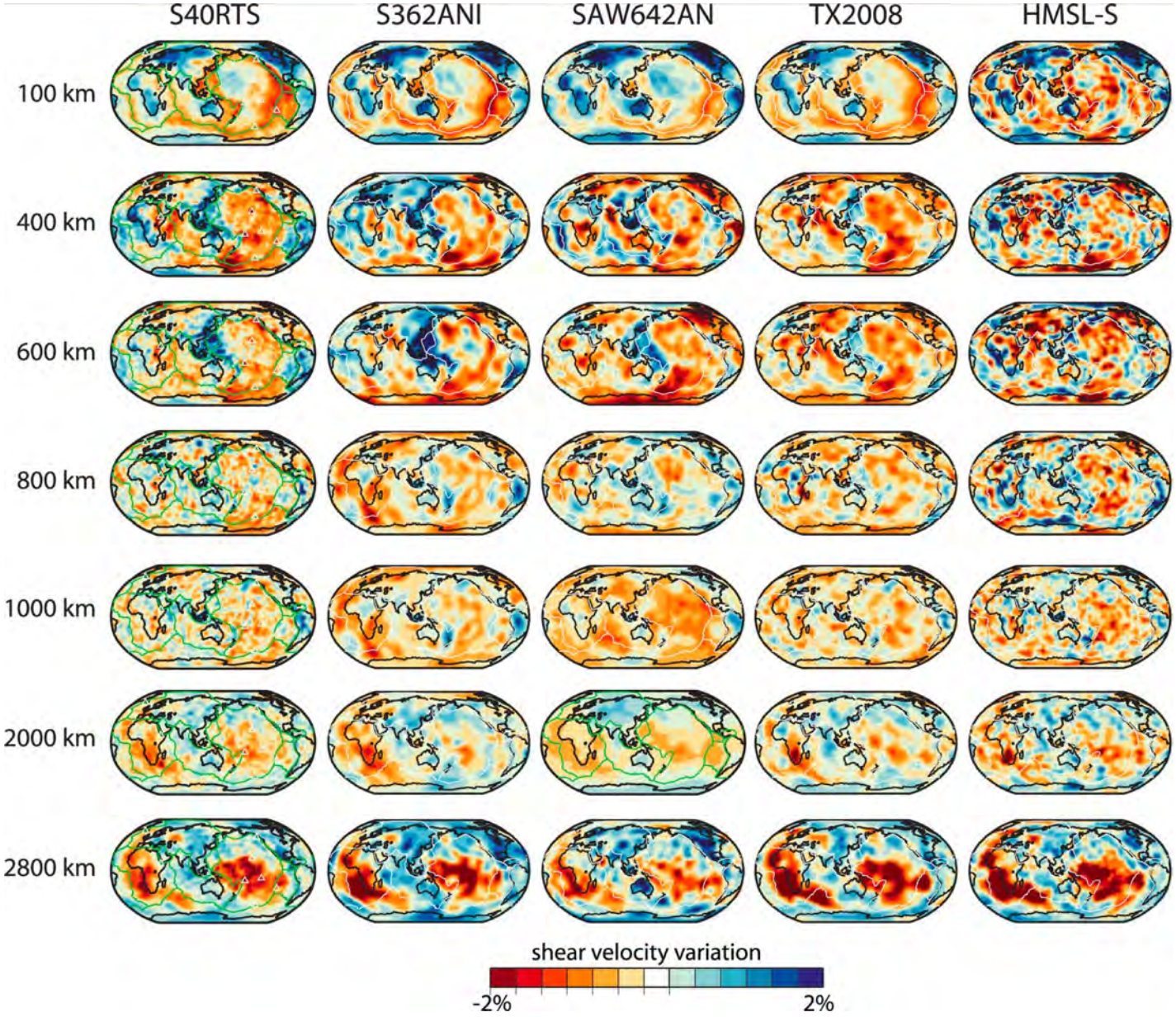

Ritsema et al. 2011

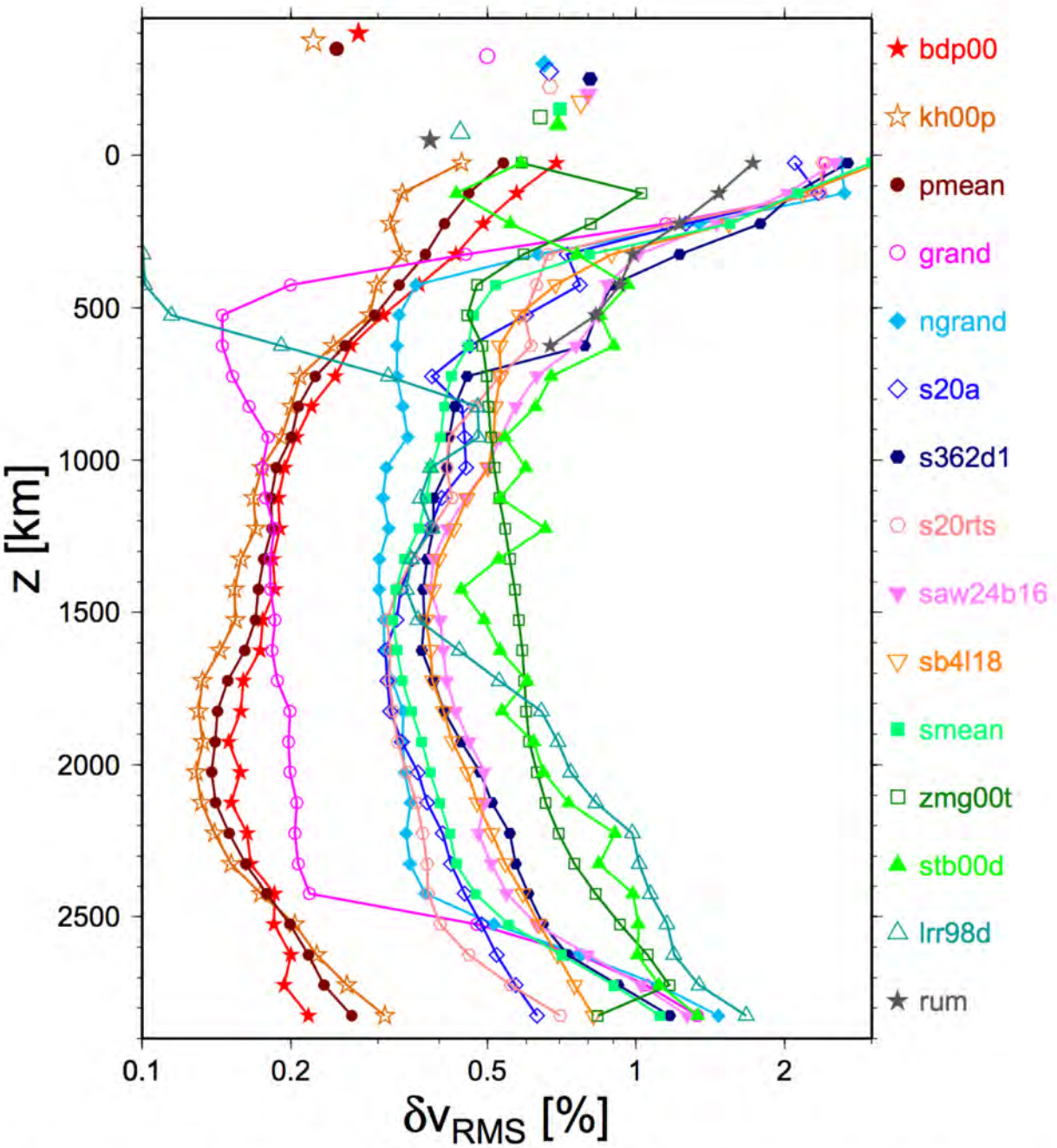

Figure 3. The δv_{RMS} versus z, $\ell_{\max} = 31$. Symbols at $z < 0$ denote depth averaged $\langle \delta v_{\mathrm{RMS}} \rangle$.

Boschi and Becker 2002

Stixrude and Lithgow-Bertelloni, 2011

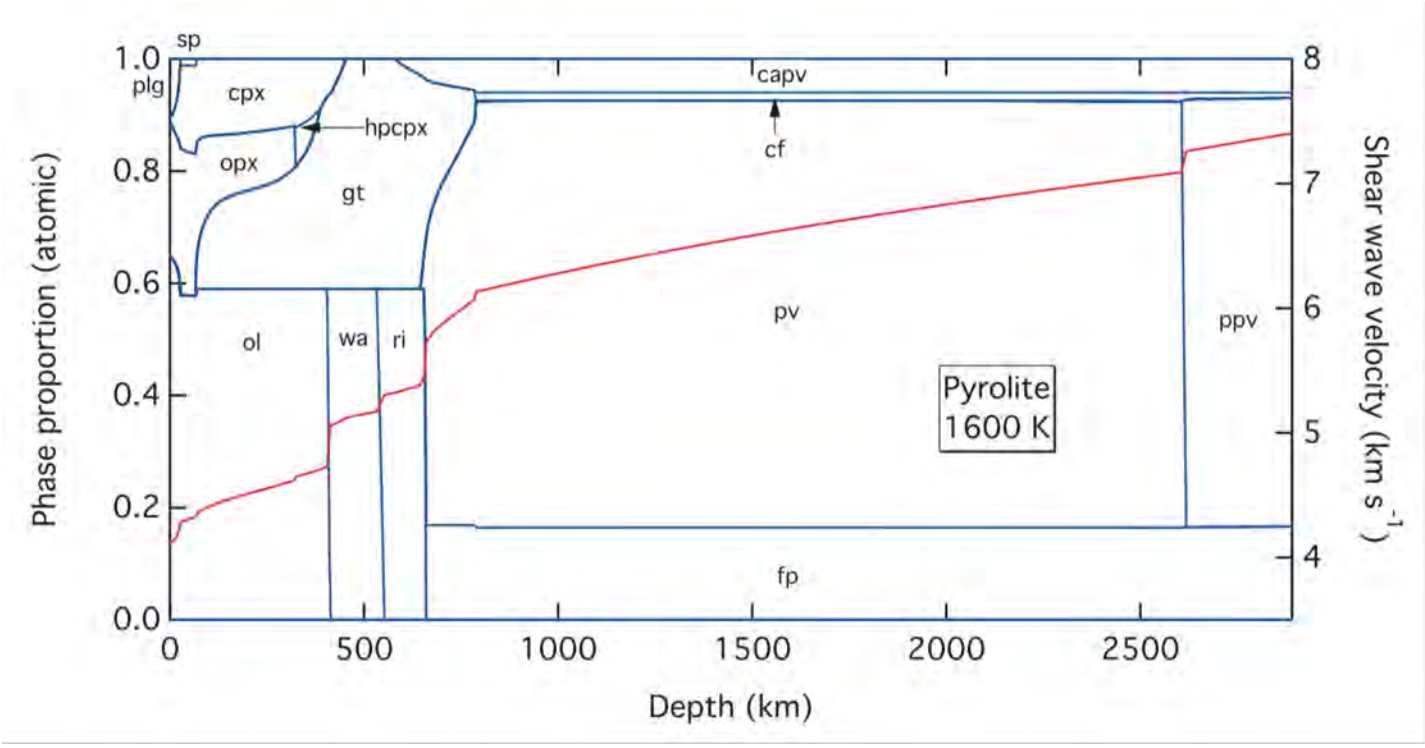

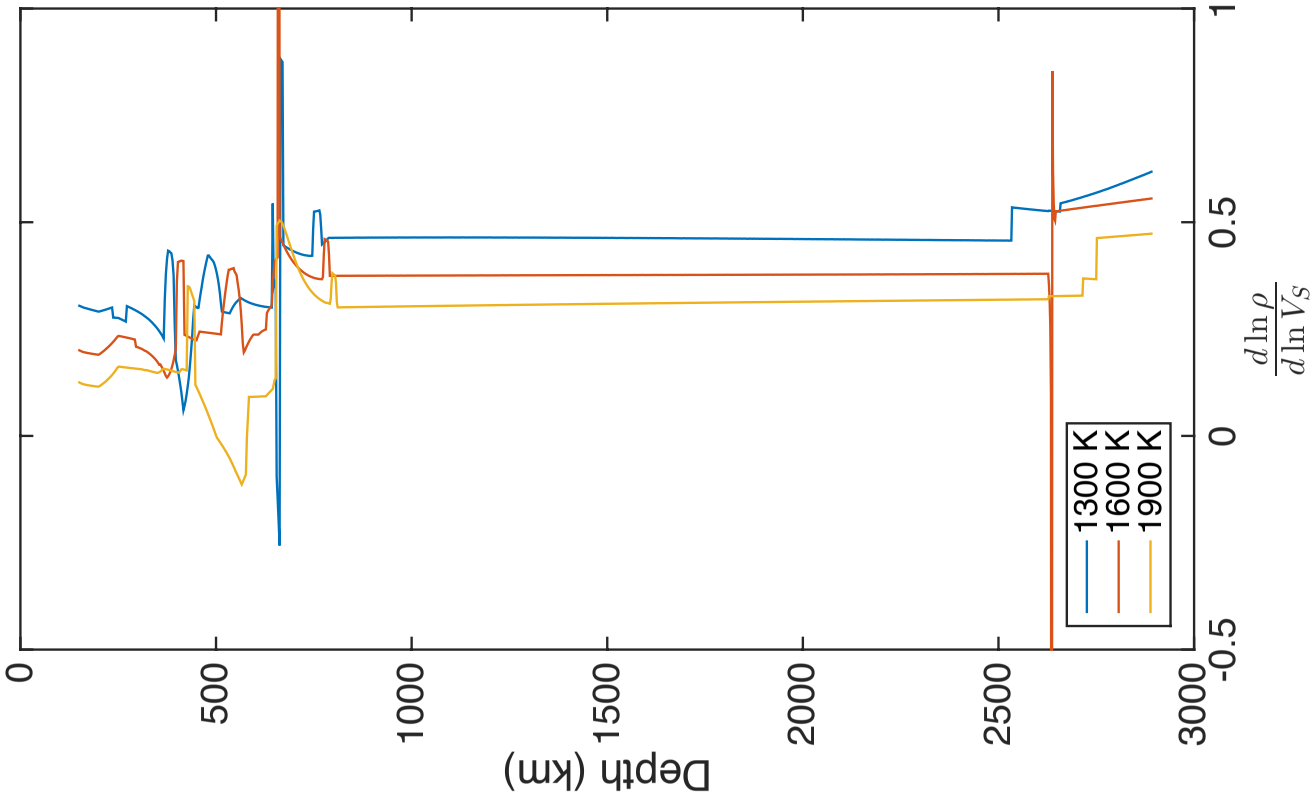

(Mantle flow models are then calculated using propagator matrix technique or finite elements)

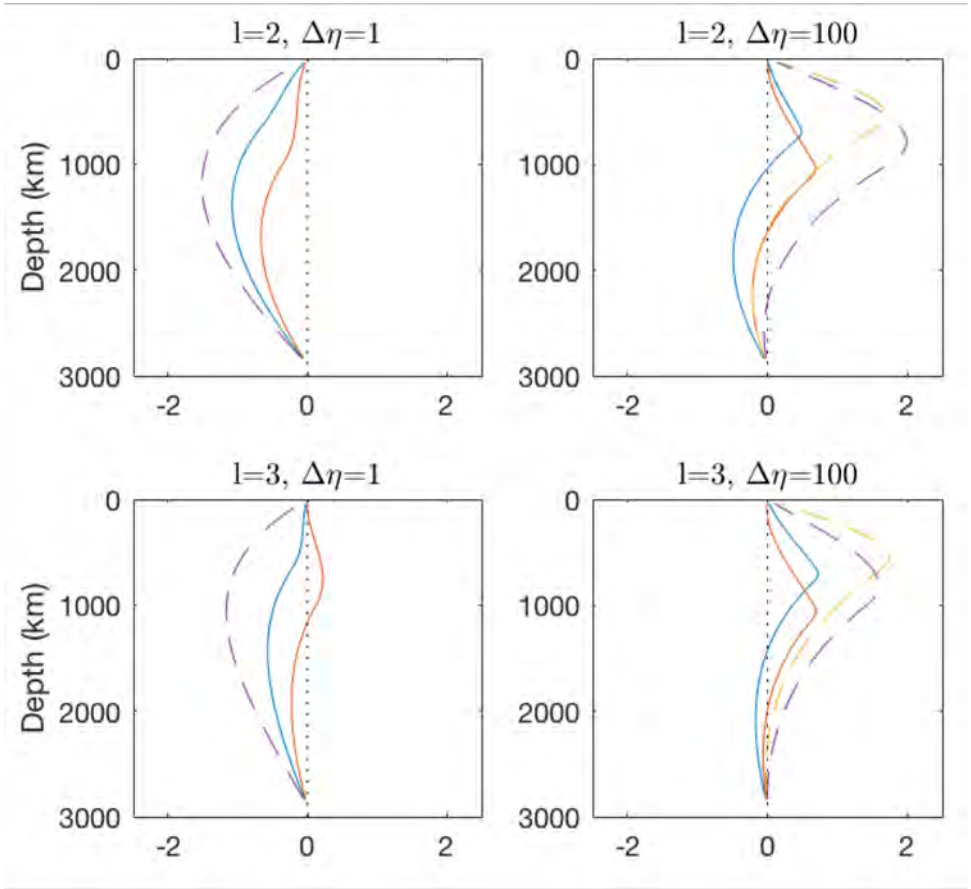

Geoid Kernels tell you a lot, but not ‘the whole story’

Kernel is a non-linear function of the viscosity structure.

We must explore parameter space to find the best kernel, i.e. the kernel that allows you to minimize misfit for a given density structure.

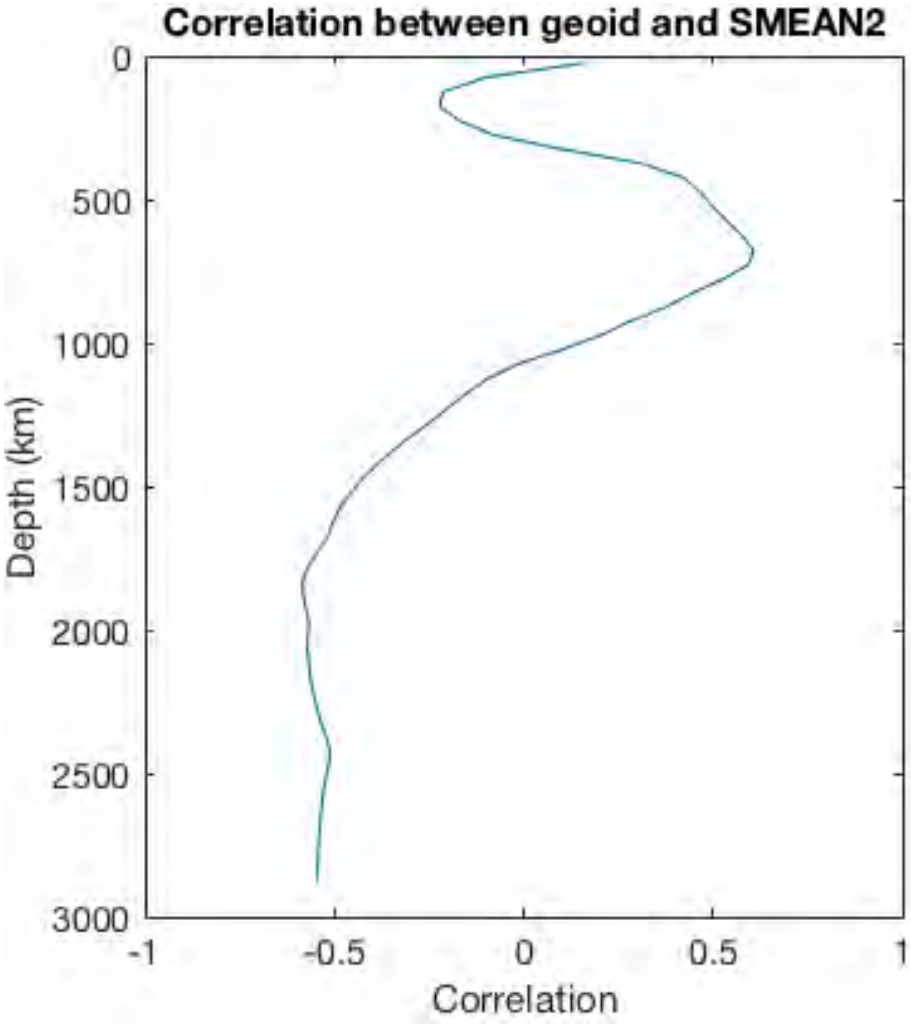
Correlation between geoid and SMEAN2
Depth (km)
0
500
1000
1500
2000
2500
3000
-1
-0.5
0
0.5
1
Correlation

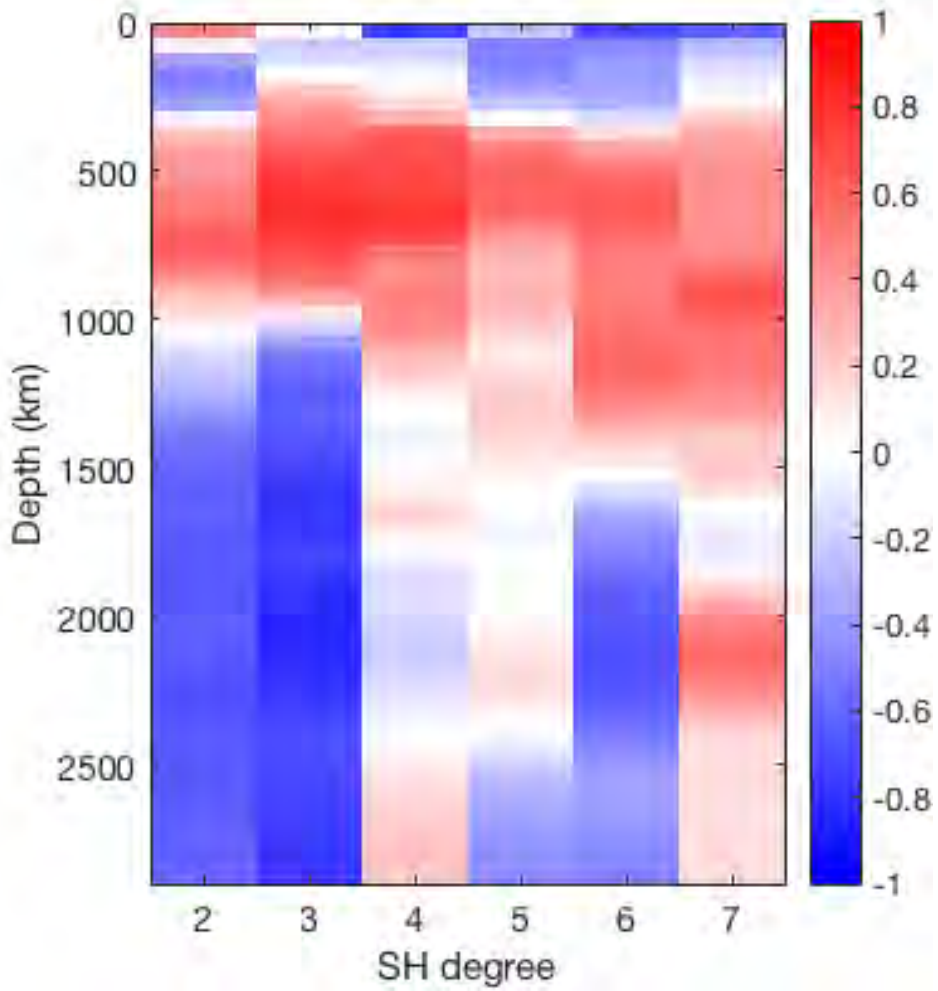
Depth (km)
0
500
1000
1500
2000
2500
2
3
4
5
6
7
SH degree
1
0.8
0.6
0.4
0.2
0
-0.2
-0.4
-0.6
-0.8
-1

Observed geoid

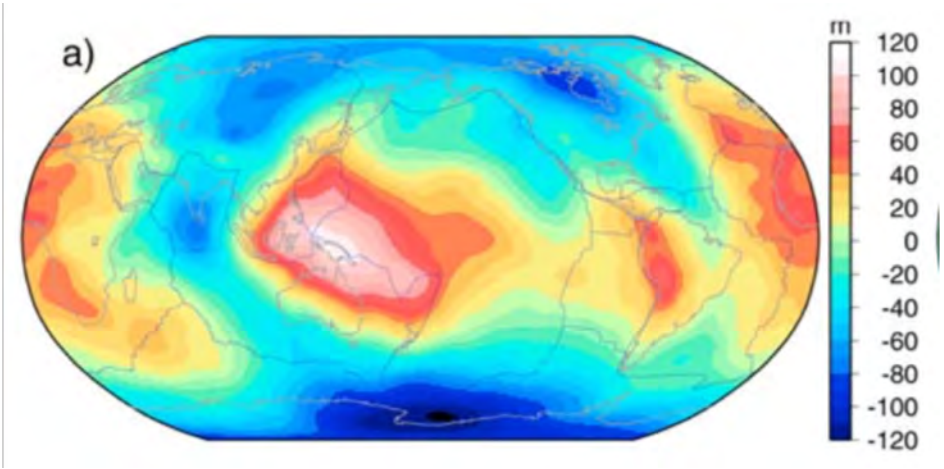

No LVVs

With LVVs

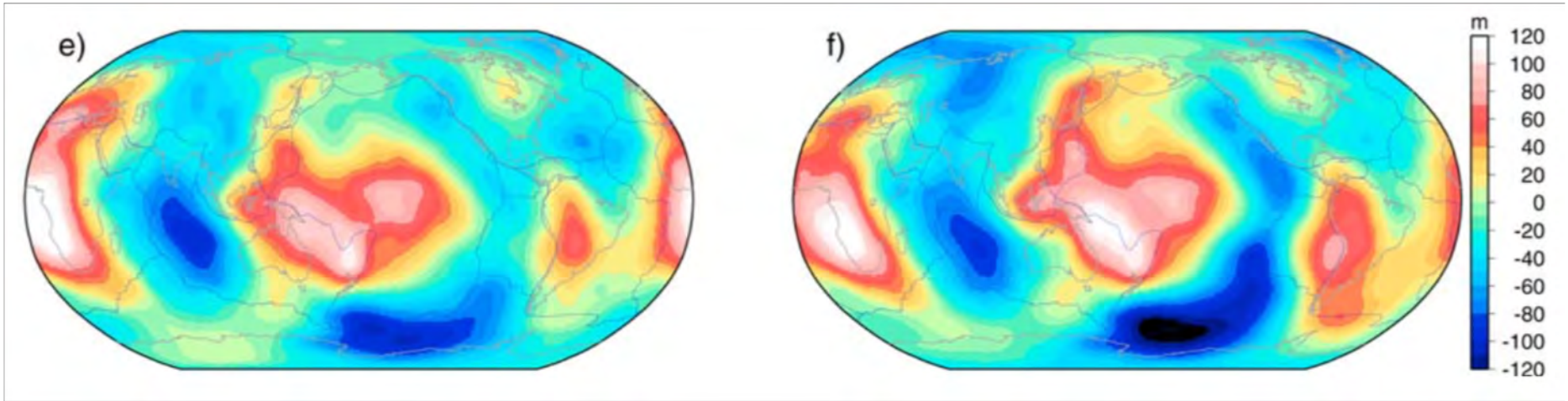

Ghosh et al. 2006

Transdimensional Inversion

Example: Find the optimal representation of some data using piecewise linear functions.

The number of discontinuities is not known *a priori*

Noise is added to the data

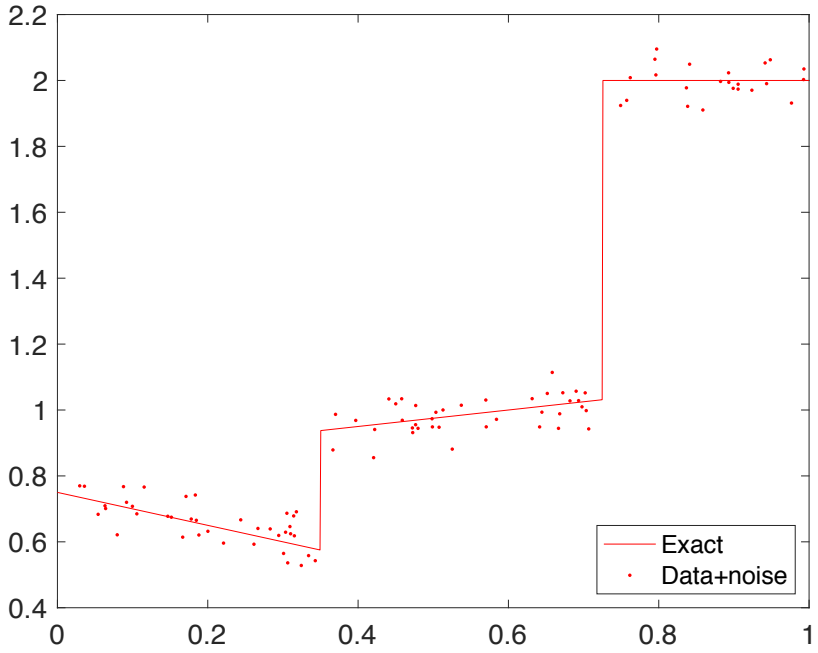

$$P(D|G) = \frac{1}{\sqrt{(2\pi)^{n_{lm}}|C_D|}} \exp\left(-\frac{\Phi(G)}{2}\right)$$

$$\Phi(G) = \underline{R}^T \underline{\underline{C}}_D^{-1} \underline{R}$$

Accept new model with k' parameters over old with k parameters
With probability:

$$min\left(1, \frac{P(D|G')}{P(D|G)} \frac{k+1}{k'+1}\right)$$

Transdimensional Inversion

Example: Find the optimal representation of some data using piecewise linear functions.

The number of discontinuities/cells is not known *a priori*

Noise is added to the data

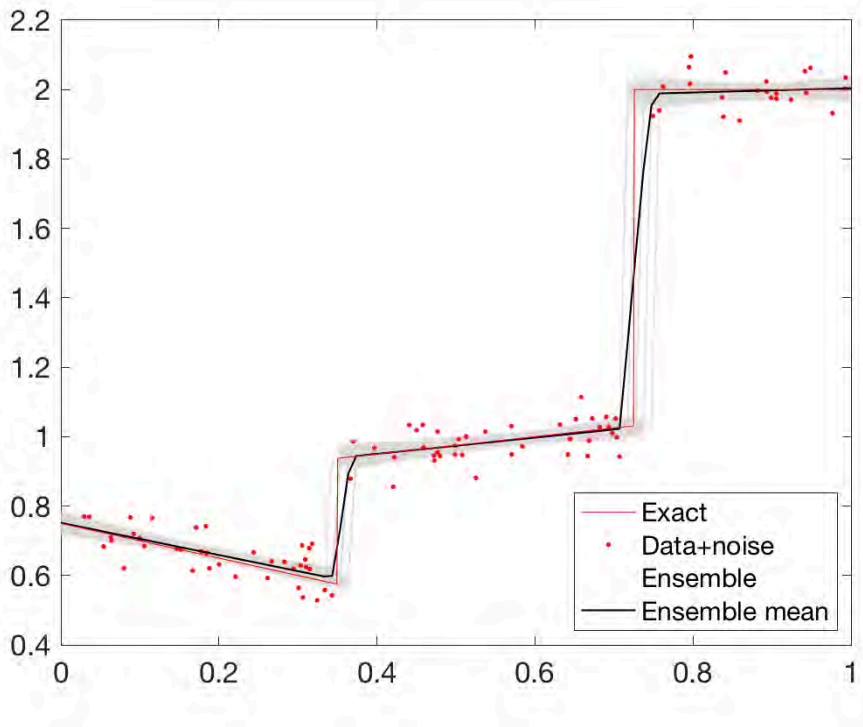

$$P(D|G) = \frac{1}{\sqrt{(2\pi)^{n_{lm}}|C_D|}} \exp\left(-\frac{\Phi(G)}{2}\right)$$

$$\Phi(G) = \underline{R}^T \underline{\underline{C}}_D^{-1} \underline{R}$$

Accept new model with k' parameters over old with k
With probability:

$$min\left(1, \frac{P(D|G')}{P(D|G)} \frac{k+1}{k'+1}\right)$$

Penalizes over-parameterization

Transdimensional Hierarchical Inversion

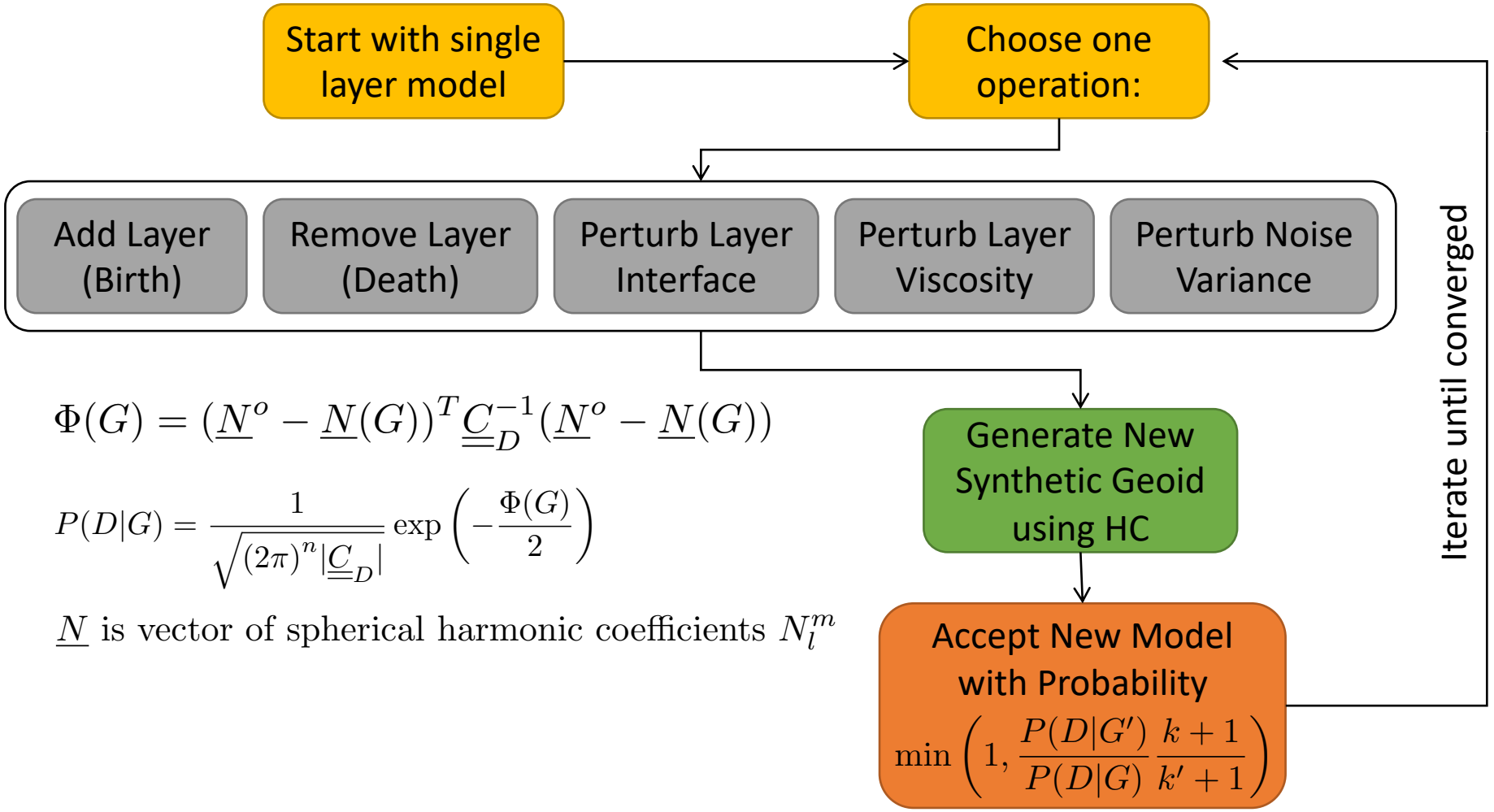

(Similar to Kolb and Lekic, 2013)

Transdimensional Inversion

Example: Find the optimal representation of some data using piecewise linear functions.

The number of discontinuities is not known *a priori*

Noise is added to the data

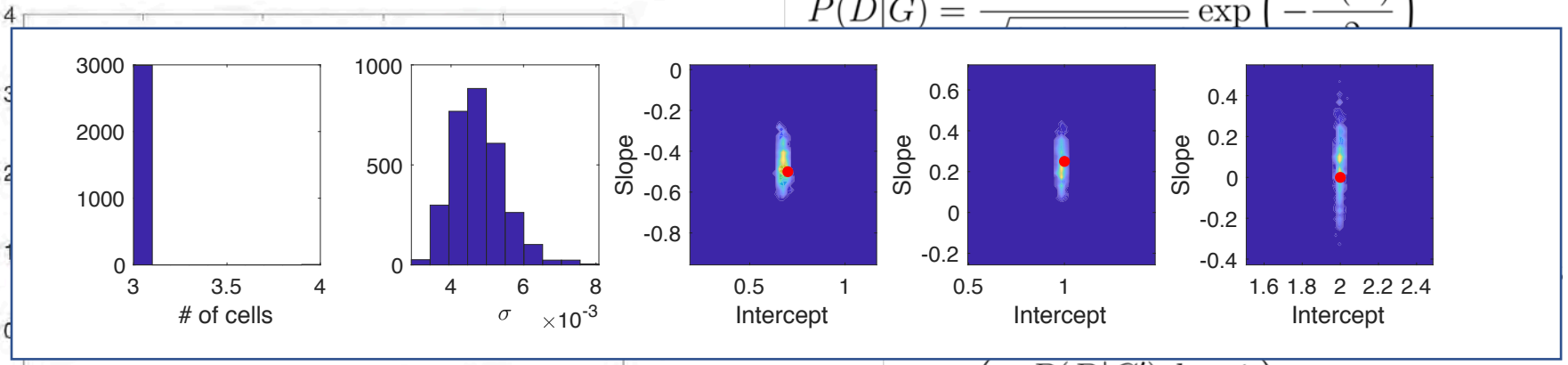

$$P(D|G) = \frac{1}{\qquad} \exp\left(-\frac{\Phi(G)}{\qquad}\right)$$

$$min\left(1, \frac{P(D|G')}{P(D|G)} \frac{k+1}{k'+1}\right)$$

Penalizes over-parameterization

Viscosity profiles and 95% confidence intervals

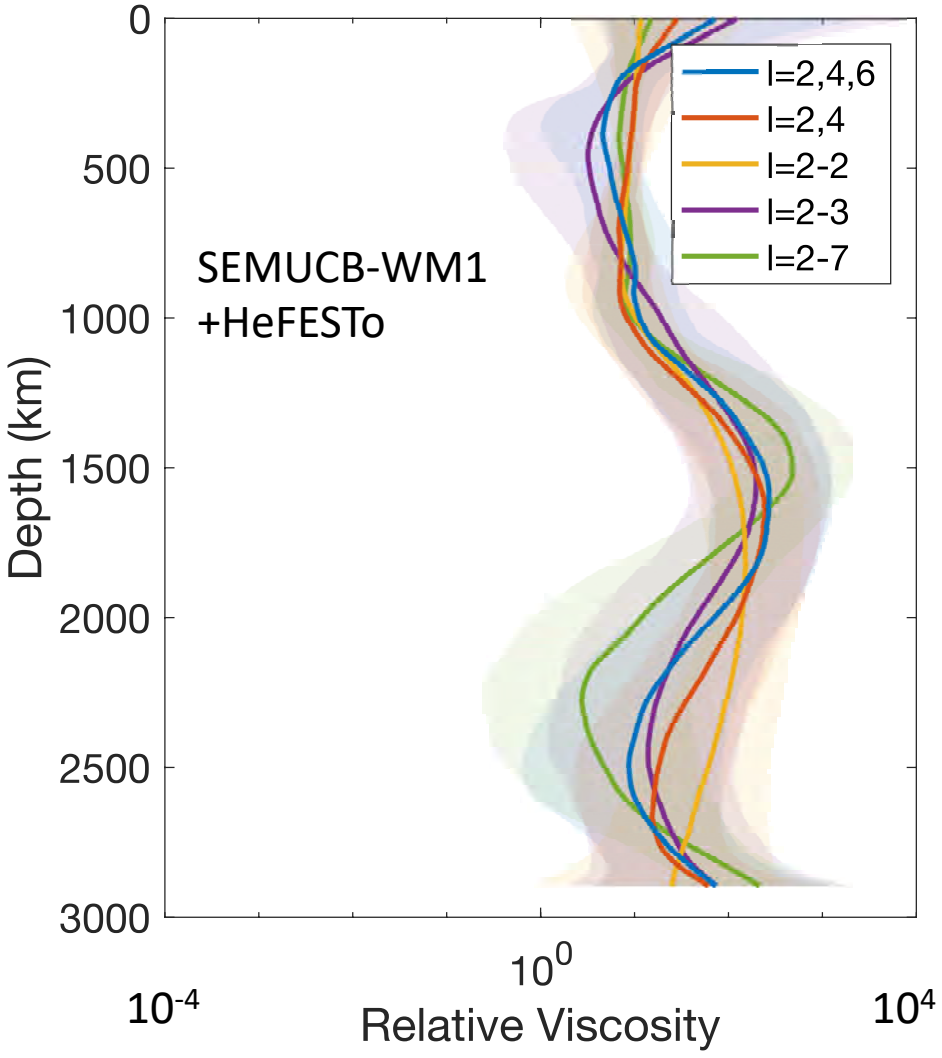

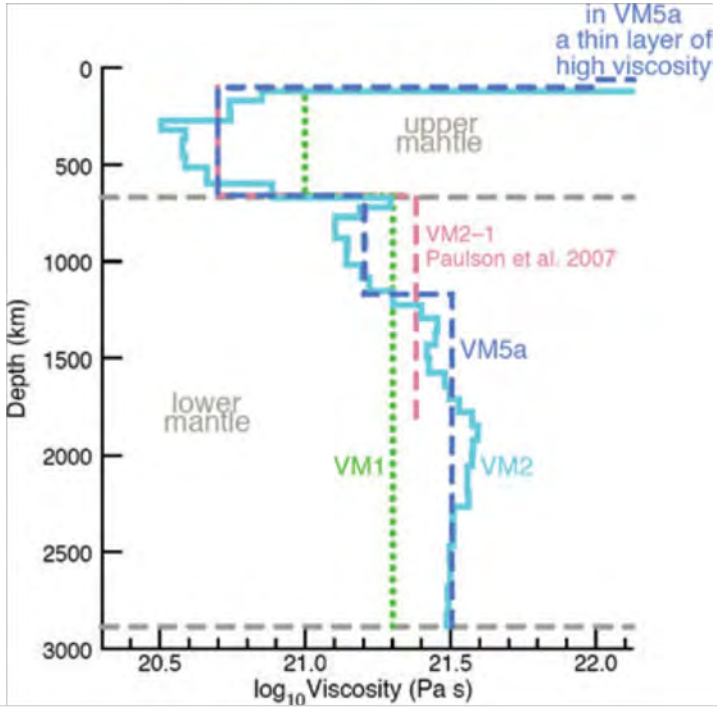

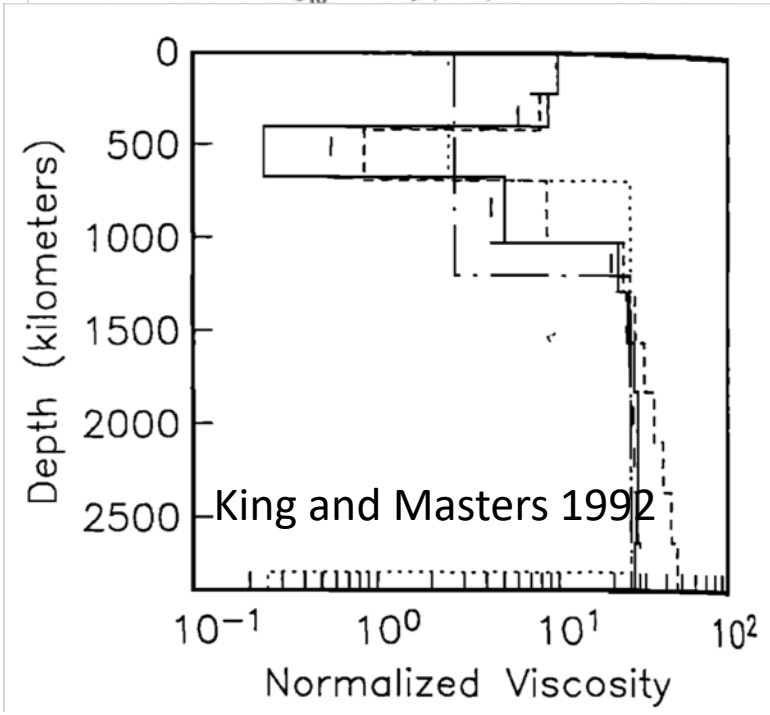

Changes in radial correlation / vertical coherence

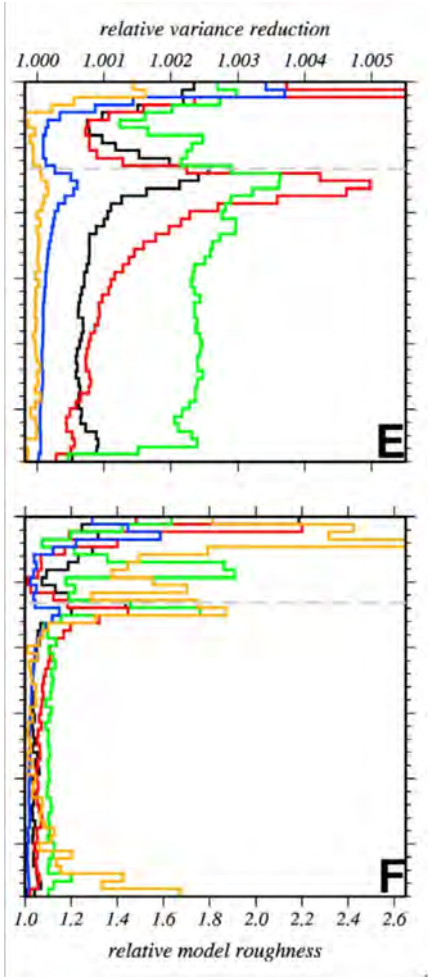

Boschi and Becker 2011

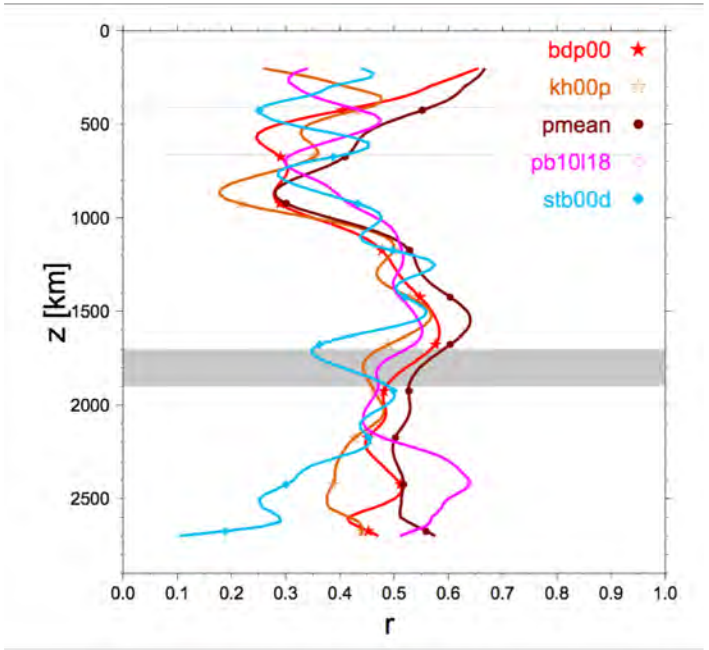

Boschi and Becker 2002

Seismic scatterers in the shallow lower mantle

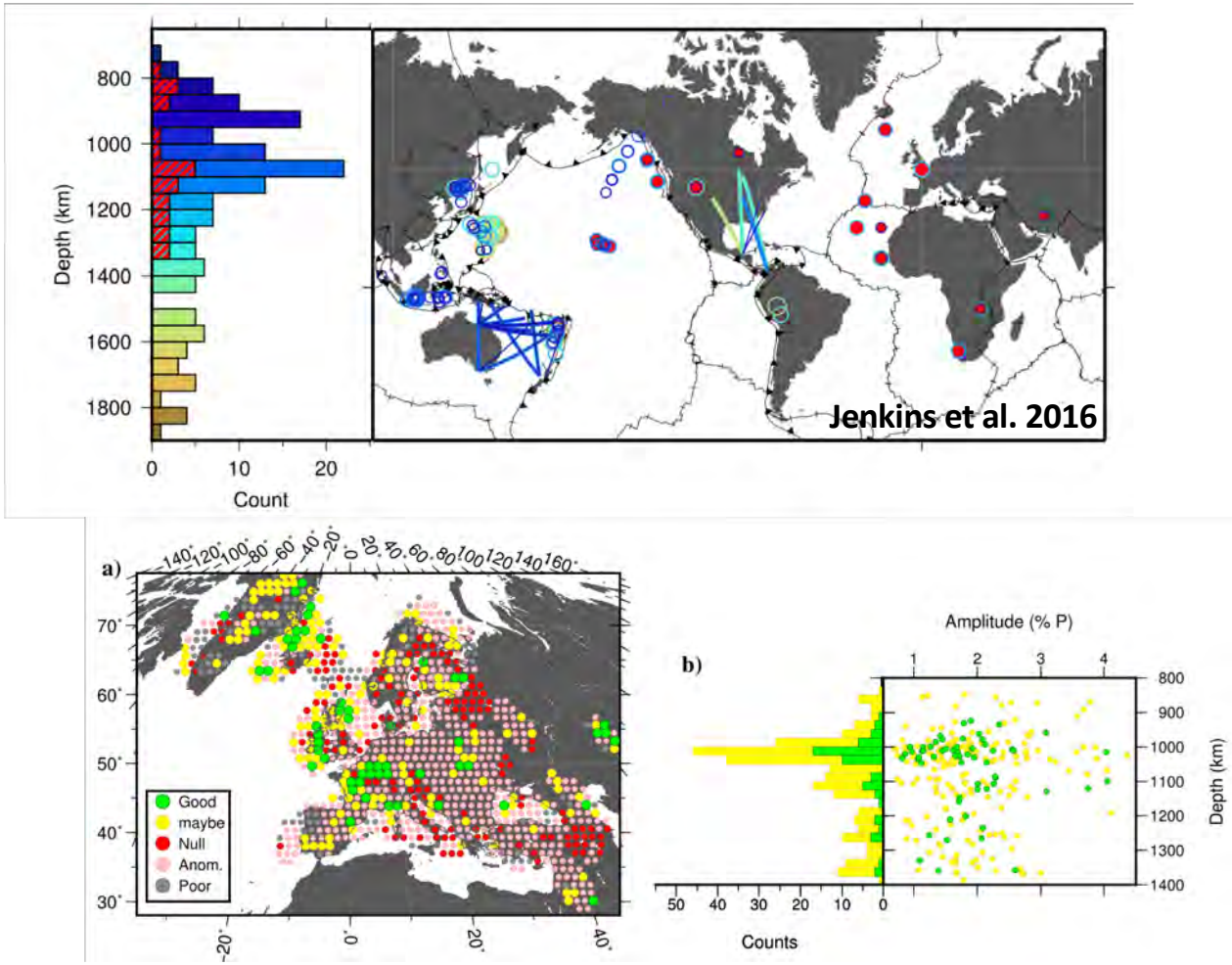

Changes in radial correlation / vertical coherence

$$R_\beta(r,r') = \frac{1}{4\pi\sigma_\beta(r)\sigma_\beta(r')}\int_{S_1}\delta\beta(r,\Omega)\delta\beta(r',\Omega)d\Omega$$

(Jordan et al. 1993)

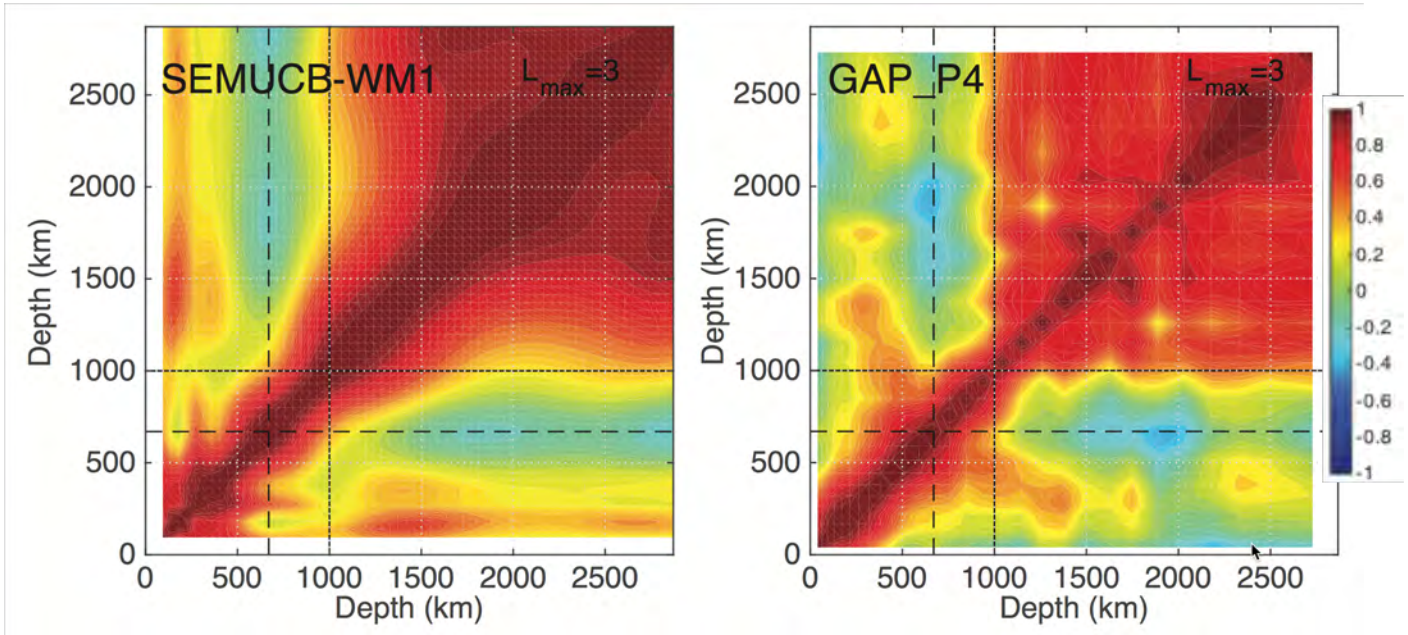

Very long wavelength radial correlation

Slab stagnation below the transition zone

Tonga and Kermadec

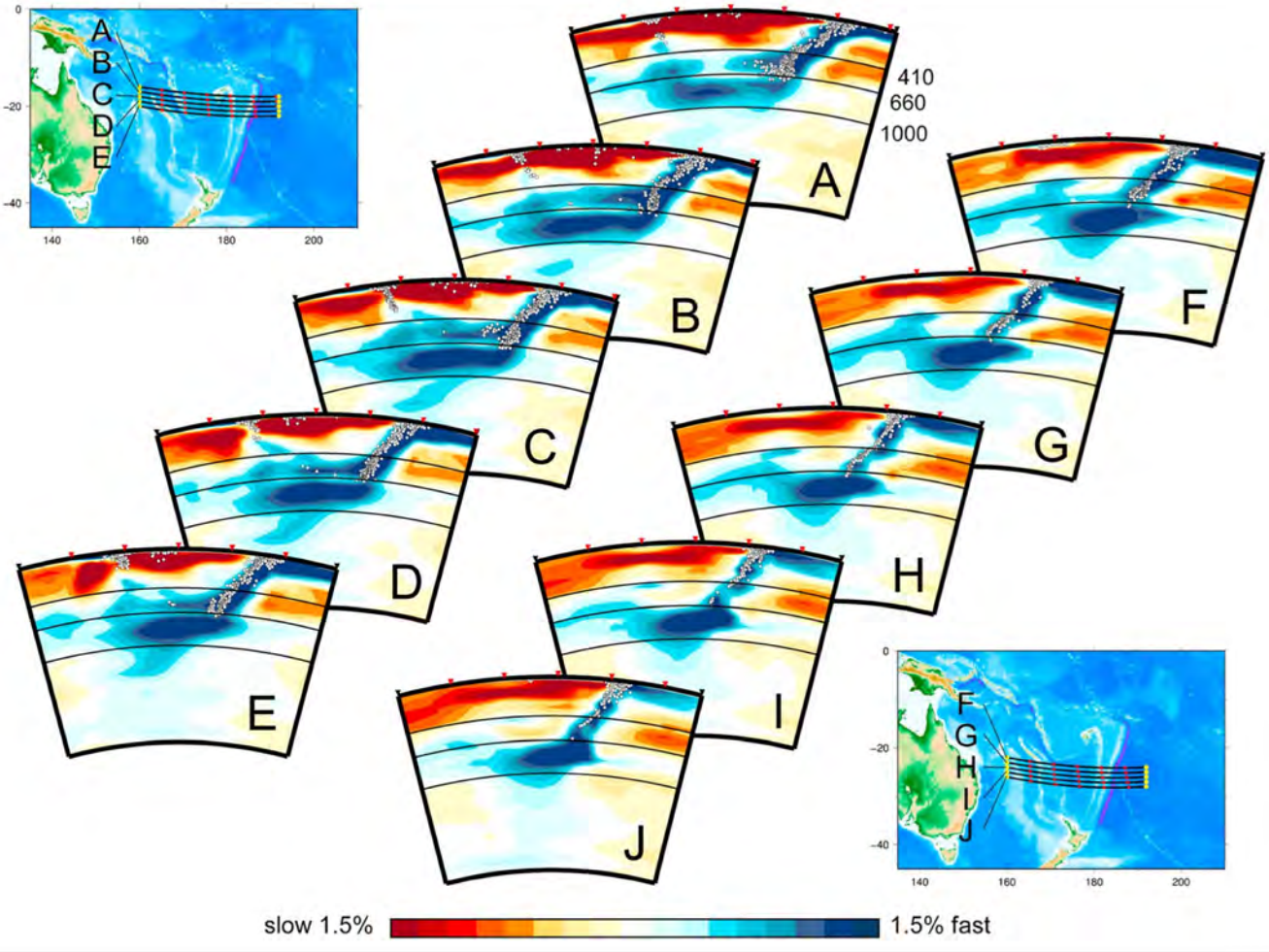

(not ubiquitous)

Central American Arc

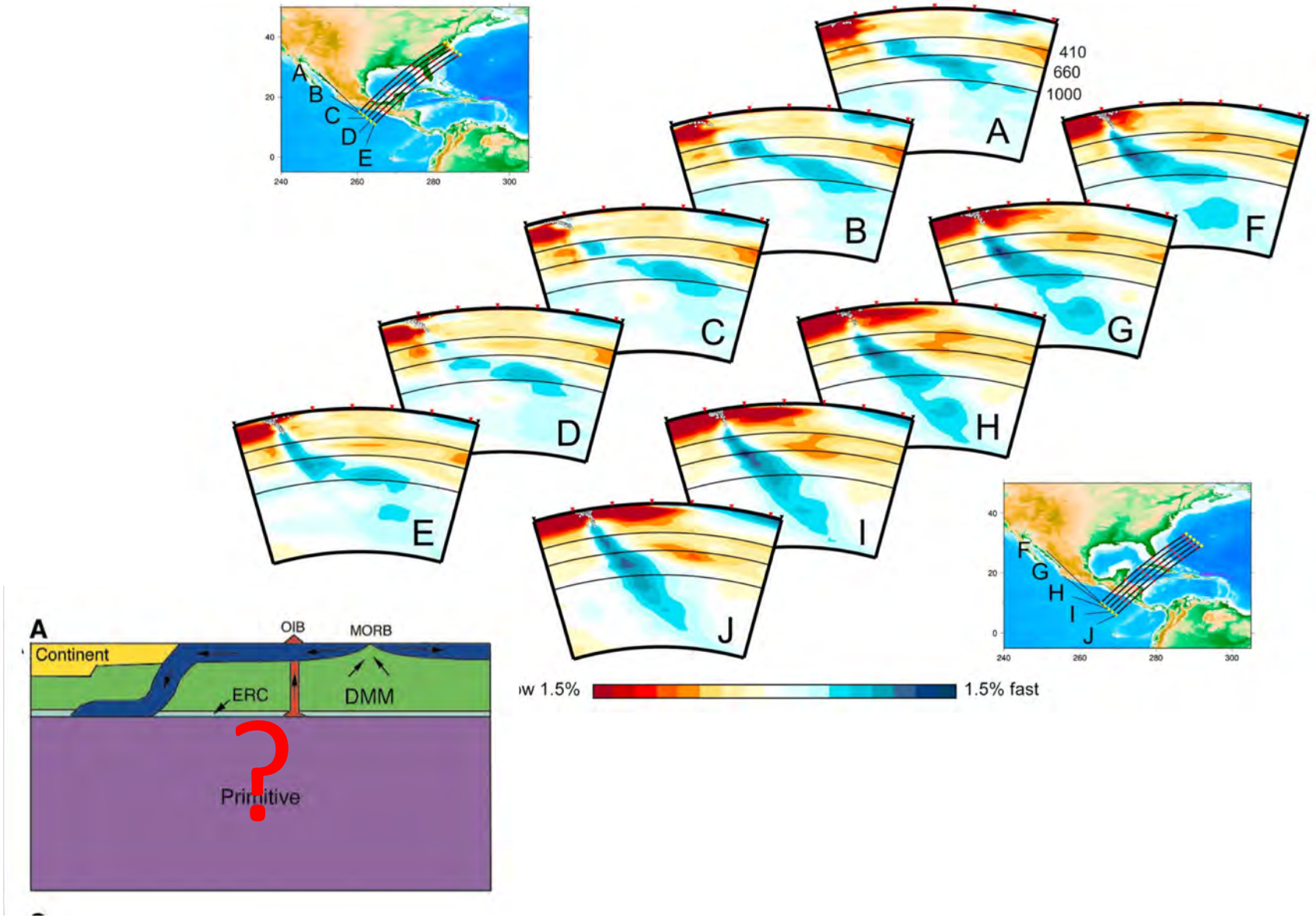

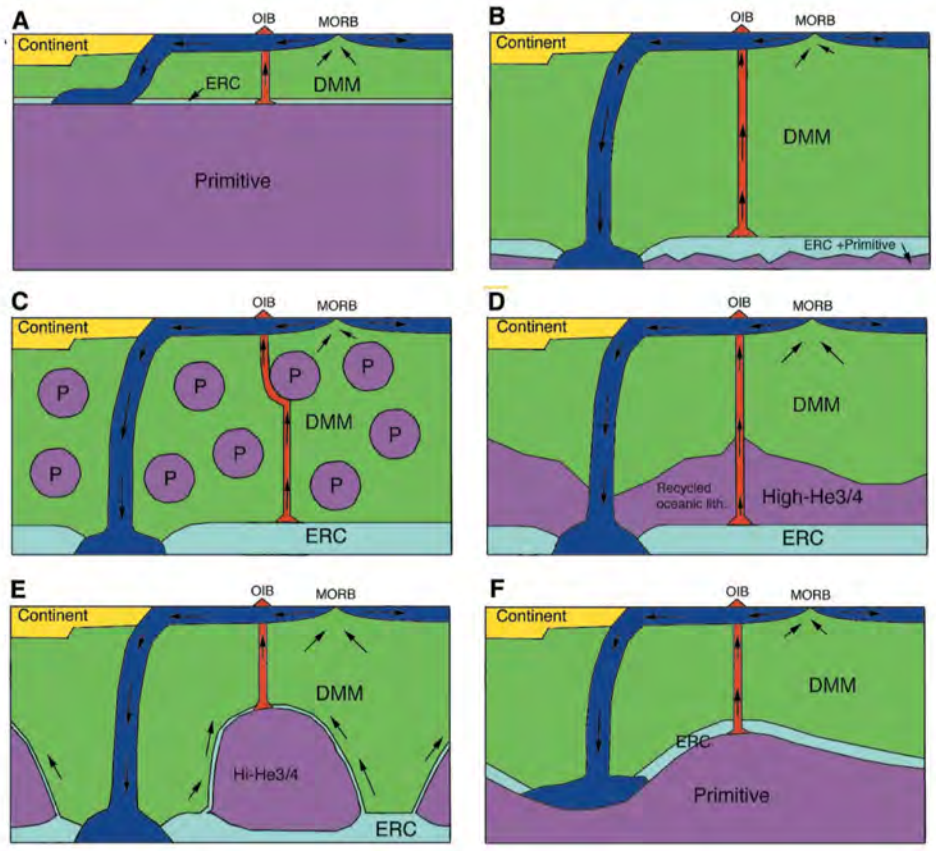

How do variations in viscosity affect mixing?

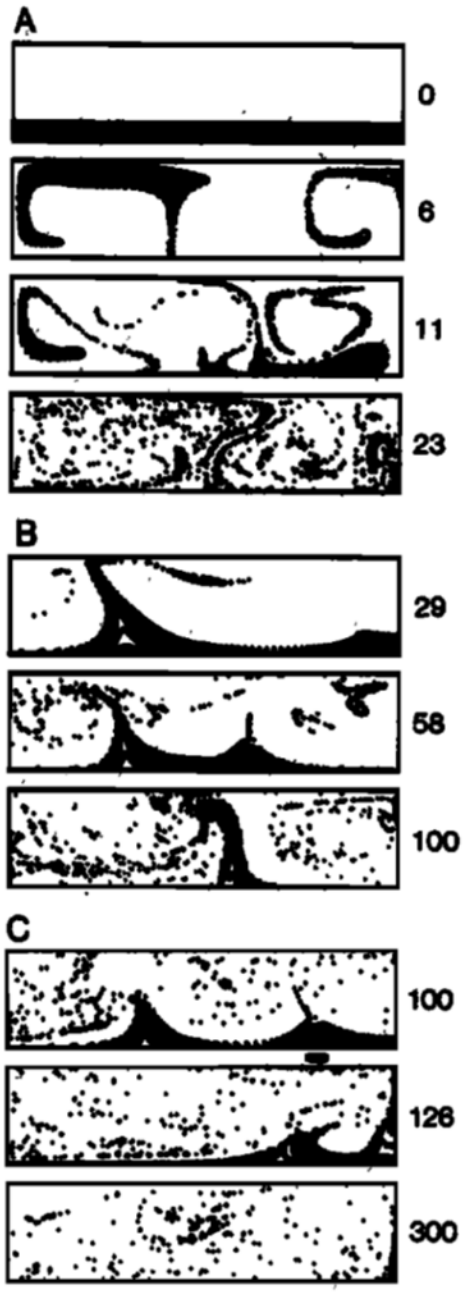

Fig. 2. Positions of tracers at different instants in the model runs A. Case 1 β=0, B. Case 3 β=2.5 and C. Case 4 β=3.5.

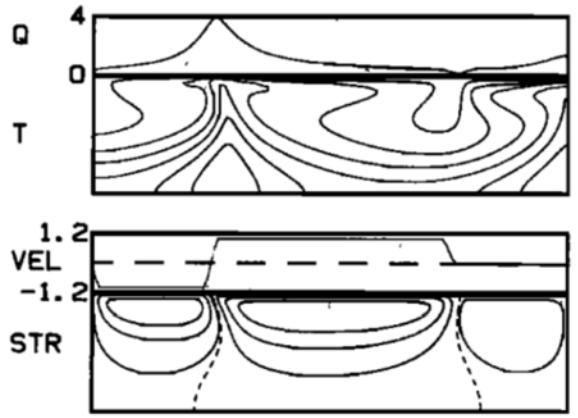

Fig. 1. Initial state for Case 4, with Ra=5×10^6, Pe=700, β=3.5. Q is the top surface heat flux, T are the isotherms, VEL is the imposed top velocity (positive to the right), and STR are the stream lines.

$$\eta' = \frac{\eta}{\eta_o} 10^{\beta(1-y')}$$

Gurnis and Davies 1986

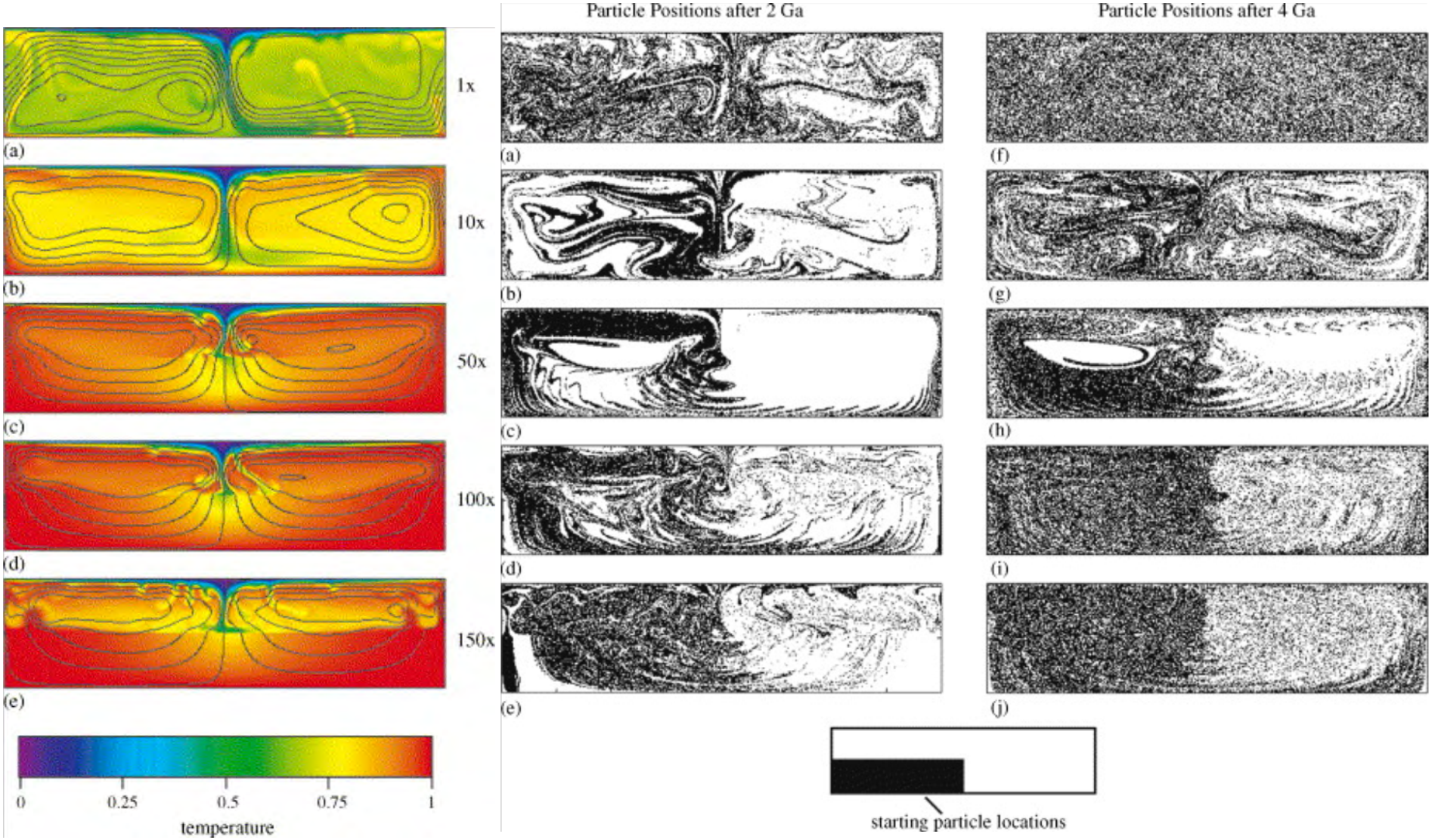

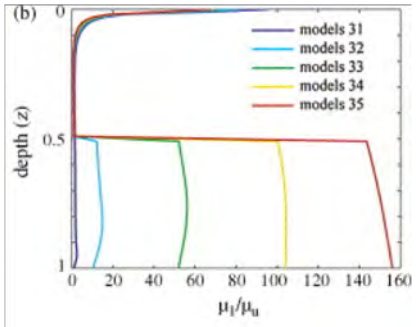

Naliboff and Kellogg 2007

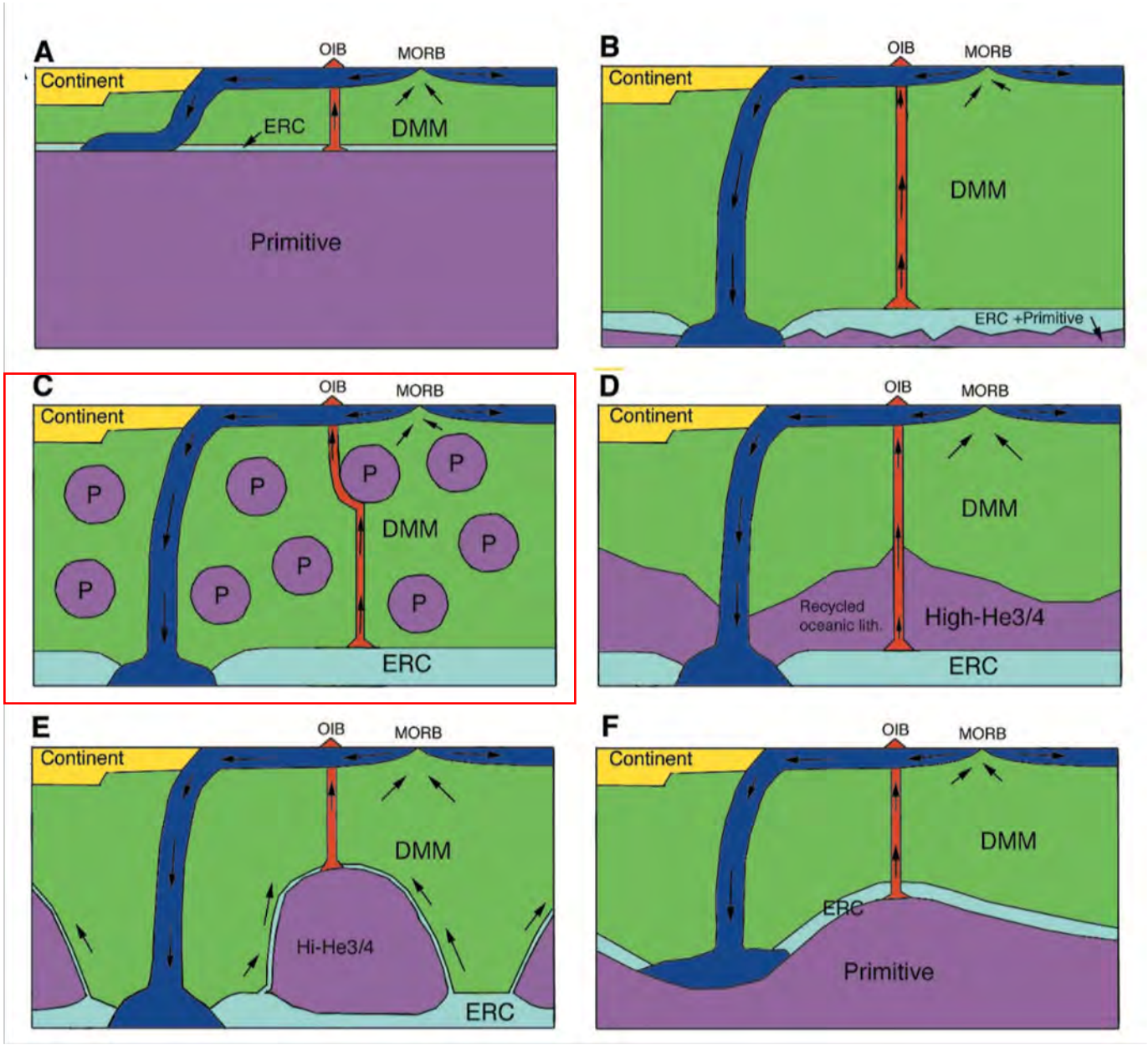

Primitive Blobs

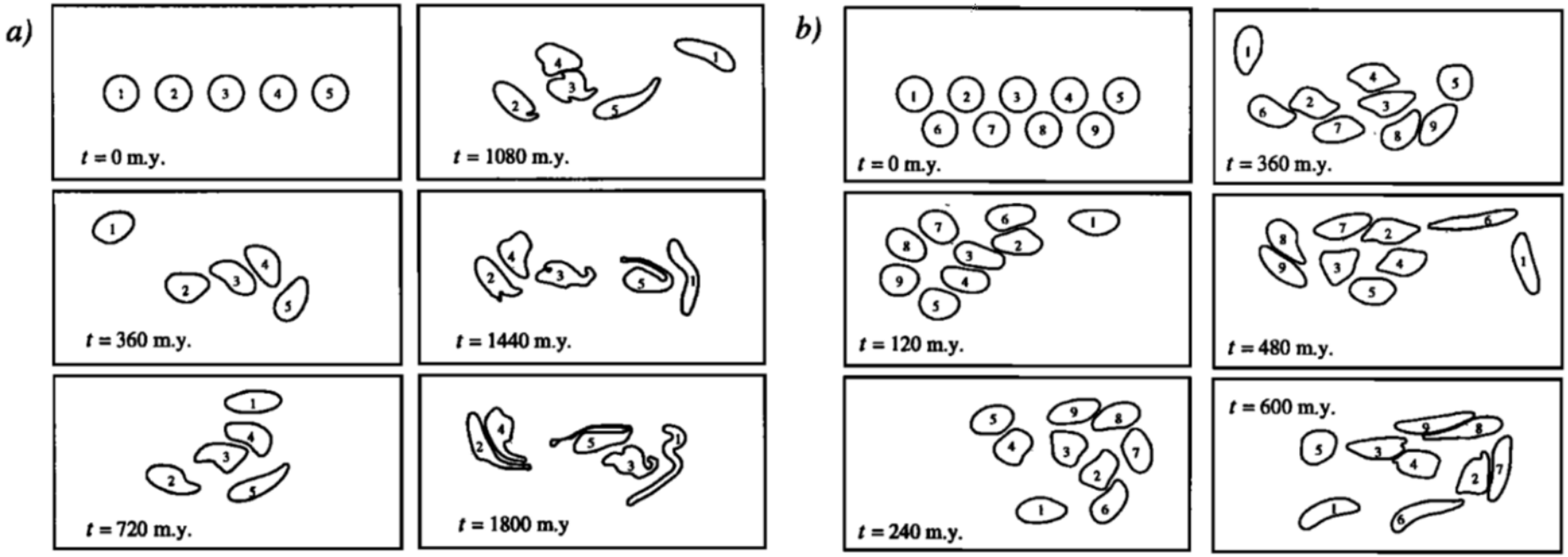

Figure 4. Stretching of blobs in simulations with *a)* five and *b)* nine blobs for $\lambda = 10$. Times are based on a mantle thickness of 3000 km and a plate velocity of 10 cm/year.

Manga (1996)

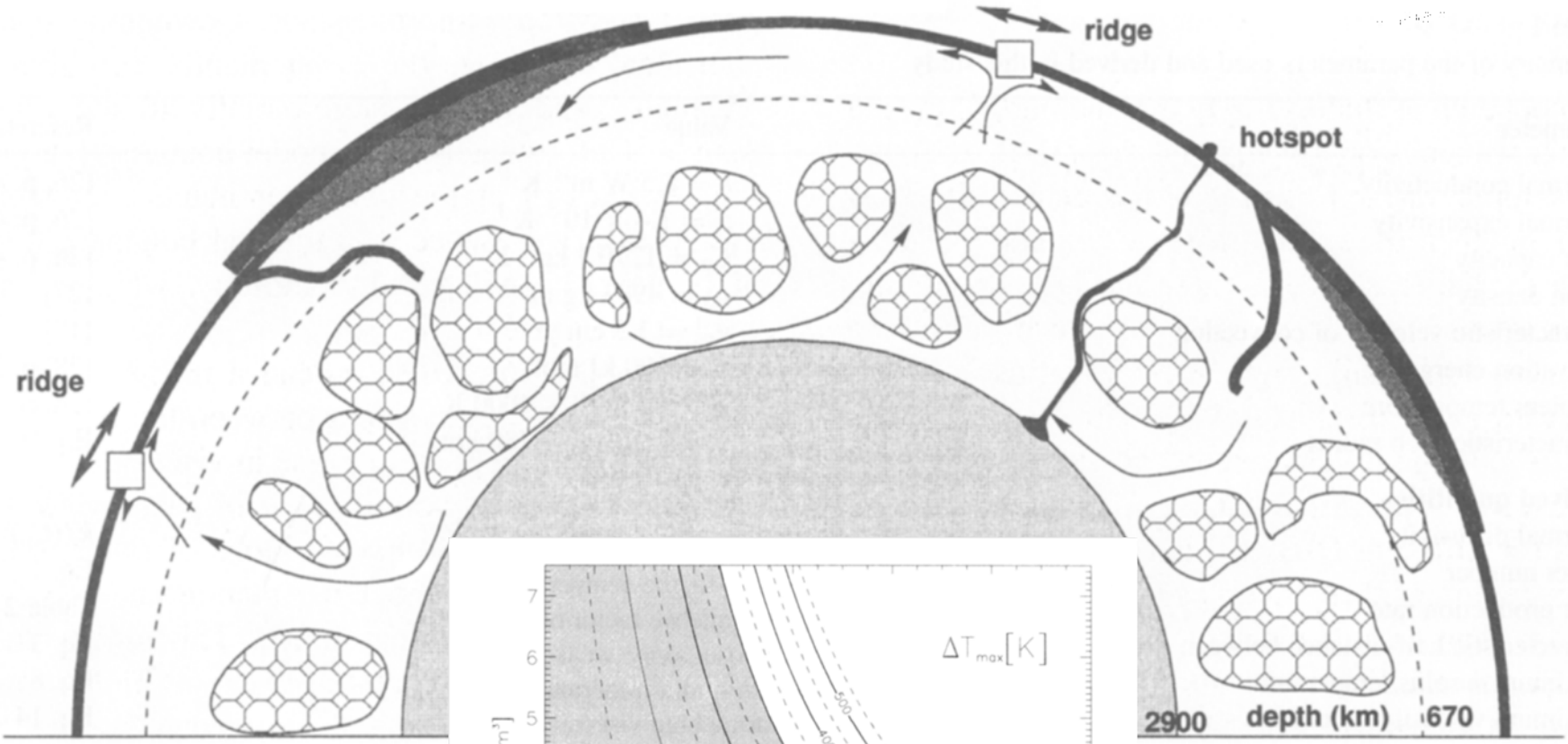

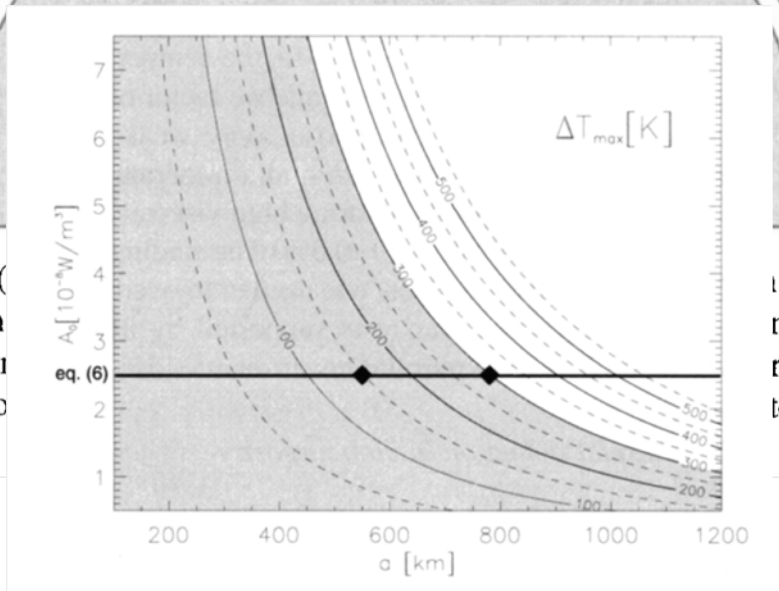

Fig. 1. The blob model of convection (the whole mantle mode with varying morphology of slab penetration through n the cores of the convective cells and represent the primitive reservoir. Surrou re depleted and degassed by melting at the ridges and earlier continent-formatio terial and lead to a heterogeneous OIB isotope source.

Becker et al. 1999

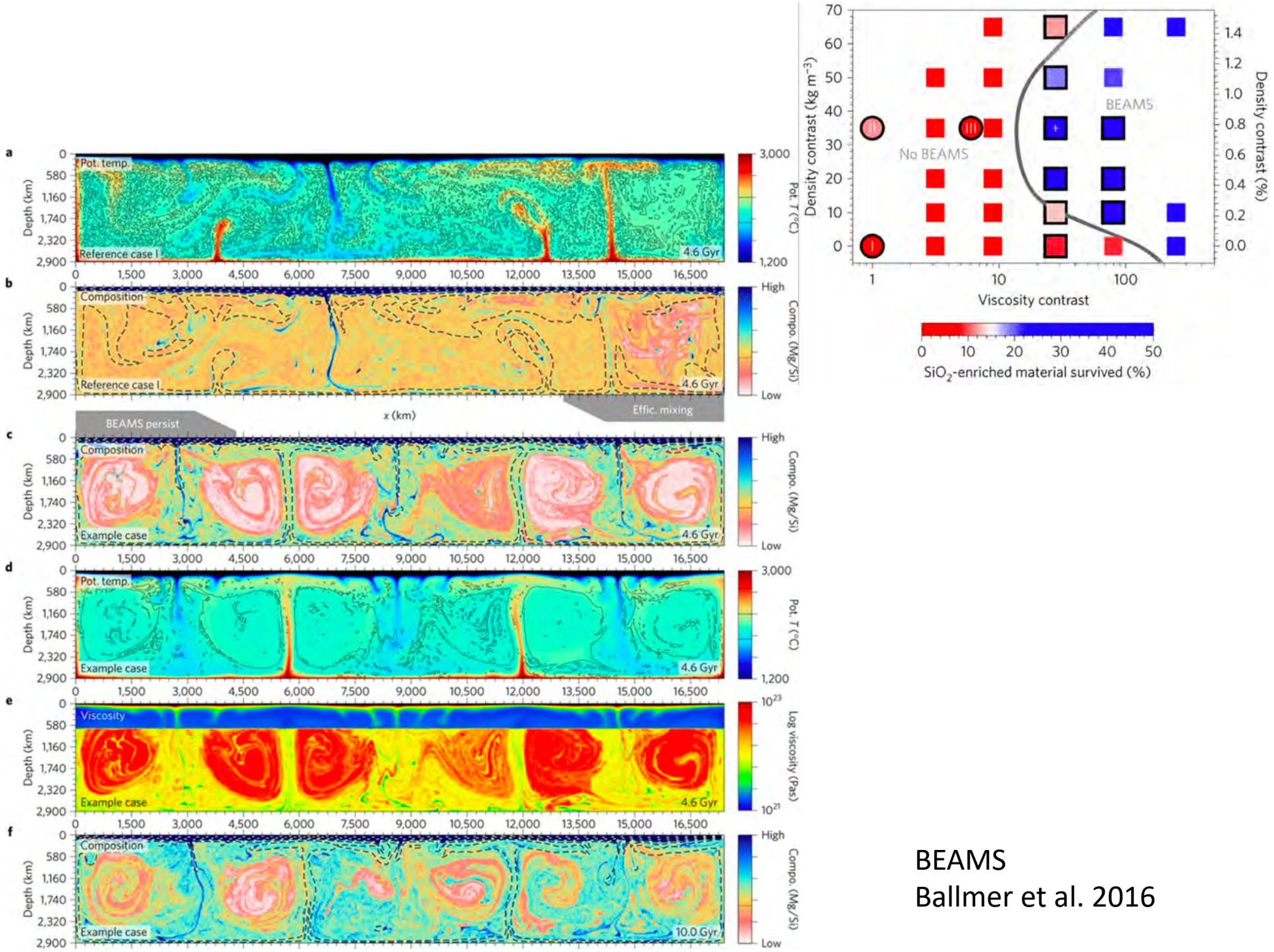

BEAMS
Ballmer et al. 2016

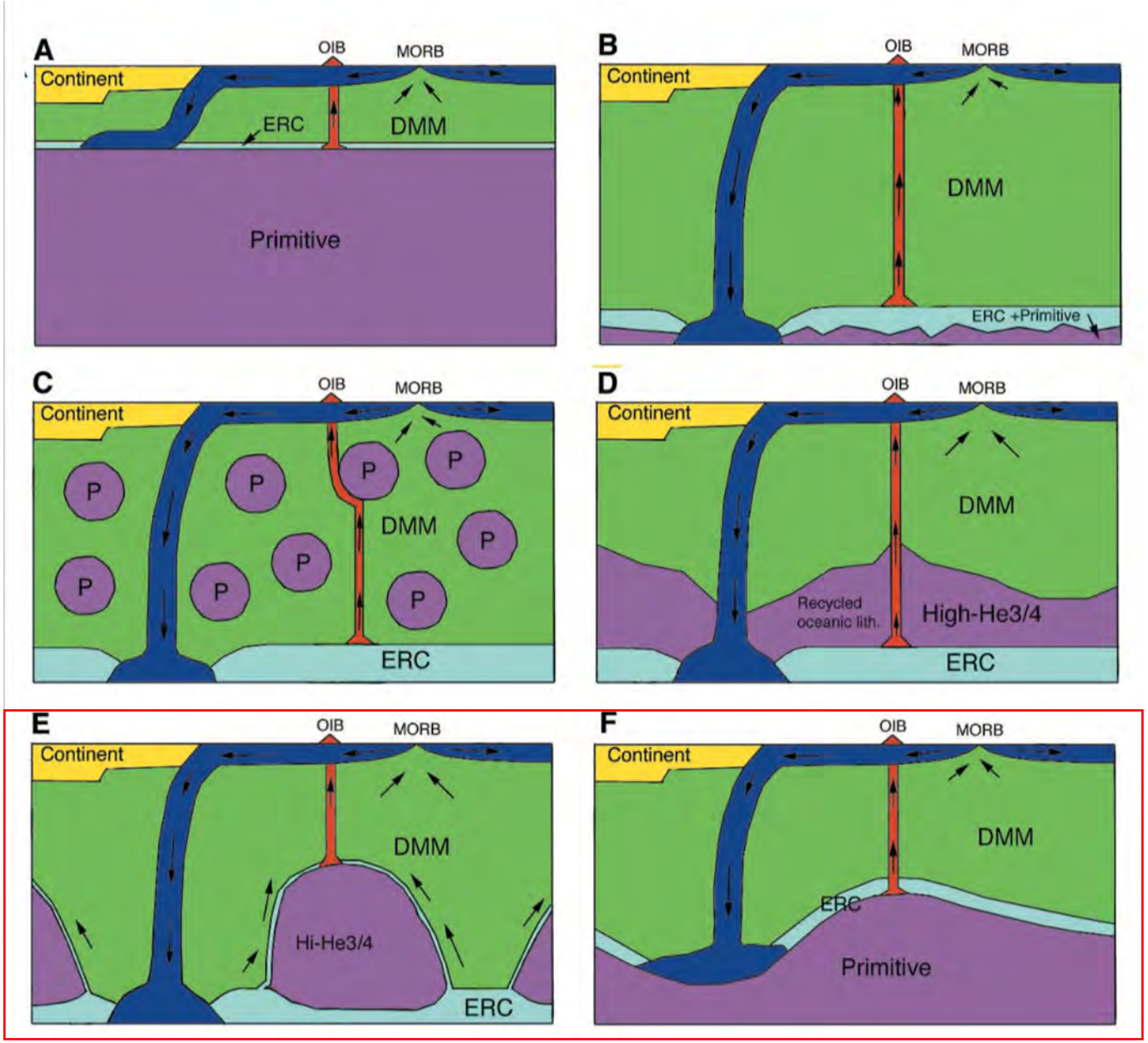
A
OIB
MORB
Continent
ERC
DMM
Primitive
B
OIB
MORB
Continent
DMM
ERC +Primitive
C
OIB
MORB
Continent
P
P
P
P
P
P
P
P
DMM
ERC
D
OIB
MORB
Continent
DMM
Recycled
oceanic lith.
High-He3/4
ERC
E
OIB
MORB
Continent
DMM
Hi-He3/4
ERC
F
OIB
MORB
Continent
DMM
ERC
Primitive

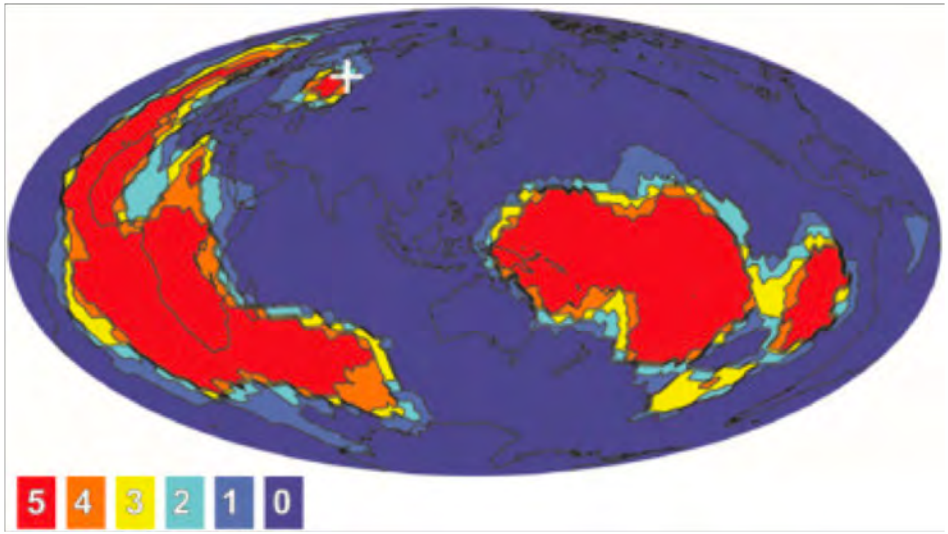

Lekic et al. 2012

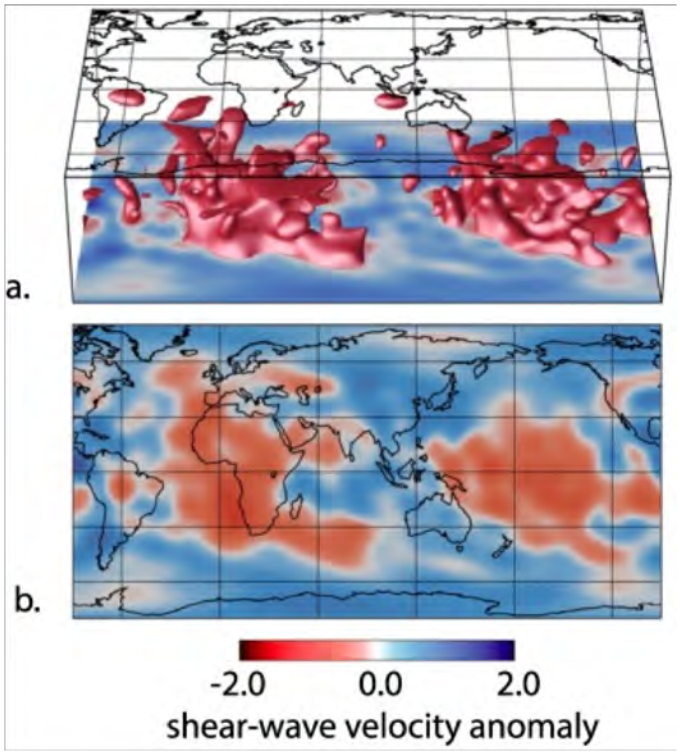

McNamara 2018 Tectonophysics
(tomography is s20rts, Ritsema et al. 1999)

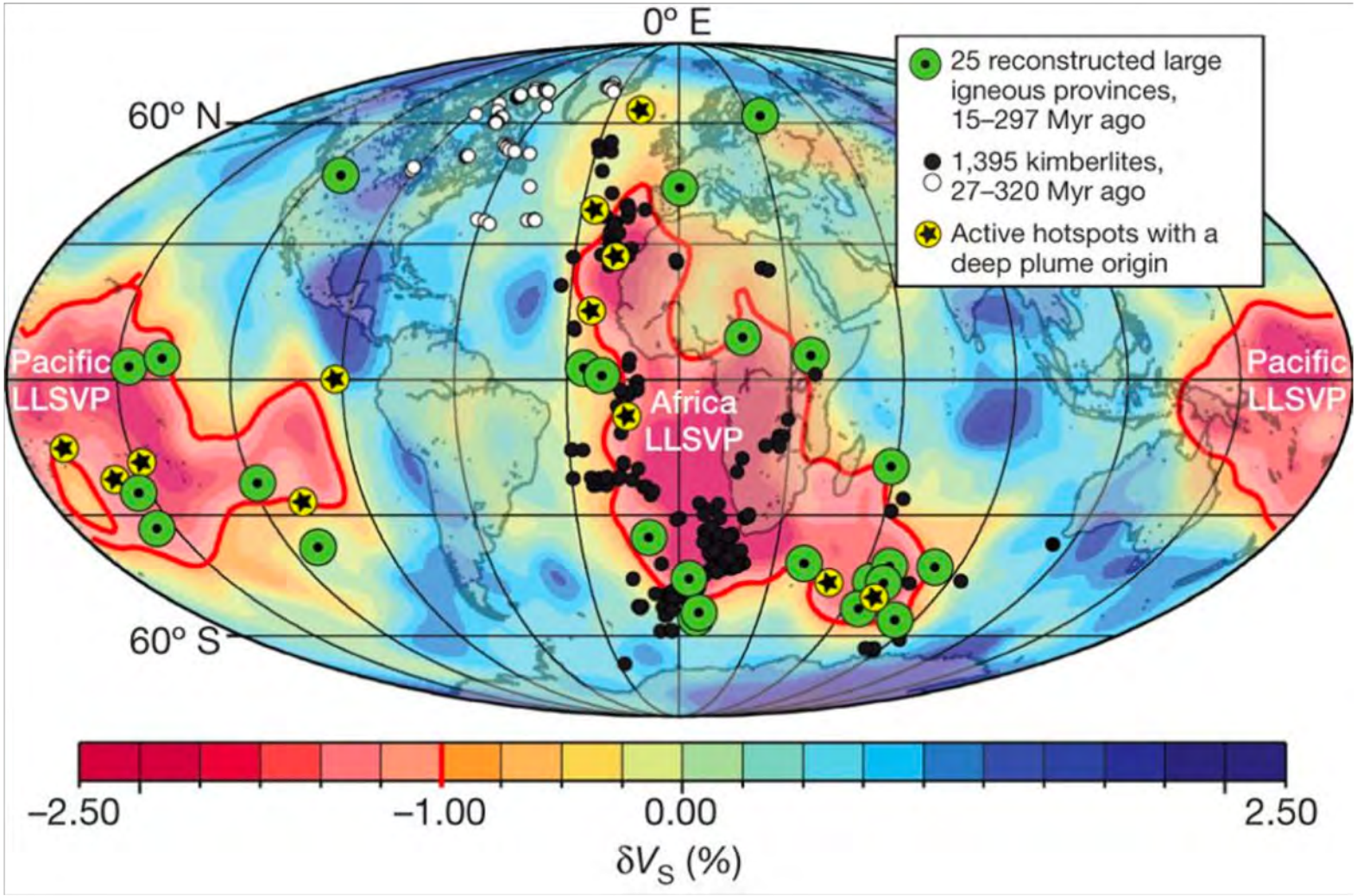

Torsvik et al. 2010

Fixed LLSVPs are being assumed to extend plate reconstructions further back in geologic time

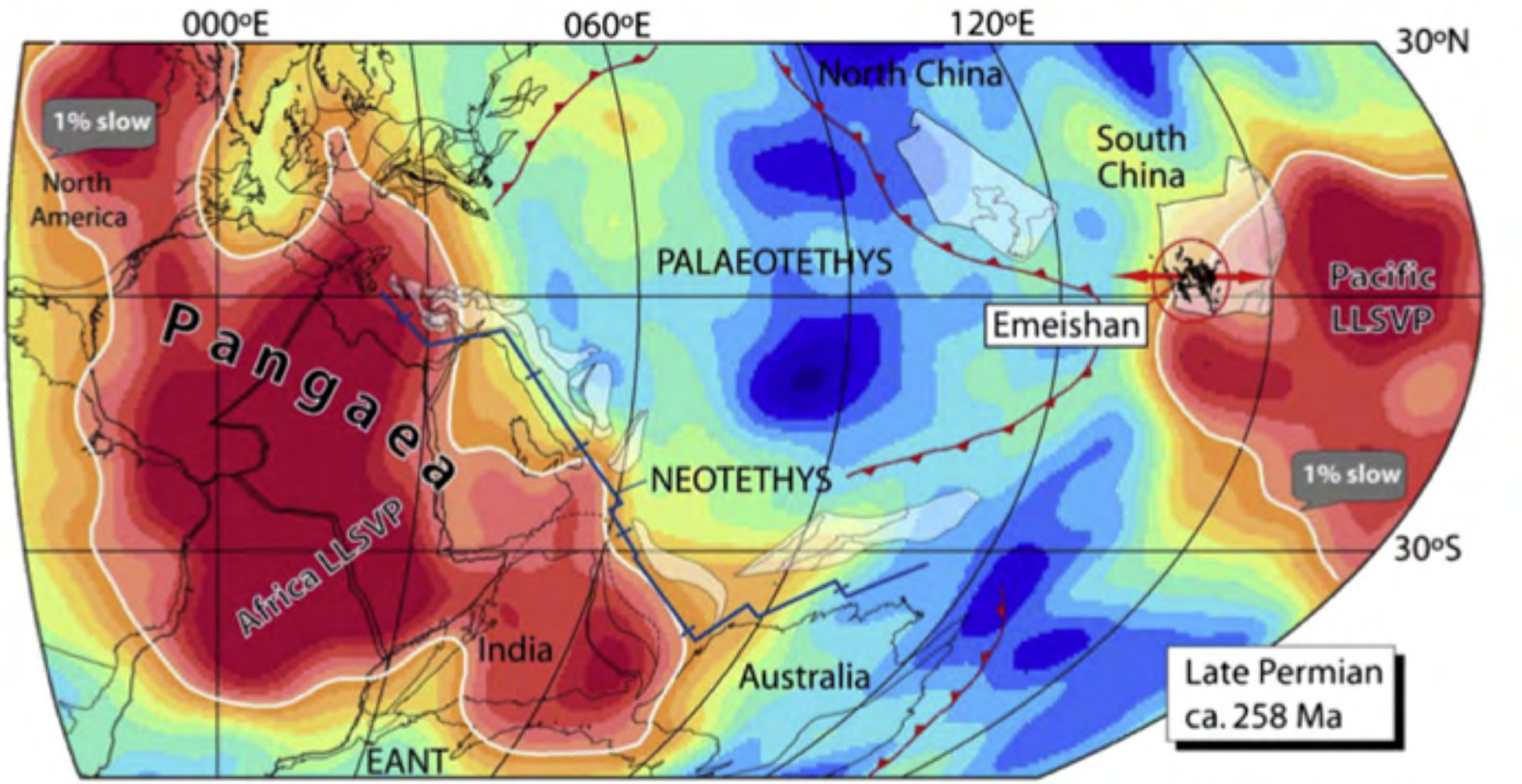

Emeishan LIP – paleolongitude uncertain

Torsvik et al. 2008

Journal of Geophysical Research: Solid Earth

RESEARCH ARTICLE
10.1002/2015JB012679

Key Points:
- Imaged global variations in elastic properties and density using complementary data sets

The relationships between large-scale variations in shear velocity, density, and compressional velocity in the Earth's mantle

P. Moulik[1,2] and G. Ekström[1]

Joint Vp, Vs, ρ model

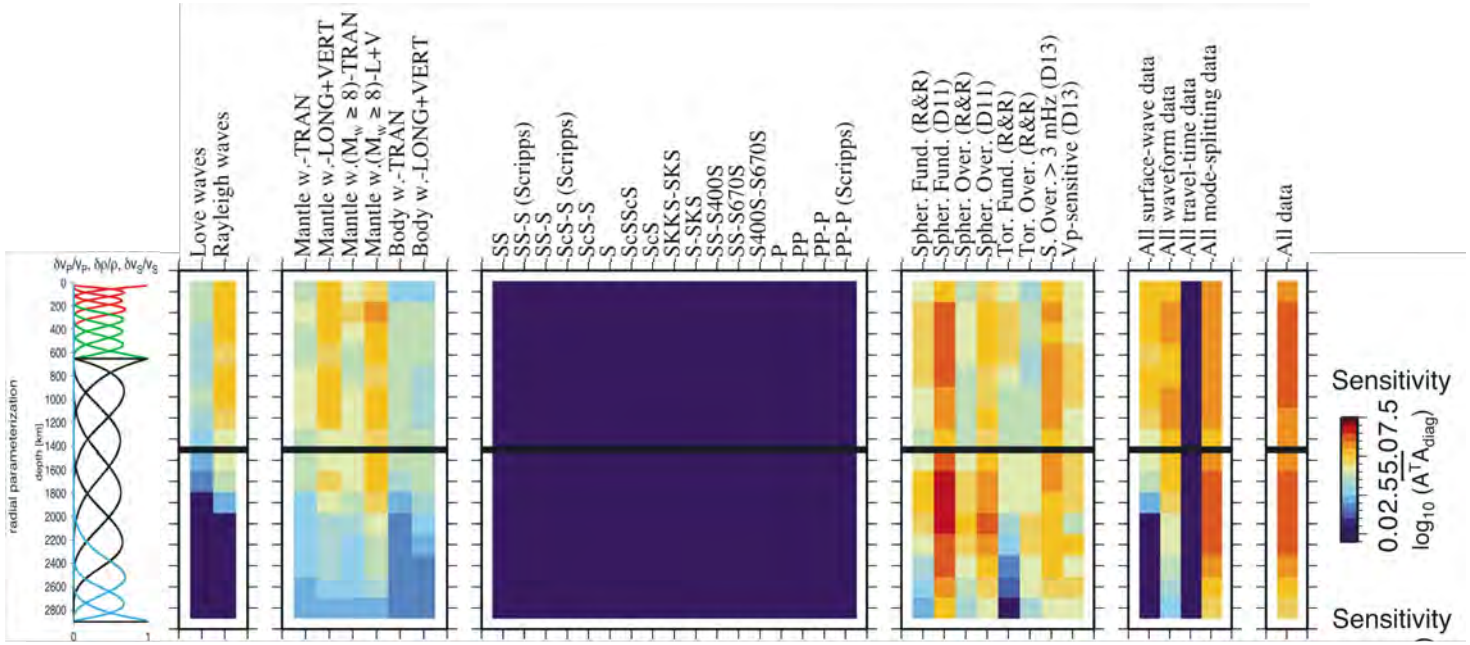

Sensitivity to density structure

Moulik and Ekström 2016

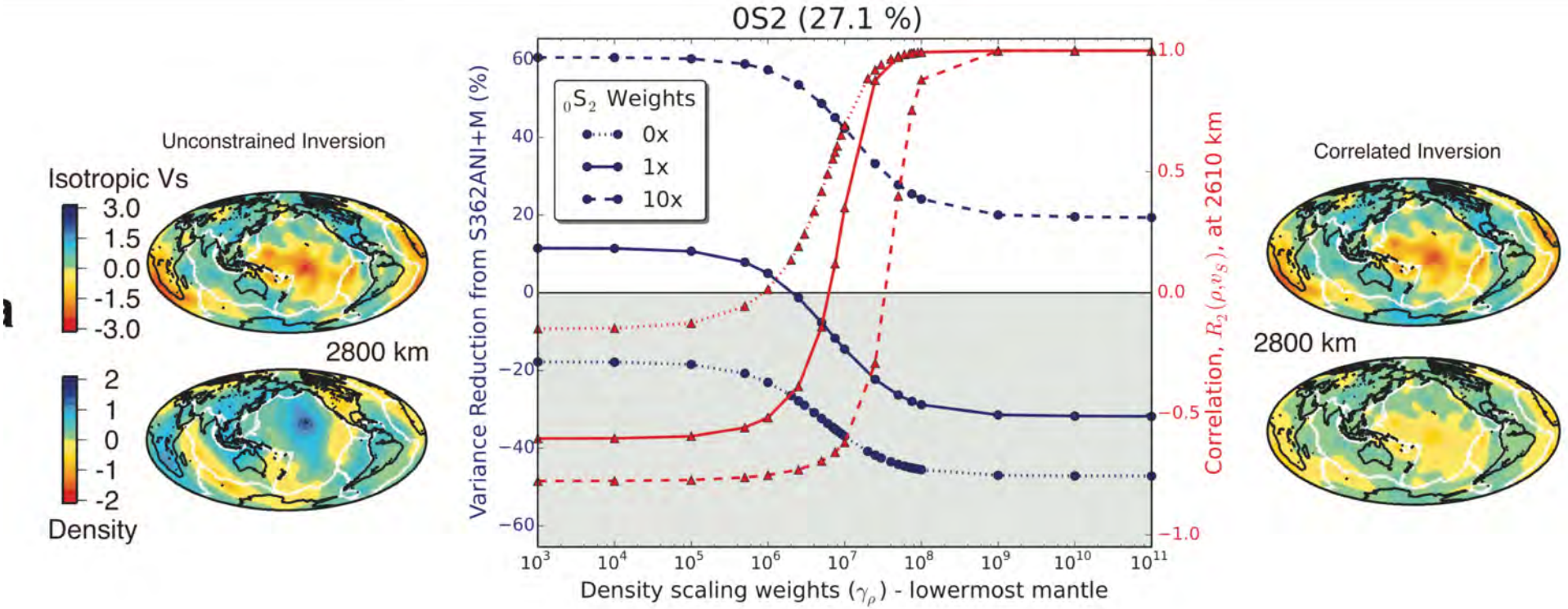

Moulik and Ekström (2016)

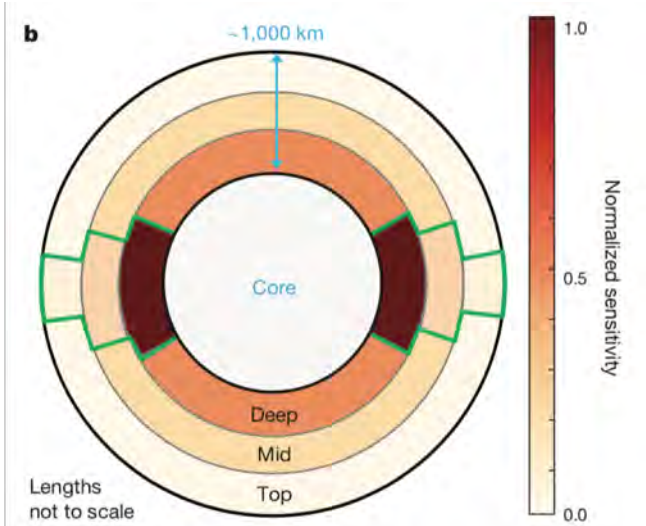

Region	Average area (%)
Deep LLSVP	19
Mid LLSVP	12
Top LLSVP	5

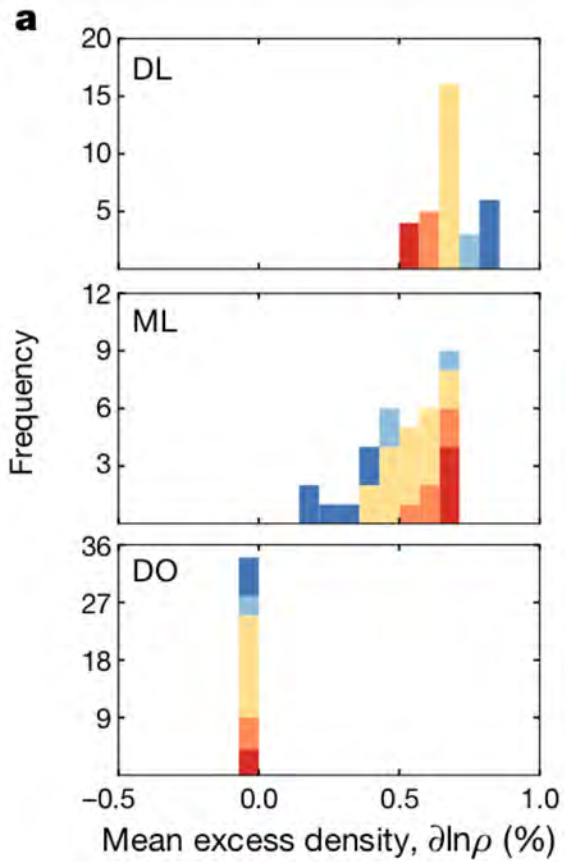

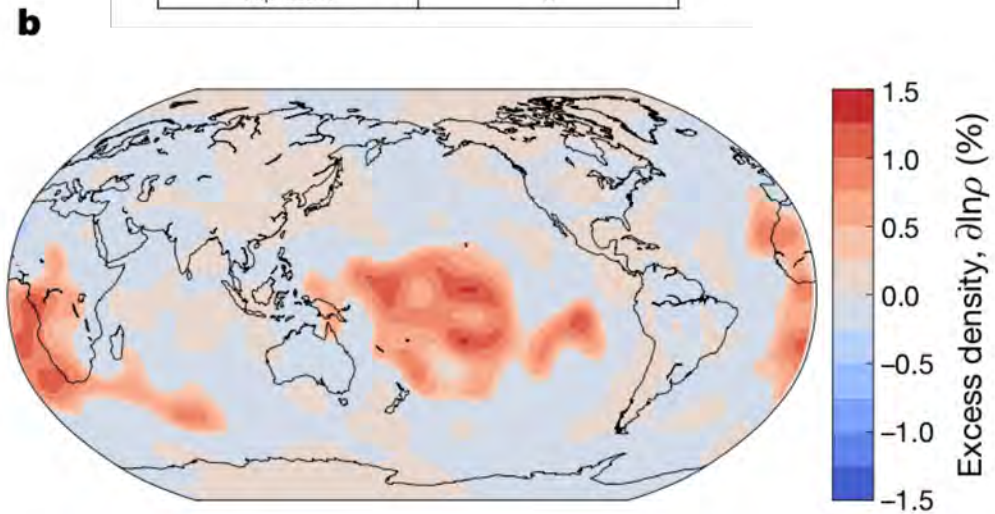

Lau et al. 2017

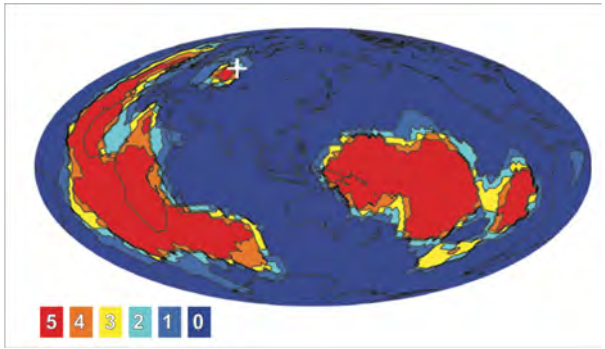

LLSVP boundaries from cluster analysis
Lekic et al. 2012

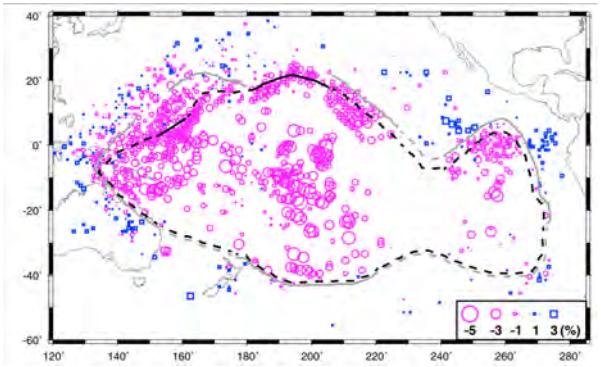

Shear and bulk sound speed anticorrelated

Waveform modeling reveals sharp boundaries

Tidal tomography

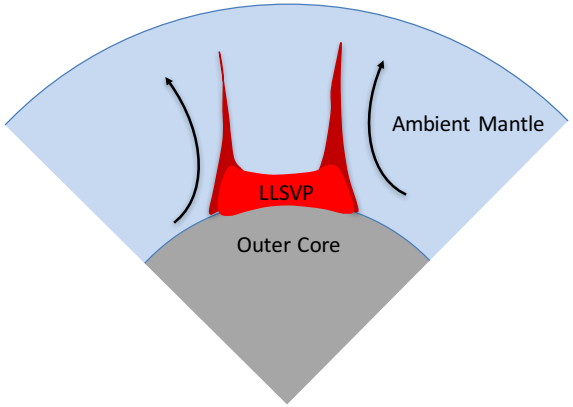

Thermal Buoyancy

Compensated over bottom 1000 km?

Compositional Buoyancy

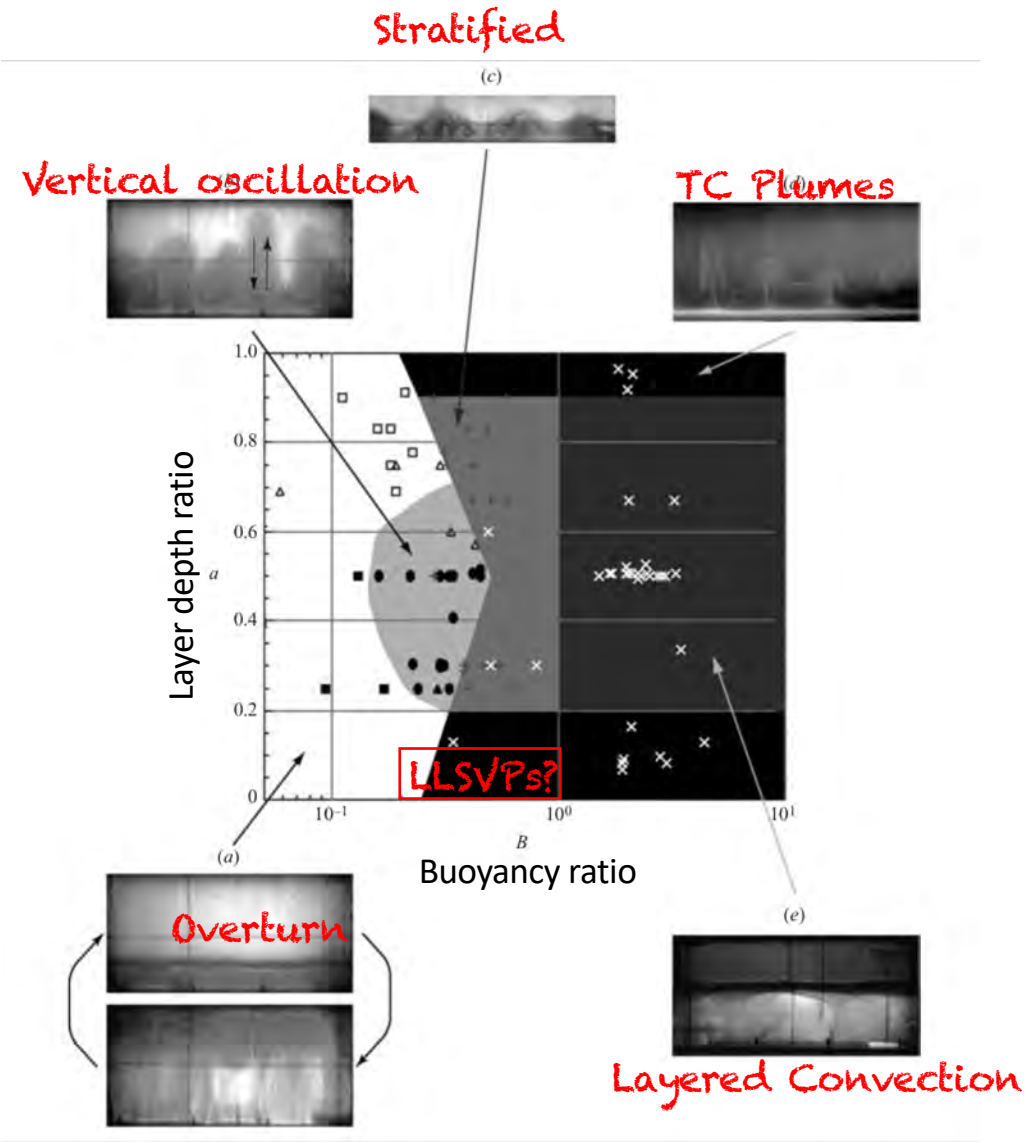

Le Bars and Davaille 2004 *JFM*

Regime diagram from Laboratory analogue experiments

$$B = \frac{\Delta\rho_\chi}{\alpha\rho_0\Delta T},$$

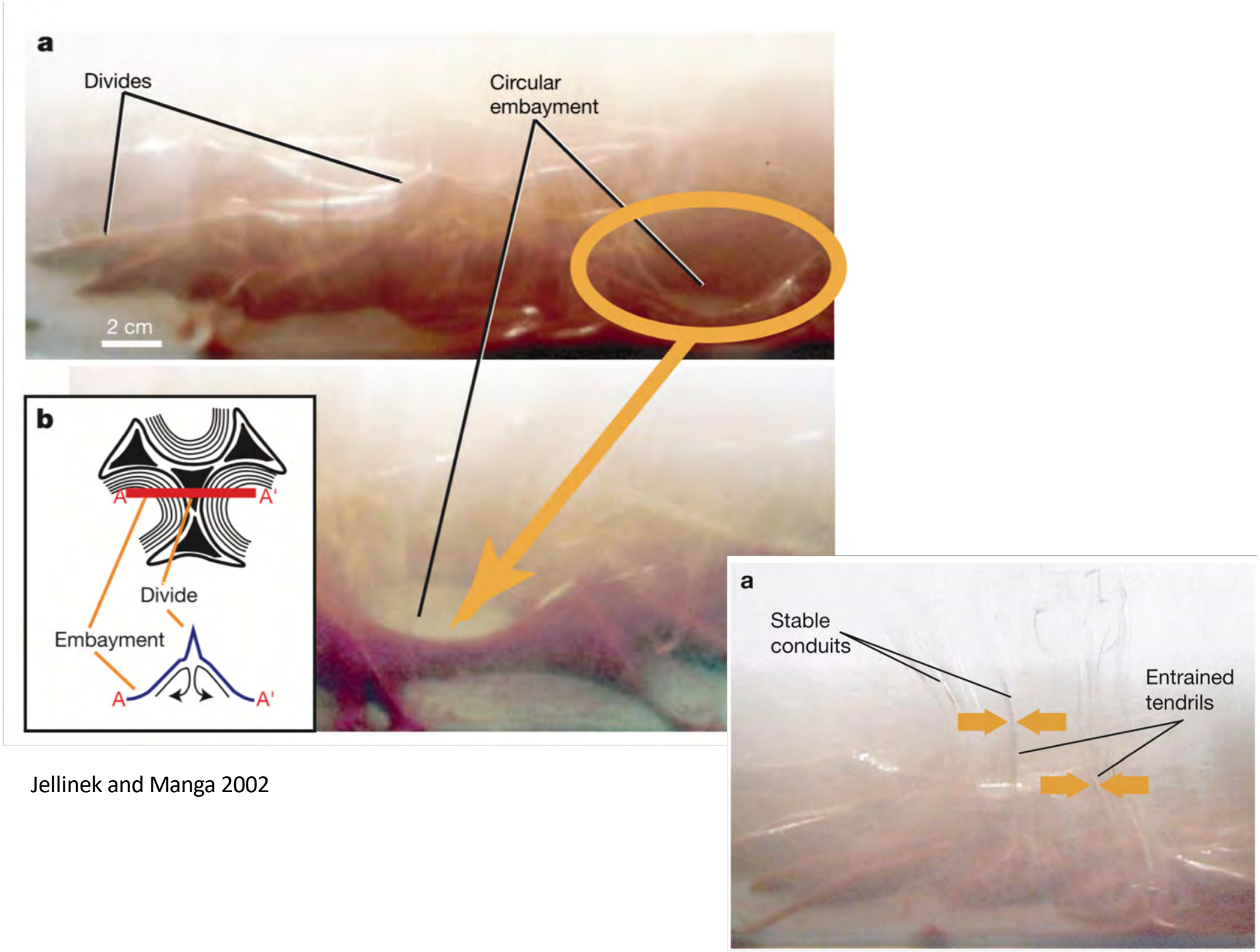

Jellinek and Manga 2002

Chemical piles – what controls shape?

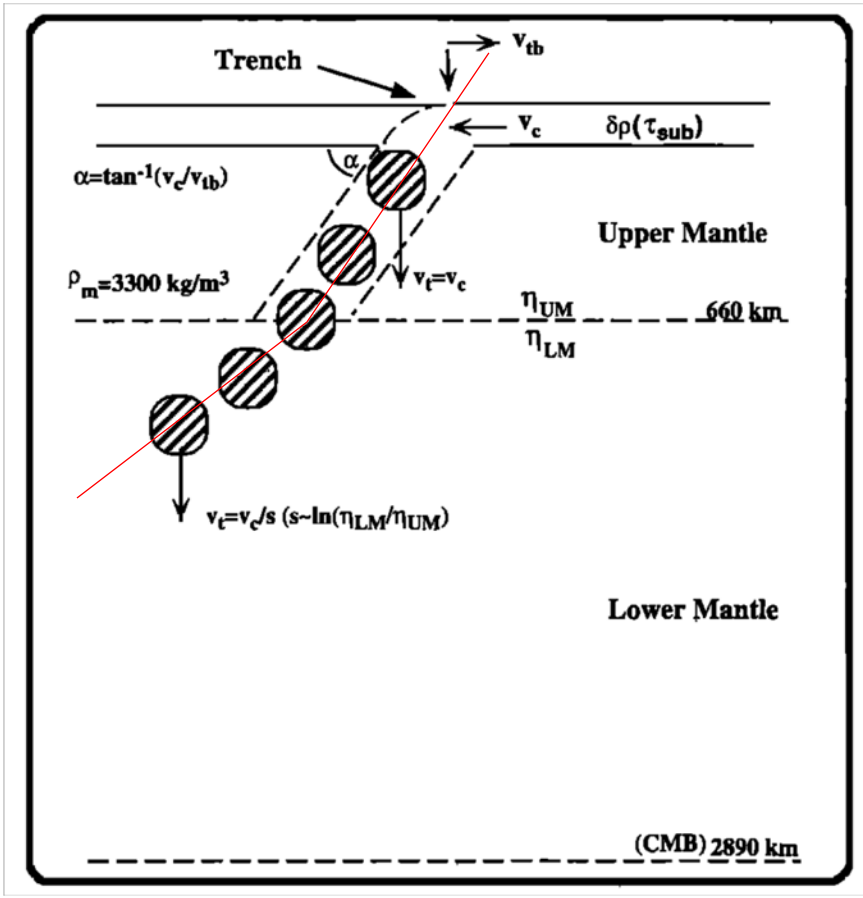

Simplest models of slab sinking

'Slablets' introduced, sink vertically.

Ricard et al. 1993
Lithgow-Bertelloni and Richards 1998 *Rev. Geophys.*

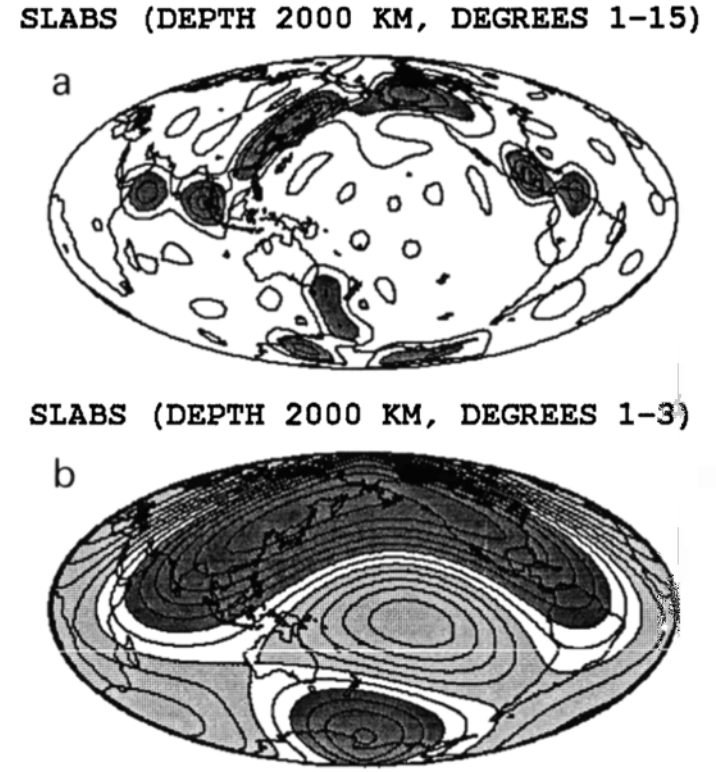

Put slabs into the mantle based on 180 Myr subduction history.

Use resulting ‘slablet’ density model to drive
Mantle flow

Lower mantle density structure not so different from tomography.

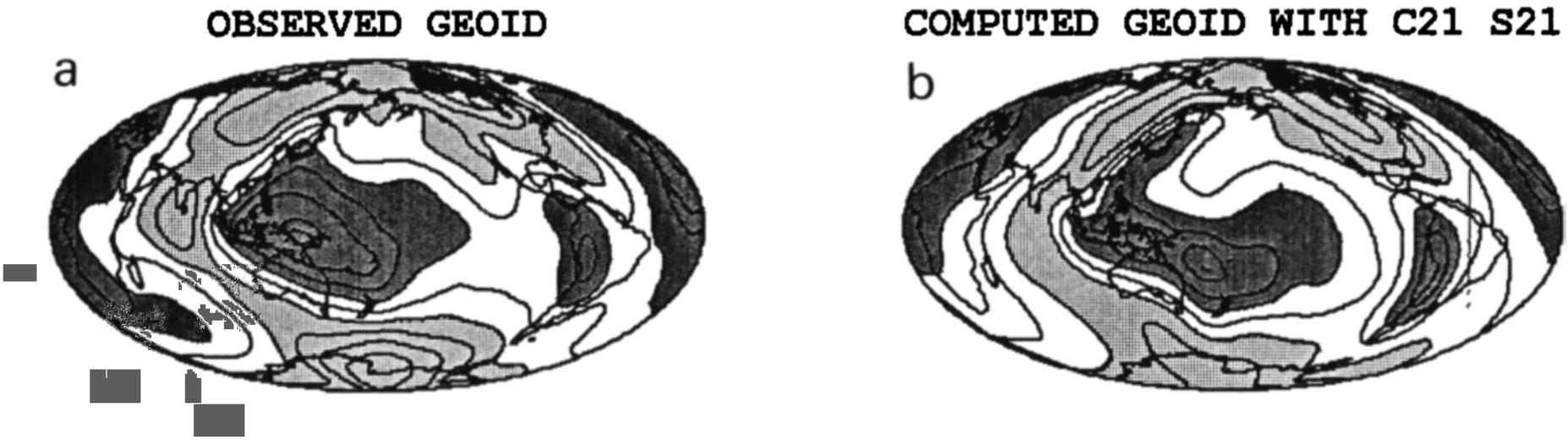

Ricard et al. 1993

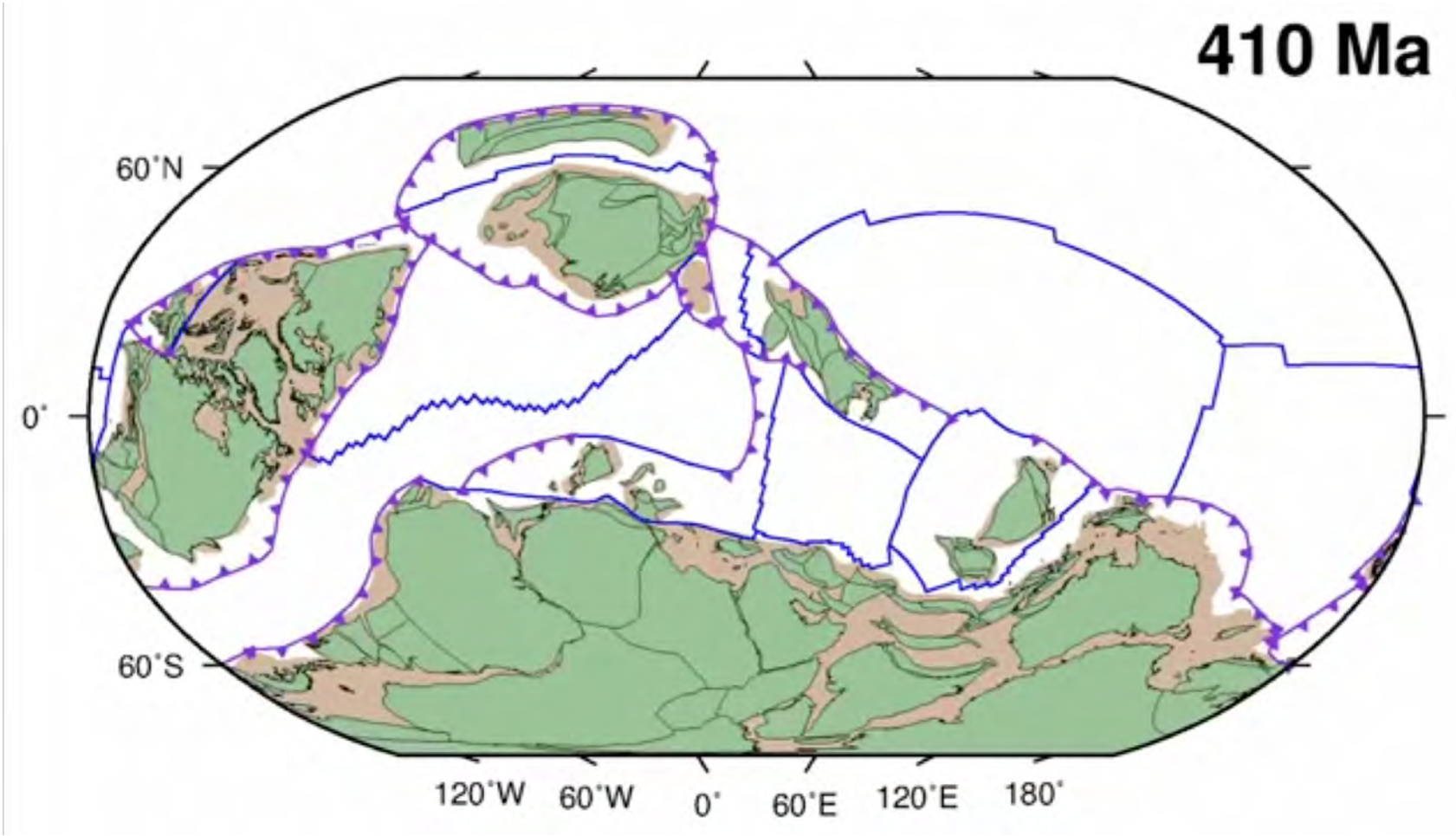

Time-dependent plate boundary configuration from Matthews et al. 2016

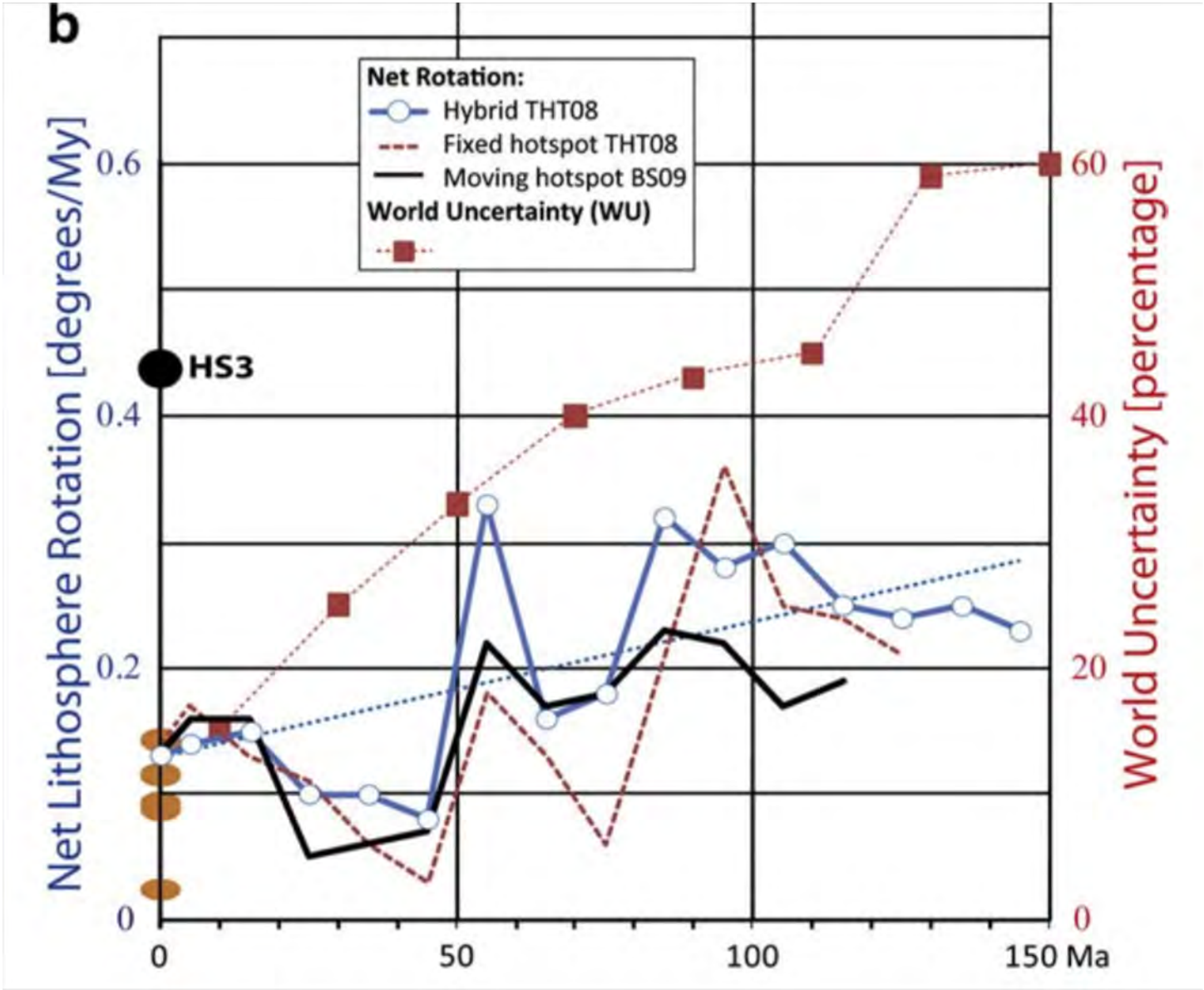

Torsvik et al. 2010

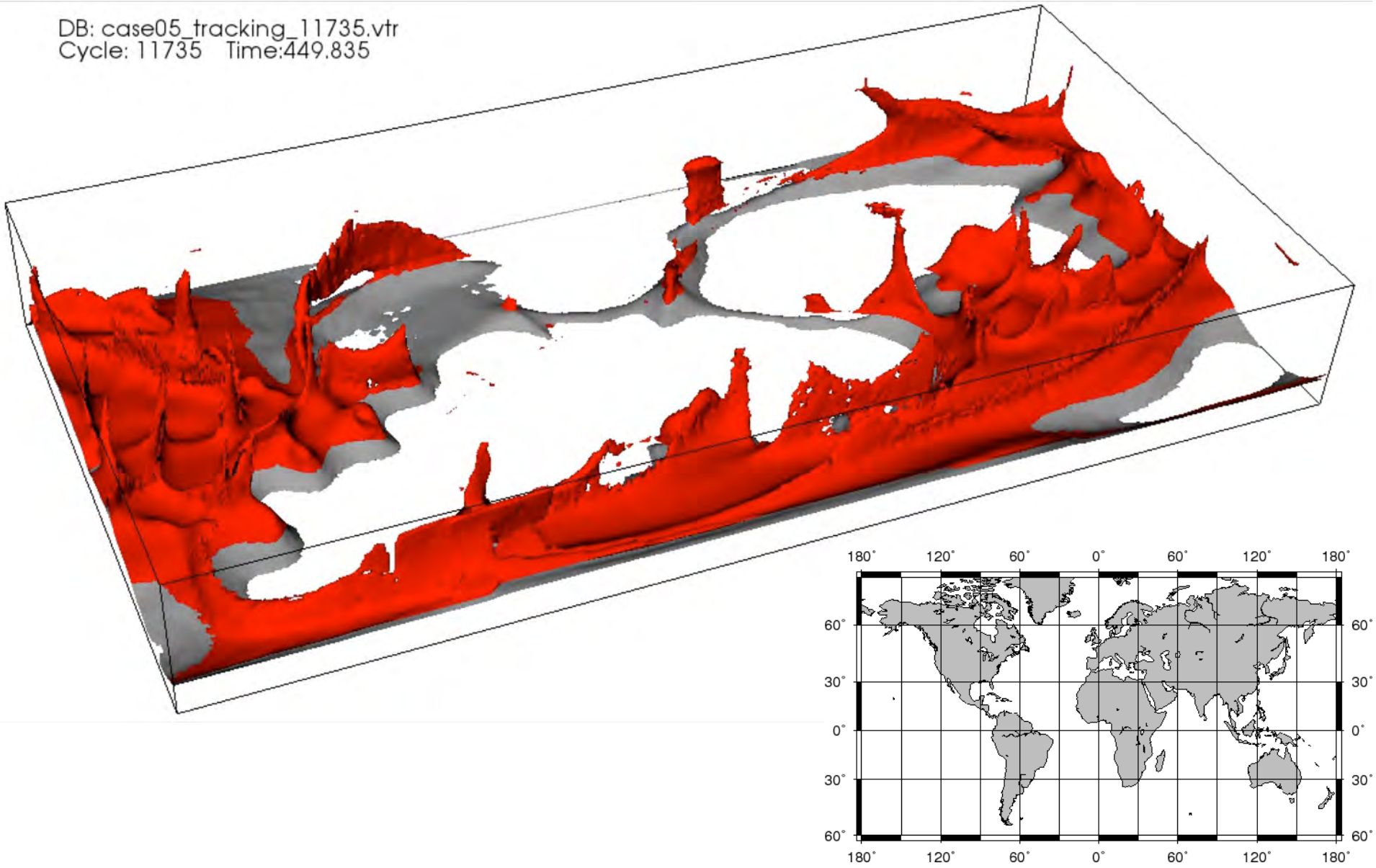
DB: case05_tracking_11735.vtr
Cycle: 11735 Time:449.835
180˚ 120˚ 60˚ 0˚ 60˚ 120˚ 180˚
60˚
30˚
0˚
30˚
60˚

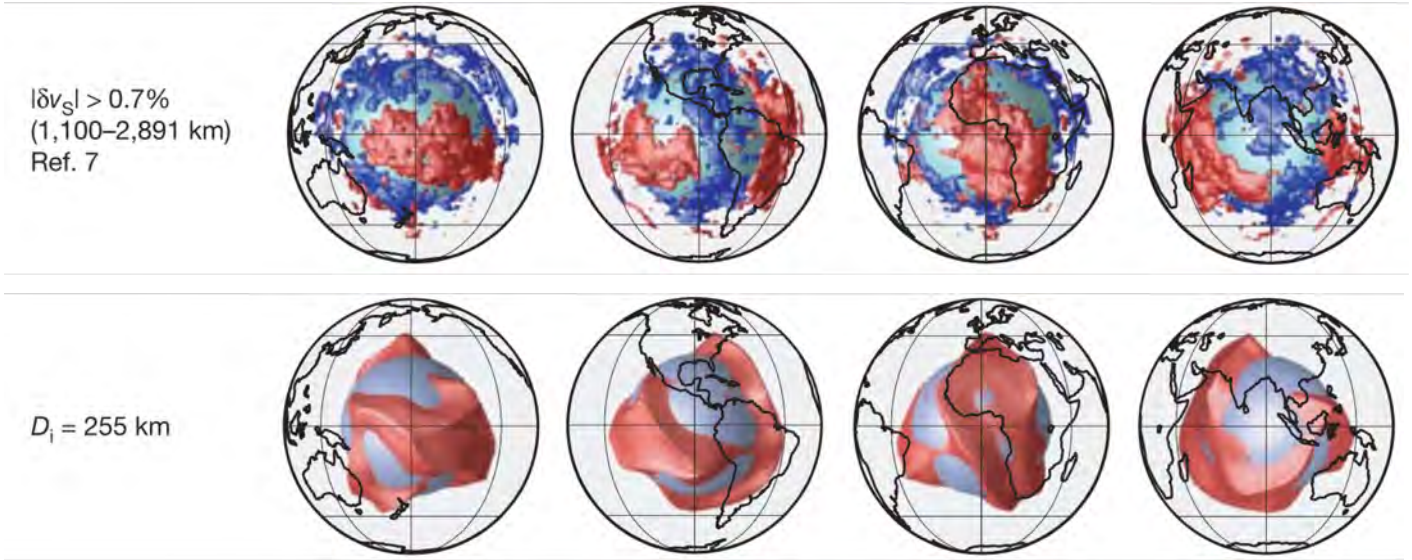

McNamara and Zhong 2004

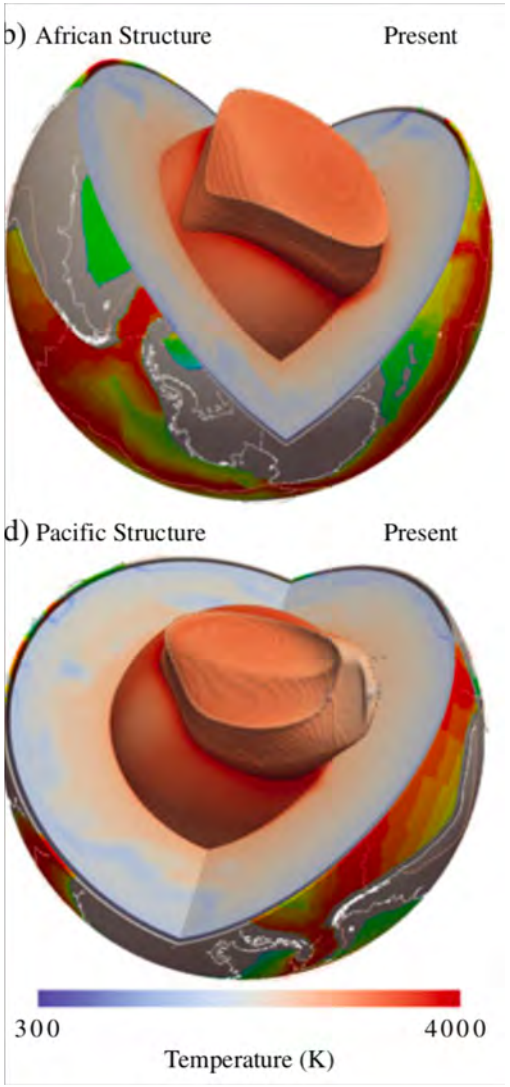

Bower et al. 2013

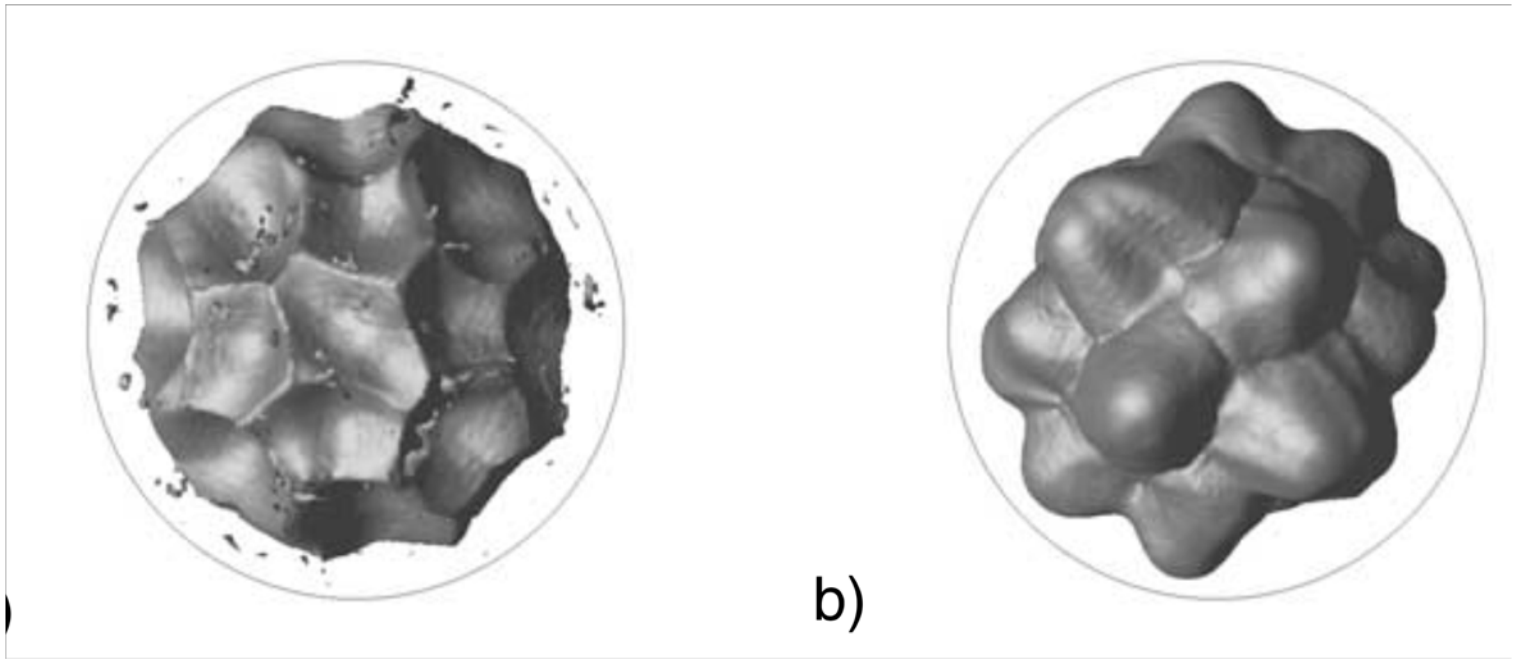

50X lower viscosity

50X higher viscosity

McNamara and Zhong 2004

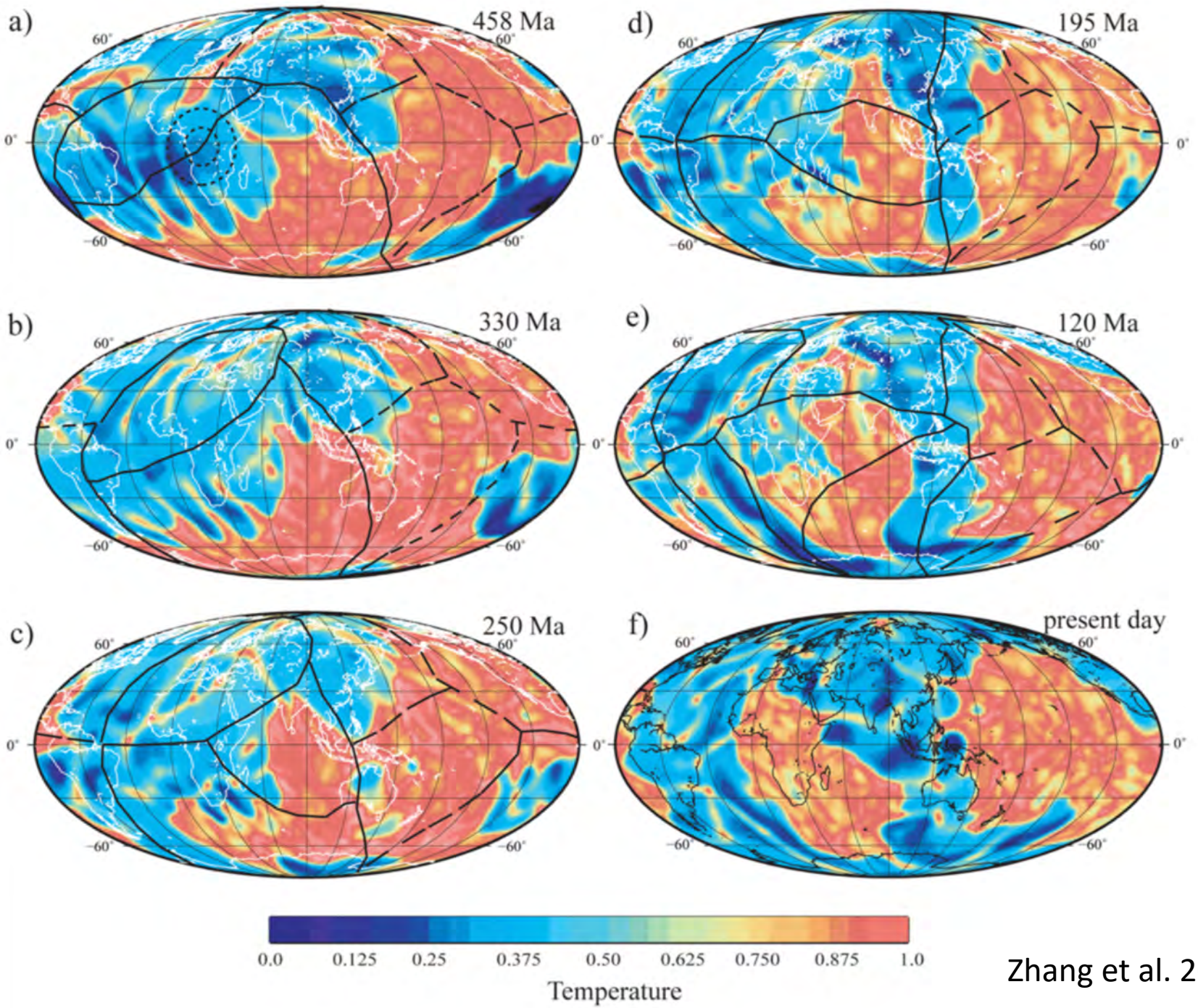

Zhang et al. 2010

Lower-mantle mysteries

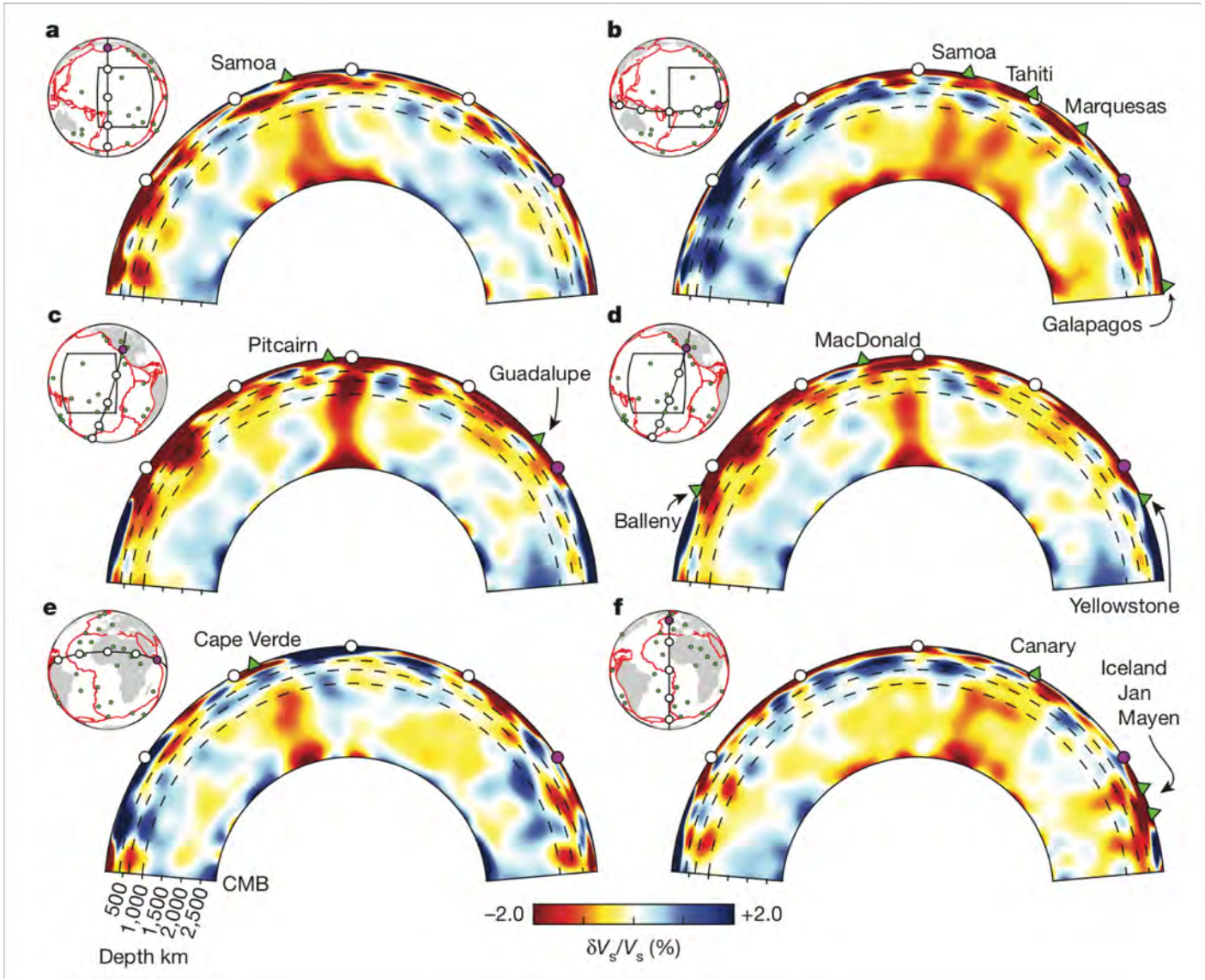

French and Romanowicz 2015

Rheological explanation for broad plumes, ponding below 1000?

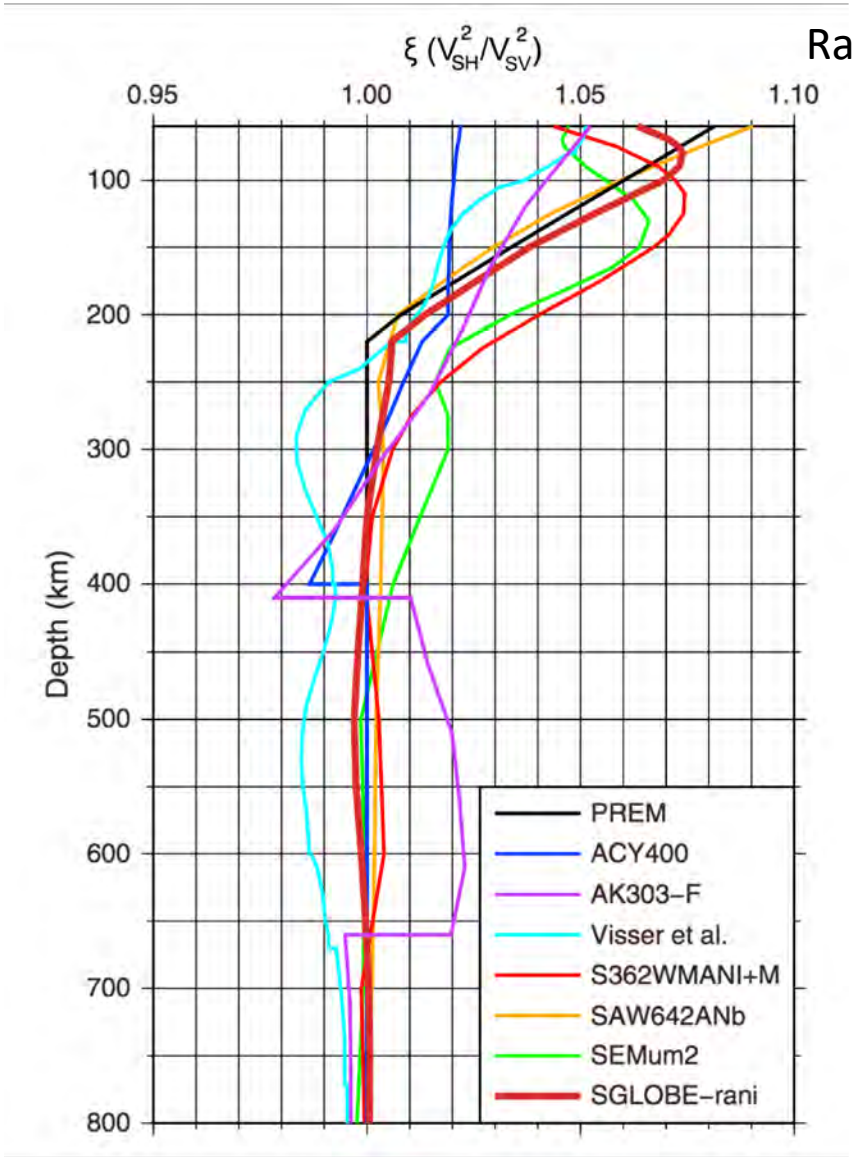

Radial anisotropy from SGLOBE-RANI and other models

Diffusion creep – grain size sensitive but no CPO.

Dislocation creep – not grain size dependent, produces CPO

Chang et al. 2018

Grain size evolution?

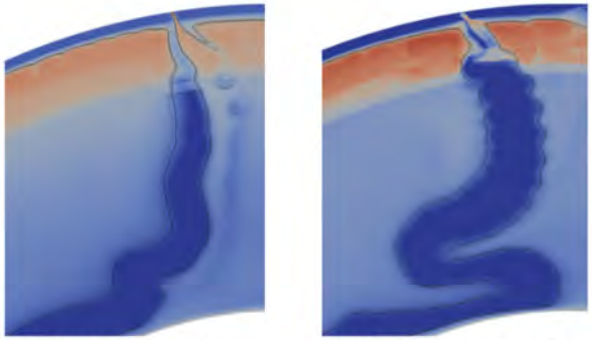

(a) Steinberger & Calderwood, 2006

(b) Constant grain size

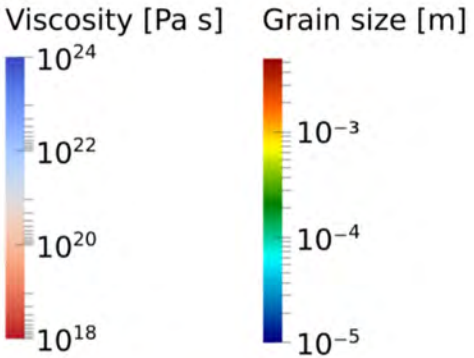

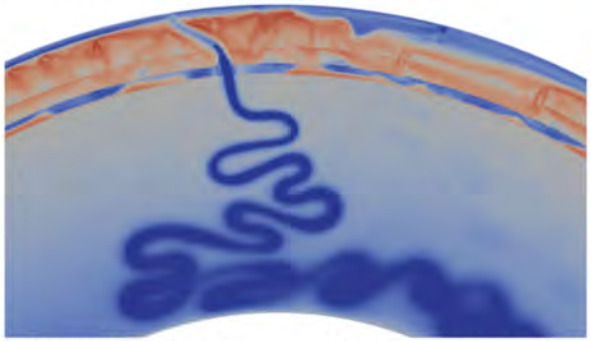

(c) Evolving grain size, LM V_{diff} = 2e-6

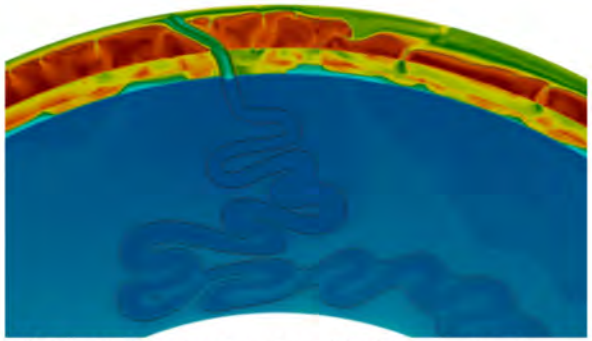

(d) Evolving grain size, LM V_{diff} = 2e-6

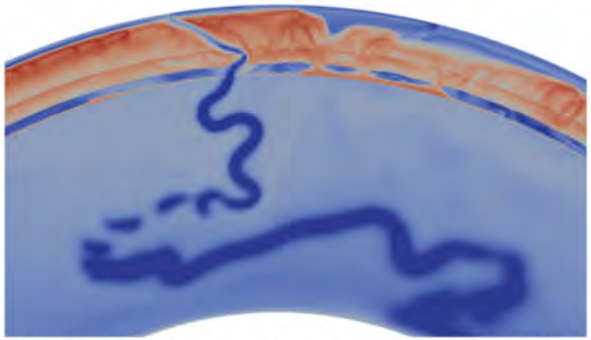

(e) Evolving grain size, LM V_{diff} = 1.5e-6

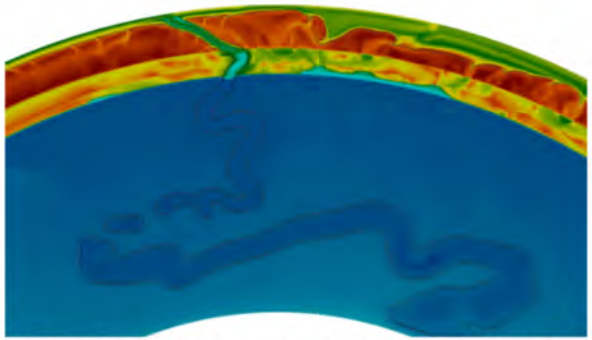

(f) Evolving grain size, LM V_{diff} = 1.5e-6

$$\eta_{diff} = \frac{1}{2} A_{diff}^{-1} d^m \exp\left(\frac{E^*_{diff} + PV^*_{diff}}{RT}\right),$$

$$\eta_{dis} = \frac{1}{2} A_{dis}^{-\frac{1}{n}} \dot{\varepsilon}_{dis,II}^{\frac{1-n}{n}} \exp\left(\frac{E^*_{dis} + PV^*_{dis}}{nRT}\right),$$

$$\dot{d}_{growth} = p_g^{-1} d^{1-p_g} k_g \exp\left(-\frac{E_g + PV_g}{RT}\right),$$

$$\dot{d}_{reduce} = 4 \dot{\varepsilon}_{II} \dot{\varepsilon}_{dis,II} \eta_{eff} \frac{\lambda d^2}{c\gamma},$$

Dannberg et al. 2017
CIDER project!

Is diffusion creep the dominant LM mechanism?

Pure climb creep mechanism drives flow in Earth's lower mantle

Francesca Boioli,[1]* Philippe Carrez,[1] Patrick Cordier,[1†] Benoit Devincre,[2] Karine Gouriet,[1] Pierre Hirel,[1] Antoine Kraych,[1] Sebastian Ritterbex[1‡]

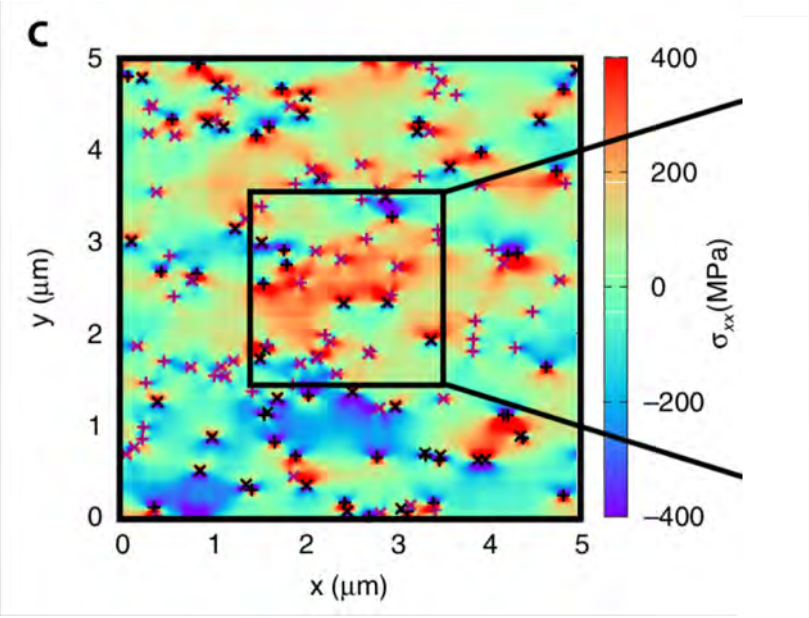

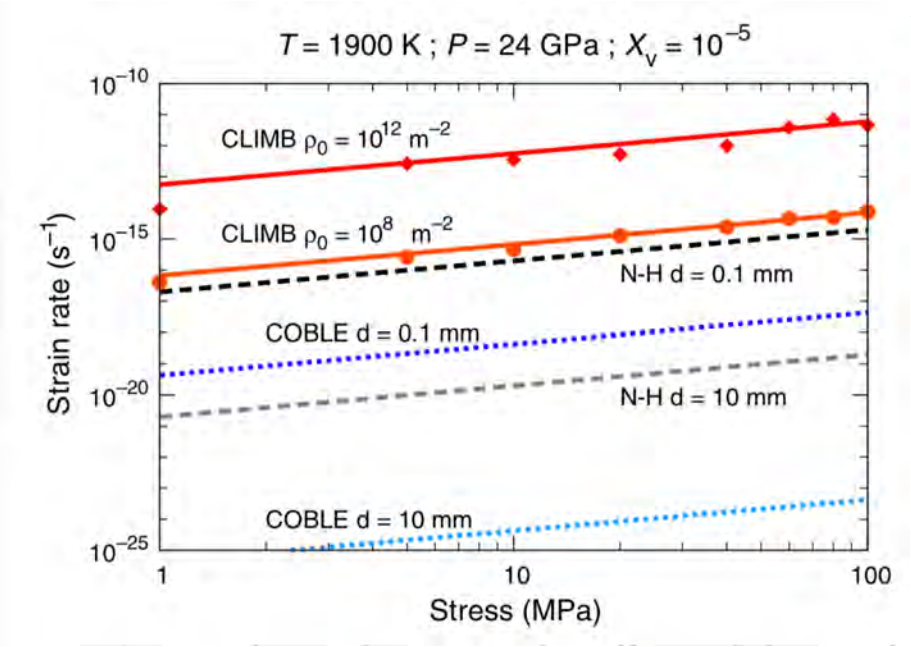

Newtonian? Probably, but grain size **insensitive** and no **CPO**

Ferropericlase strength increase?

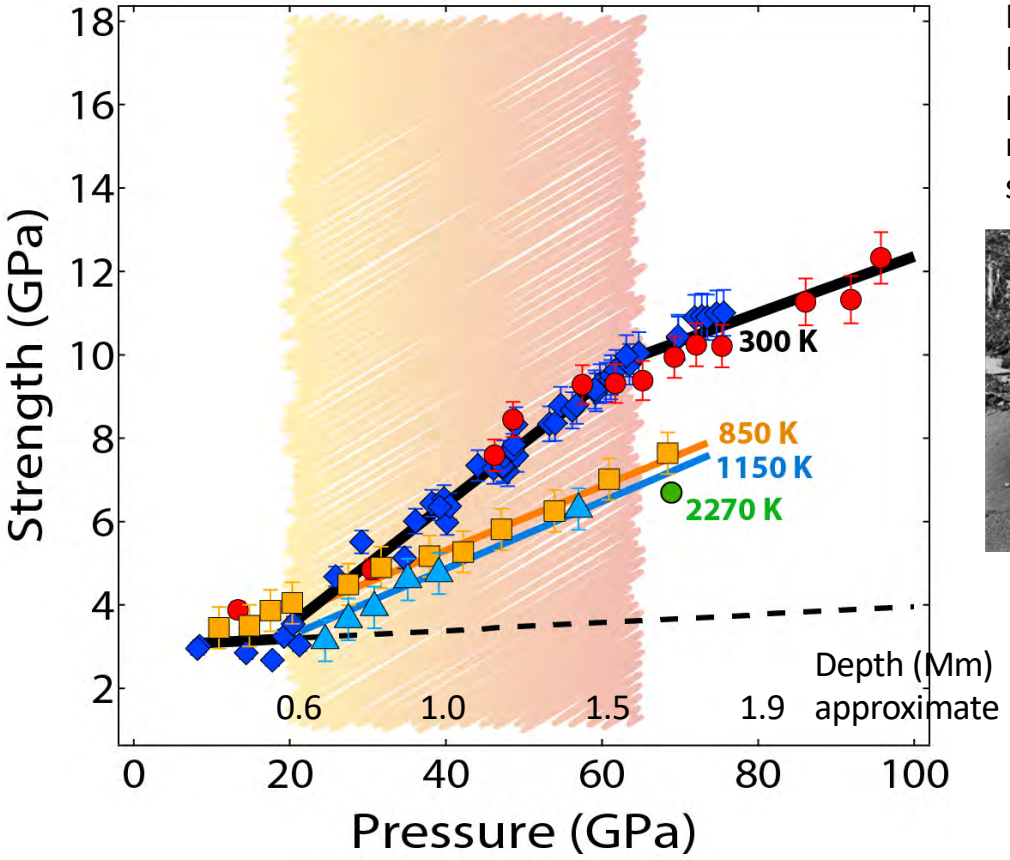

Marquardt and Miyagi 2015 and unpublished data

Increase in strength of Ferropericlase. Minor phase but could control rheology if arranged in sheets.

Effective viscosity could be nonlinear

Energy budget

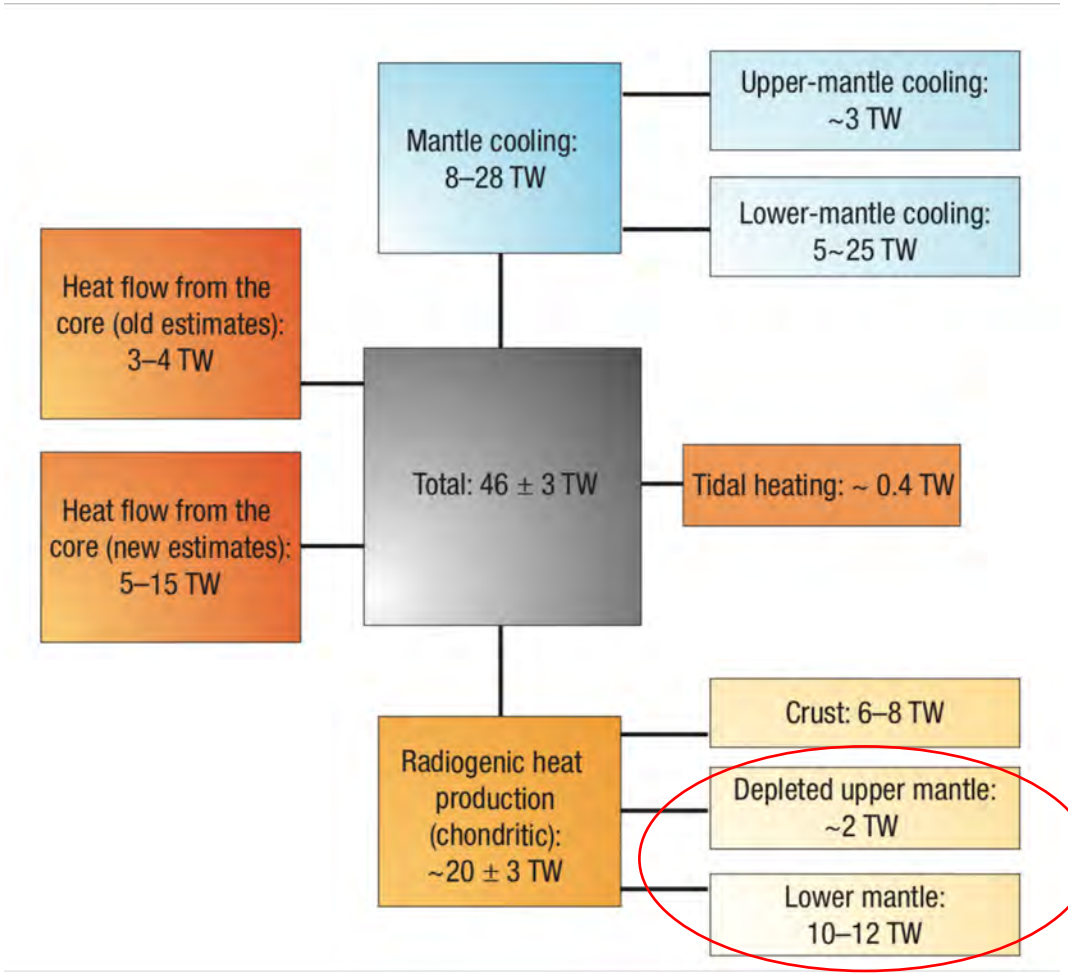

Viability of chemical blobs etc. sensitive to this and how it is distributed

Lay et al. 2008

Thursday Tutorial Preview

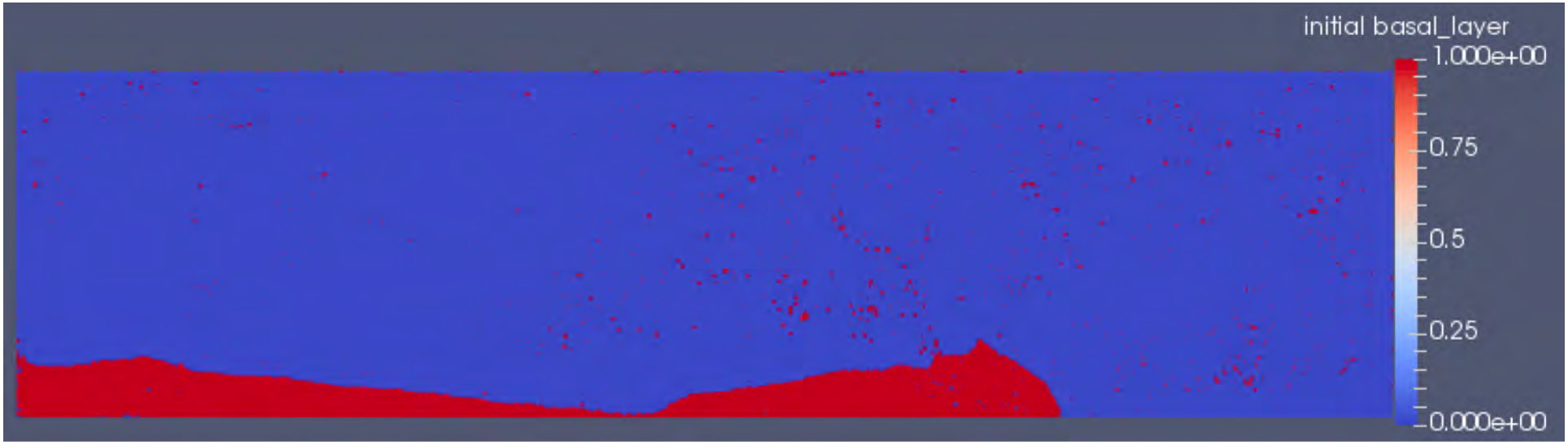

With thermochemical piles: